

March 2019

## **Analysis of Adhesive Anchorage Systems Under Extreme In-Service Temperature Conditions**

Rachel Wang

*University of Massachusetts Amherst*

Follow this and additional works at: [https://scholarworks.umass.edu/masters\\_theses\\_2](https://scholarworks.umass.edu/masters_theses_2)



Part of the Civil Engineering Commons

---

### **Recommended Citation**

Wang, Rachel, "Analysis of Adhesive Anchorage Systems Under Extreme In-Service Temperature Conditions" (2019). *Masters Theses*. 752.  
<https://doi.org/10.7275/13071979> [https://scholarworks.umass.edu/masters\\_theses\\_2/752](https://scholarworks.umass.edu/masters_theses_2/752)

This Open Access Thesis is brought to you for free and open access by the Dissertations and Theses at ScholarWorks@UMass Amherst. It has been accepted for inclusion in Masters Theses by an authorized administrator of ScholarWorks@UMass Amherst. For more information, please contact [scholarworks@library.umass.edu](mailto:scholarworks@library.umass.edu).

**ANALYSIS OF ADHESIVE ANCHORAGE SYSTEMS UNDER EXTREME IN-SERVICE TEMPERATURE CONDITIONS**

A Thesis Presented

by

RACHEL L. WANG

Submitted to the Graduate School of the  
University of Massachusetts Amherst in partial fulfillment  
of the requirements for the degree of

MASTER OF SCIENCE IN CIVIL ENGINEERING

February 2019

Civil and Environmental Engineering

**ANALYSIS OF ADHESIVE ANCHORAGE SYSTEMS UNDER EXTREME IN-SERVICE TEMPERATURE CONDITIONS**

A Thesis Presented

by

RACHEL L. WANG

Approved as to style and content by:

---

Scott Civjan, Chair

---

Sergio Breña, Member

---

Richard N. Palmer, Department Head  
Civil and Environmental Engineering

## **DEDICATION**

This work is dedicated to my family, who have always believed in me.

## **ACKNOWLEDGMENTS**

I would like to thank my advisor, Dr. Scott Civjan, for guiding me and mentoring me throughout this project, whose advice and support has proved invaluable to my education.

I would also like to thank the Structural Engineering group at the University of Massachusetts Amherst, all of whom have taught me and guided me in some way over the past few years. I am in their debt.

## **ABSTRACT**

### **ANALYSIS OF ADHESIVE ANCHORAGE SYSTEMS UNDER EXTREME IN-SERVICE TEMPERATURE CONDITIONS**

FEBRUARY 2019

RACHEL L. WANG, B.S., THE OHIO STATE UNIVERSITY

M.S. UNIVERSITY OF MASSACHUSETTS AMHERST

Directed by: Professor Scott A. Civjan

Adhesive anchorage systems have found widespread use in structural applications, including bridge widening, concrete repair and rehabilitation, and barrier retrofitting. Because these applications typically require adhesive anchorage systems to be installed outdoors, the effects of climate conditions and day-to-day temperature fluctuations on adhesive behavior and performance should be considered. The purpose of this thesis is to simulate pullout tests of adhesive anchorage systems for threaded rod and reinforcing bars and to emulate effects under various temperature conditions through the use of finite element analysis. Results from the finite element simulation are then compared to the physical tests conducted at UMass Amherst to determine the validity of the finite element model and to assess any notable differences in adhesive anchor performance in hot, cold, and ambient temperatures. In addition, differences in adhesive stresses when anchoring threaded rod versus reinforcing steel are evaluated.

## TABLE OF CONTENTS

	<b>Page</b>
ACKNOWLEDGMENTS .....	iv
ABSTRACT.....	v
LIST OF TABLES .....	ix
LIST OF FIGURES .....	x
CHAPTER	
1. INTRODUCTION .....	1
1.1. Overview.....	1
1.2. Motivation for Study.....	2
1.3. Research Objectives.....	4
2. LITERATURE REVIEW .....	5
2.1. Behavior Models and Failure Modes of Bonded Anchors.....	5
2.2. Current Test Standards For Bonded Anchors .....	7
2.2.1. ASTM E488 (2010): Standard Test Methods for Strength of Anchors in Concrete and Masonry Elements.....	8
2.2.2. ICC-ES AC308 (2013) Acceptance Criteria for Post-Installed Adhesive Anchors in Concrete Elements .....	8
2.2.3. ACI 355.4 (2011): Qualification of Post-Installed Anchors in Concrete .....	9
2.2.4. AASHTO TP-84 (2013): Evaluation of Adhesive Anchors in Concrete Under Sustained Loading .....	9
2.3. Epoxy Behavior and Effect of Temperature .....	9
2.4. Effect of Temperature on Concrete Behavior .....	14
2.5. Effect of Temperature on Steel Behavior .....	16
3. PHYSICAL TESTING PREPARATION .....	19
3.1. Test Specimens .....	19
3.1.1. Concrete .....	19
3.1.2. Anchor.....	21
3.1.3. Bonding Material .....	22
3.2. Testing Program.....	22

3.3. Specimen Preparation .....	23
3.3.1. Condition Prior to Drilling.....	23
3.3.2. Drilling.....	23
3.3.3. Hole Cleaning .....	24
3.3.4. Anchor Installation.....	25
3.3. Environmental Conditioning.....	27
3.3.1. Freezers .....	27
3.3.2. Heat Chamber .....	28
3.5. Short-Term Test Components.....	28
3.5.1. Loading Rod.....	33
3.5.2. Non-Rigid Coupler.....	33
3.5.3. Lenton Terminator D6 .....	33
3.5.4. Confining Plate .....	34
3.5.5. Confining Sheet .....	34
3.5.6. Hydraulic Jack .....	34
3.6. Instrumentation .....	34
3.6.1. Temperature and Relative Humidity.....	34
3.6.2. Displacement.....	35
3.6.3. Load .....	36
3.7. Data Management .....	36
3.7.1. Data Acquisition System and Sampling .....	36
3.8. Test Procedure .....	36
4. FINITE ELEMENT MODELING.....	38
4.1. Overview.....	38
4.2. Finite Element Model .....	38
4.2.1. Geometry.....	38
4.2.2. Mesh and Element Type .....	45
4.2.3. Material Properties.....	49
4.5. Contact Conditions.....	54
4.6. Parameters.....	55
4.6.1. Boundary Conditions .....	55

4.6.2. Applied Force.....	55
4.7. Analysis Procedure .....	56
4.8. Nomenclature .....	57
5. RESULTS OF PHYSICAL TESTING AND FEA.....	58
5.1. Nomenclature .....	58
5.2. Physical Testing Results .....	58
5.2.1. Material 1B .....	64
5.2.2. Material 7 .....	68
5.2.3. Material 2 .....	72
5.2.4. Reinforcing Bar Pullout Tests.....	74
5.2.5. Exceptions to Manufacturer Specifications .....	76
5.3. Finite Element Analysis Results .....	79
5.3.1. TR-NB.....	79
5.3.2. TR-CB.....	89
5.3.3. RB-NB .....	93
5.3.4. RB-CB.....	102
5.3.5. Comparison of the Physical Test and FEM Results.....	105
5.3.6. Larger Hole Diameter Results .....	107
5.4. Summary .....	115
6. CONCLUSION.....	117
REFERENCES .....	119

## LIST OF TABLES

<b>Table</b>	<b>Page</b>
Table 3-1. Concrete Compressive Strength .....	20
Table 3-2: Hole Cleaning Procedure for All Materials.....	24
Table 3-3: Cure Times For Material 1B, Material 2, and Material 7.....	26
Table 4-1. Adhesive Layer Element Sizes.....	48
Table 4-2. Young's Modulus for Adhesive at Various Temperatures.....	54
Table 5-1. Material 1B Results .....	61
Table 5-2. Material 7 Results.....	62
Table 5-3. Material 2 Results.....	63
Table 5-4. Summary of Finite Element Results.....	79
Table 5-5. Summary of Finite Element (Larger Hole) Results.....	107

## LIST OF FIGURES

<b>Figure</b>	<b>Page</b>
Figure 1-1. Types of anchorage systems. (Cook. & Burtz., 2003) .....	1
Figure 1-2. Adhesive anchor failure in I-90 tunnel ceiling collapse. (NSTB, 2007, p.1) .....	3
Figure 2-1. Bonded anchor failure modes (Cook et al., 1998). ....	5
Figure 2-2. Hyperbolic tangent stress distribution (left); load transfer behavior of a bonded anchor (right) (Cook et al., 2013). Authorized reprint from the Transportation Research Board. ....	6
Figure 2-3. Stress distribution along length of adhesive anchor for $hef/d = 5.33$ .....	7
Figure 2-4. Dynamic mechanical properties of epoxy resin undergoing cure at 25°C (May, 1987).....	11
Figure 2-5. The effect of elevated temperatures on bond strength for three hypothetical adhesive products (Cook et al., 1998).....	12
Figure 2-6. Stress-strain curve of amorphous neat epoxy resin (Fielder et al., 2005). .....	13
Figure 2-7. Stress-strain relationship of concrete at ambient and elevated temperatures. (Ma et al., 2015) Authorized reprint from Construction and Building Materials Volume 93. ....	14
Figure 2-8. Modulus of Elasticity vs. Temperature at different concrete cure times (Shoukry et al., 2009). Authorized reprint from Construction and Building Materials Volume 25. ....	15
Figure 2-9. Stress-strain curve of ASTM A514 high strength steel at ambient and elevated temperatures (Chen et al., 2006).....	17
Figure 2-10. Stress-strain curves of ASTM A709 Grade 100 steel at ambient and elevated temperatures (Neuenschwander et al., 2017). Authorized reprint from Materials & Design Volume 136.....	17
Figure 2-11. Stress-strain curve for steel reinforcement under ambient and reduced temperatures (Yan and Xie, 2017). Authorized reprint from Construction and Building Materials Volume 141. ....	18

Figure 3-1. Concrete specimens with the center marked.....	21
Figure 3-2. Concrete specimens with drilled anchor holes and thermistor holes.....	24
Figure 3-3. Threaded rod anchor. ....	26
Figure 3-4. Cold chest freezer with one specimen inside. ....	27
Figure 3-5. Short-term test setup. ....	29
Figure 3-6. Short-Term Test Apparatus Section A-A. (Droesch, 2015).....	30
Figure 3-7. Short-Term Test Apparatus Section B-B. (Droesch, 2015) .....	31
Figure 3-8. Coupler details. (Droesch, 2015) .....	32
Figure 3-9. Displacement reading apparatus with two sensors attached to a steel flat bar, slipped through the non-rigid coupler atop the steel confining plate and polytetrafluoroethylene sheet. ....	35
Figure 4-1. Full geometry with reinforcing bar anchor (RB). ....	39
Figure 4-2. Section cut of the full geometry (RB-NB). ....	40
Figure 4-3. Concrete geometry. ....	41
Figure 4-4. Model of #4 threaded rod anchor. ....	42
Figure 4-5. Model of #4 rebar anchor.....	43
Figure 4-6. Geometry of the threaded rod adhesive layer (left). Section cut (right). ....	44
Figure 4-7. Geometry of the rebar adhesive layer (left). Section cut (right). ....	45
Figure 4-8. Concrete mesh.....	46
Figure 4-9. Rebar mesh (left) and threaded rod mesh (right). ....	47
Figure 4-10. Section cut of mesh of the adhesive layer of the rebar anchor.....	48
Figure 4-11. Mesh of the adhesive layer of the threaded rod. ....	49

Figure 4-12. Engineering stress vs. engineering strain plot for ASTM A354 BD steel (Ocel & Provines, 2015). Authorized reprint by the Federal Highway Administration.....	51
Figure 4-13. Engineering stress vs. engineering strain plot for A1035 Grade 120 steel (Rautenberg et al., 2012). Authorized reprint from Engineering Structures Volume 37.....	51
Figure 4-14. Engineering stress vs. engineering strain plot for A36 carbon steel. (Brockenbrough, 2006).....	52
Figure 4-15. Plastic Strain vs. True Stress of the adhesive at 104°F (40°C). .....	53
Figure 4-16. Plastic Strain vs. True Stress of the adhesive at 77°F (25°C). .....	53
Figure 4-17. Plastic Strain vs. True Stress of the adhesive at -40°F (-40°C).....	54
Figure 4-18. Section cut showing fixed support underneath the confining plate.....	55
Figure 4-19. Force applied to the top surface of the anchor rod.....	56
Figure 5-1. Adhesive failure in the anchor. ....	59
Figure 5-2. Summary of Extreme Testing Results.....	60
Figure 5-3. Material 1B Tested at 0°F (-18°C): Load vs. Displacement. ....	65
Figure 5-4. Material 1B Tested at 110°F to 120°F (43°C to 49°C): Load vs. Displacement.....	66
Figure 5-5. Material 1B Tested at Ambient: Load vs. Displacement. ....	66
Figure 5-6. Material 1B Cured at Ambient and Tested at 0°F (-18°C): Load vs. Displacement.....	67
Figure 5-7. Material 1B Stiffness Tested Under Different Temperatures. ....	67
Figure 5-8. Material 7 Tested at 0°F (-18°C): Load vs. Displacement .....	68
Figure 5-9. Material 7 Tested at 30°F (-1°C): Load vs. Displacement.....	69
Figure 5-10. Material 7 Tested at 20°F (-7°C): Load vs. Displacement.....	69
Figure 5-11. Material 7 Tested at Ambient: Load vs. Displacement.....	71

Figure 5-12. Material 7 Cured at 20°F (-7°C) and 30°F (-1°C) and Tested at Ambient: Load vs. Displacement.....	71
Figure 5-13. Material 7 Tested at 110°F to 120°F (43°C to 49°C): Load vs. Displacement.....	72
Figure 5-14. Material 2 Tested at 0°F (-18°C): Load vs. Displacement.....	73
Figure 5-15. Material 2 Tested at 110°F to 120°F (43°C to 49°C): Load vs. Displacement.....	74
Figure 5-16. Material 2 Reinforcing Bar and Threaded Rod Results: Load vs. Displacement.....	75
Figure 5-17. Material 1B Insufficiently Cured and Tested at 0°F (-18°C): Load vs. Displacement.....	77
Figure 5-18. Material 2 Cured Outside Manufacturer Specifications and Tested at 0°F (-18°C): Load vs. Displacement.....	78
Figure 5-19. Material 7 Cured Outside Manufacturer Specifications and Tested at 110°F to 120°F (43°C to 49°C): Load vs. Displacement.....	78
Figure 5-20. Shear stress contour plot of the adhesive layer at time 12 kips (53 kN) (a), 14 kips (62 kN) (b), and 18 kips (80 kN) (c). .....	81
Figure 5-21. Shear stress contour plot of the adhesive layer of the TR-NB model at 104°F (40°C) before failure (a), at failure (b), and after failure (c) as load increases.....	84
Figure 5-22. Section cut of the adhesive layer of the TR-NB model at 104°F (40°C).....	84
Figure 5-23. Contour plot of the equivalent stress in the adhesive layer at 104°F (40°C) at failure.....	85
Figure 5-24. Contour plot of the normal vertical-direction stress in the adhesive layer at 104°F (40°C) at failure.....	86
Figure 5-25. Material 2 Threaded Rod Results and the TR-NB Model Results with assumed adhesive material properties at 104°F (40°C): Load vs. Displacement.....	87
Figure 5-26. Shear Stress Distribution at the hole diameter for TR-NB at 104°F (40°C).....	87

Figure 5-27. Shear stress contour plot of the adhesive layer of the TR-NB model at 77°F (25°C) at failure.....	88
Figure 5-28. Shear stress contour plot of the adhesive layer of the TR-CB model at 104°F (40°C) at failure.....	90
Figure 5-29. Shear Stress Distribution at the hole diameter for TR-CB at 104°F (40°C) .....	91
Figure 5-30. Shear stress contour plot of the adhesive layer of the TR-CB model at 77°F (25°C) at failure.....	92
Figure 5-31. Shear stress pattern, which follows the shape of the reinforcing bar lugs (left), and the pockets of high stress at the lugs and low stress between the lugs.....	94
Figure 5-32. Evenly distributed shear stress on the outside face of the adhesive (left) and consistently distributed shear stress on the inside of the adhesive (right).....	95
Figure 5-33. Shear Stress Distribution at the steel/adhesive interface for RB-NB at 104°F (40°C).....	96
Figure 5-34. Shear stress contour plot of the adhesive layer of the RB-NB model at 104°F (40°C) before failure (a), at failure (b), and after failure (c) as load increases.....	99
Figure 5-35. Material 2 Reinforcing Bar Test Results and RB-NB Model Results with assumed adhesive material properties at 104°F (40°C).....	100
Figure 5-36. Shear Stress Distribution at the hole diameter for RB-NB at 104°F (40°C). ....	100
Figure 5-37. Shear stress contour plot of the outer face (left) and inner face (right) of the adhesive layer of the RB-NB model at 77°F (25°C)) at failure. ....	101
Figure 5-38. Shear stress contour plot of the outer face (left) and inner face (right) of the adhesive layer of the RB-CB model at 104°F (40°C) at failure. ....	103
Figure 5-39. Shear Stress Distribution at the hole diameter for RB-CB at 104°F (40°C). ....	104

Figure 5-40. Material 2 Reinforcing Bar Test and FEM Results: Load vs. Displacement.....	104
Figure 5-41. Material 2 Threaded Rod Results Compared With the TR-NB and TR-CB FEM Results: Load vs. Displacement.....	106
Figure 5-42. Material 2 Reinforcing Bar Results Compared With the RB-NB and RB-CB FEM Results: Load vs. Displacement.....	106
Figure 5-43. Shear stress contour plot of the adhesive layer of the TR-NB- BD model at 104°F (40°C) before failure (a), at failure (b), and after failure (c) as load increases. ....	110
Figure 5-44. Material 2 Threaded Rod Test Results and TR-NB-BD Result: Load vs. Displacement.....	111
Figure 5-45. Shear stress contour plot of the adhesive layer of the RB-NB- BD model at 104°F (40°C) before failure (a), at failure (b), and after failure (c) as load increases. ....	114
Figure 5-46. Material 2 Reinforcing Bar Test Results and RB-NB-BD Result: Load vs. Displacement. ....	115

# CHAPTER 1

## INTRODUCTION

### 1.1. Overview

Adhesive anchorage systems have found widespread use in structural applications over the years. An anchorage system is normally characterized by the embedment of a steel anchor or reinforcing bar into hardened concrete, which can then be used to connect further members. They are typically used for bridge widening, concrete repair and rehabilitation, barrier retrofitting, and mounting of structural or architectural features to concrete.

Two variations of anchorage systems exist: cast-in place anchors and post-installed anchors, as defined in Figure 1-1. Post-installed anchors can be further subcategorized into bonded and mechanical anchors, of which bonded anchors will be the primary focus of this thesis.

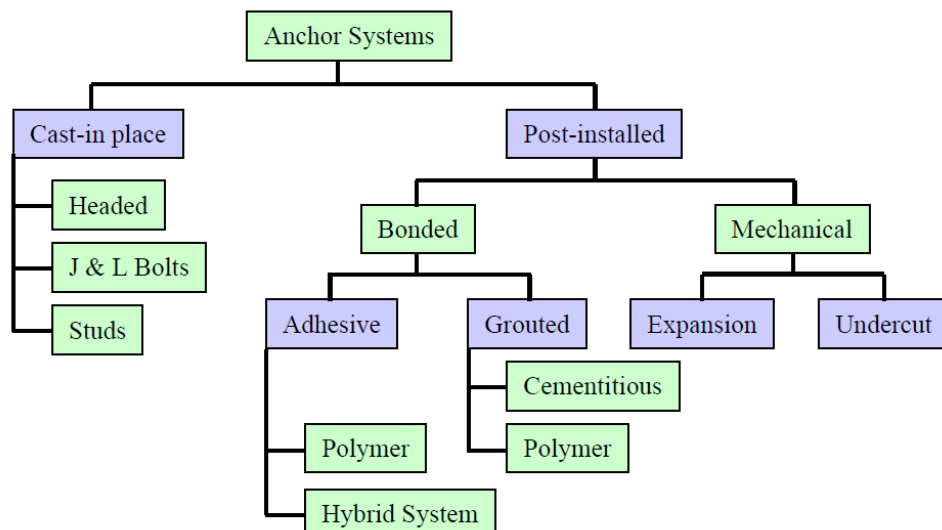


**Figure 1-1.** Types of anchorage systems. (Cook. & Burtz., 2003)

A cast-in-place anchor is installed in wet concrete before the concrete sets, while a post-installed anchor is installed after the concrete has hardened. Cast-in-place anchors are advantageous in that they exhibit predictable and reliable behavior; however, they are difficult to install with precision and cannot be moved once the concrete hardens. Meanwhile, post-installed anchors allow easier and more accurate alignment during the embedment process but may exhibit more variability in performance in addition to requiring proprietary methods of installation based on the anchor system. Further information on types of anchorage systems was presented by Drolesch (2015).

Because bridge applications require adhesive anchorage systems to be installed outdoors, climate conditions and varying temperatures on a day-to-day basis should be considered when analyzing the strength and behavior of these systems. While adhesives with differing mechanical properties have been manufactured to account for various uses and conditions, the environment in which they are installed cannot always be controlled. Temperature is unpredictable and may rise or drop overnight, which affects the adhesive curing process and resulting bond strength. Generally, as temperatures increase, curing times for epoxy adhesives decrease; when temperatures decrease, curing times increase. Abrupt drops in temperature that are not accounted for may result in incomplete curing and weaken the adhesive, which will be explored in this report through experimental work and finite element analysis.

## **1.2. Motivation for Study**

The Massachusetts Department of Transportation (MassDOT) frequently uses post-installed anchors to add attachments to existing structures. However, recommendations on materials used in long-term situations is lacking. One incident of

post-installed anchor failure occurred in 2006, during which precast ceiling tiles collapsed in the I-90 connector tunnel in Boston, Massachusetts, causing one fatality and one injury as well as financial damages. The collapse of the precast ceiling was determined to be the result of long-term tension failure, or creep, of epoxy anchors. Upon further inspection it was discovered that remaining anchors along the tunnels had significantly displaced, in a range from less than 0.10 in (0.25 cm) to more than 1.00 in (2.54 cm). The tunnel was closed while inspections and corrective actions occurred (NTSB, 2007).



**Figure 1-2.** Adhesive anchor failure in I-90 tunnel ceiling collapse. (NSTB, 2007, p.1)

As a result of this incident, the National Transportation Safety Board (NTSB) recommended the Federal Highway Administration (FHWA) prohibit the use of adhesive anchors under long-term tension conditions until tests could be conducted and a recommendation could be adopted. Studies performed by Cook et al. (2009, 2013) and Davis (2012) proposed new standard test methods built upon existing methods from AASHTO, ASTM, and state departments of transportation to determine the ability of adhesive anchors to resist sustained tensile load. Further tests on various anchor materials

to assess the test methods prepared by Cook et al. (2009, 2013) and Davis (2012) was performed by Droesch (2015) and Mendoza (2017). This thesis will expand on the experimental work performed by Droesch (2015) and Mendoza (2017) with the addition of fluctuating temperatures during static testing and finite element modeling.

### **1.3. Research Objectives**

The addition of temperature variation may add further uncertainty to the behavior of adhesive anchors. The purpose of this thesis is to simulate pullout tests of the adhesive anchorage system for threaded rod and reinforcing bars and emulate effects under various temperature conditions through the use of the finite element analysis tool ANSYS 18.2. Results from the simulation were to be compared to the physical tests conducted at UMass Amherst to determine both the validity of the finite element model as well as to evaluate any notable differences in adhesive anchor performance in cold, hot, and ambient temperatures and determine differences in adhesive stresses when anchoring threaded rod versus reinforcing steel.

## CHAPTER 2

### LITERATURE REVIEW

This chapter presents an overview of the existing behavior models of bonded anchors as well an overview of epoxy failure and the material properties of concrete, steel and epoxy resin under various temperatures. A comprehensive literature review addressing post-installed bonded anchoring systems was presented by Drolesch (2015).

#### 2.1. Behavior Models and Failure Modes of Bonded Anchors

Bonded anchorage systems can fail in any of the three components: the base concrete, the steel anchor, or the adhesive bonding material. Five primary failure modes have been defined by the research of Cook and Burtz (2003), shown in Figure 2-1. The five failure modes include: concrete breakout failure; adhesive/concrete interface failure; steel/adhesive interface failure; both adhesive/concrete and steel/adhesive interface failure; and steel failure. Steel failure can be defined as failure of the anchor rod itself, and is typically the design failure mode for bonded anchors in an anchor system in which the bond stress capacity develops to the full capacity of the anchor.

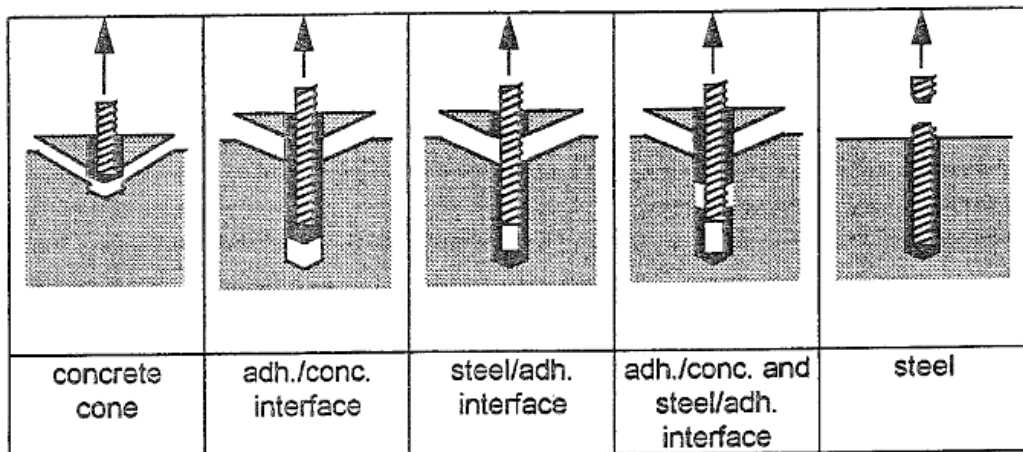


**Figure 2-1.** Bonded anchor failure modes (Cook et al., 1998).

Concrete breakout failure is predicted using the Concrete Capacity Design (CCD) Model and is addressed in ACI 318-14 Chapter 17 (2014). Though the CCD model was originally developed for cast-in-place and mechanical anchors, it is also applicable to grouted anchors that fail with a full concrete breakout cone (Fuchs, Eligenhause, & Breen, 1995). The adhesive/concrete interface, steel/adhesive interface, and adhesive/concrete + steel/adhesive interface bond failure modes are predicted using a uniform bond stress model and are exclusive to adhesive bonded anchors. In the elastic range, adhesive anchors exhibit a hyperbolic tangent stress distribution along the anchor, as shown in Figure 2-2, in which  $h_{ef}$  is the effective depth of the anchor and  $d$  is the anchor diameter. In addition, Figure 2-2 exhibits the assumed load transfer behavior of the adhesive bonded anchor, specifically for threaded rod.

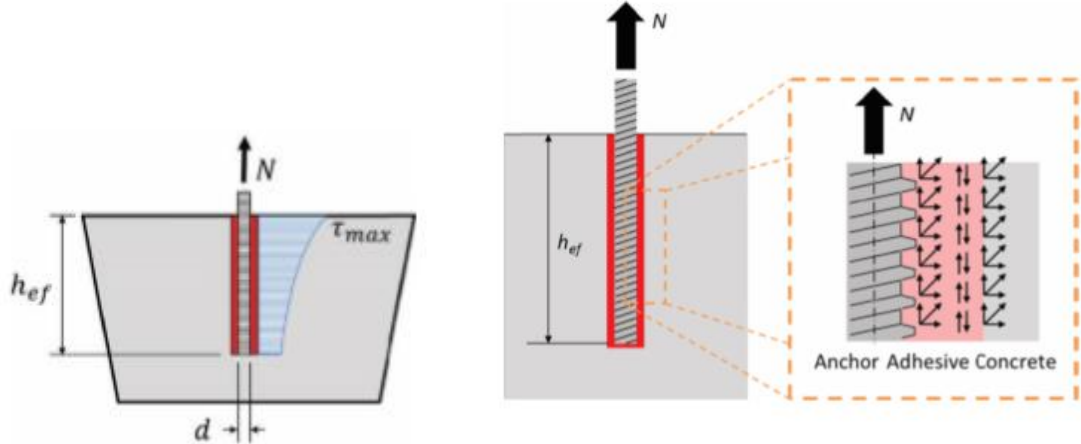


**Figure 2-2.** Hyperbolic tangent stress distribution (left); load transfer behavior of a bonded anchor (right) (Cook et al., 2013). Authorized reprint from the Transportation Research Board.

An elasto-plastic Sandler-DiMaggio constitutive model was used by McVay et al. (1996) to evaluate how bond stress is distributed along the length of the anchor under

various levels of stress. At low load levels, the adhesive closer to the surface is higher stressed than the adhesive deeper in the hole. As load increases, the adhesive closer to the surface becomes plastic, which redistributes the load further in the hole. As the load continues to increase, deeper portions of the adhesive become plastic. The stress distribution eventually becomes relatively uniform at approximately 70% of the peak stress level, seen in Figure 2-3; any further increase in load causes the adhesive to dilate, which provides increased capacity until failure (Cook et al., 2013).

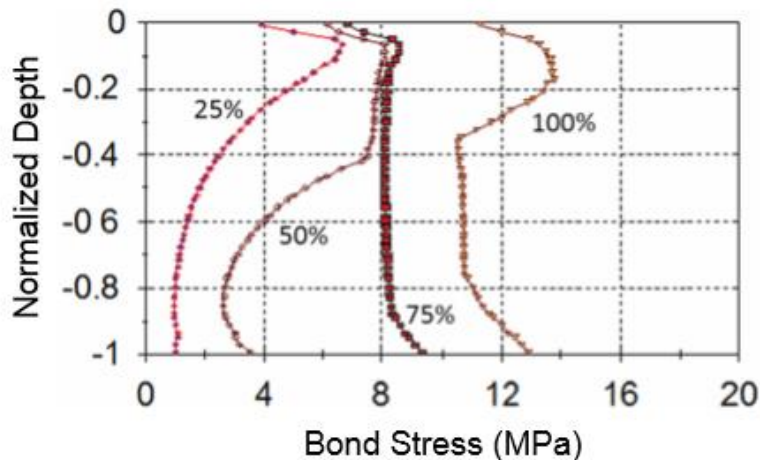


**Figure 2-3.** Stress distribution along length of adhesive anchor for  $h_{ef}/d = 5.33$  (Cook et al., 2013). Authorized reprint from the American Society of Civil Engineers (ASCE).

## 2.2. Current Test Standards For Bonded Anchors

This section discusses the current test standards and methods for bonded anchors. Test standards for bonded anchors are published by multiple agencies, including the American Society of Testing Materials (ASTM), American Concrete Institute (ACI), International Code Council-Evaluation Services (ICC-ES), and the American Association of State Highway Transportation Offices (AASHTO).

### **2.2.1. ASTM E488 (2010): Standard Test Methods for Strength of Anchors in Concrete and Masonry Elements**

ASTM E488 is a widely accepted test method that provides the procedures for determining the short-term capacity of anchors for all types of concrete anchor systems: cast-in-place, mechanical post-installed, and bonded post-installed. In addition, it covers “the fundamental test procedures to determine the static, seismic, fatigue and shock, tensile, and shear strengths of concrete and masonry anchors” (Cook et al., 2013), as well as the test procedures for environmental exposures such as freezing and thawing, moisture, decreased and elevated temperatures, and corrosion.

The test method subjects an anchor to an initial load of 5% of the estimated maximum load capacity before applying a continuous tensile load rate such that the peak load occurs  $2 \pm 1$  minutes after the start of the test. Load and displacement must be monitored and recorded throughout the test at a minimum sampling rate of once per second. ASTM E488 (2010) requires a minimum of five anchors to be tested to determine the Mean Static Load (MSL) at standard temperature, 73°F (23°C)  $\pm 8^{\circ}\text{F}$  (6°C).

### **2.2.2. ICC-ES AC308 (2013) Acceptance Criteria for Post-Installed Adhesive Anchors in Concrete Elements**

ICC-ES AC308 (2013) establishes requirements for adhesive anchors, torque-controlled adhesive anchors, and post-installed reinforcing bar systems in concrete elements to create connections between structural concrete and attachments. ICC-ES AC308 also includes assessments of adhesive anchors for bond strength, reliability, service conditions and quality control. The standard directly references ACI 355.4 (2011).

### **2.2.3. ACI 355.4 (2011): Qualification of Post-Installed Anchors in Concrete**

ACI 355.4 (2011) prescribes testing programs and evaluation requirements for the usage of post-installed adhesive anchors in concrete under the provisions of ACI 318 (2014). Provided in the standard are assessment criteria of the adhesive system for bond strength, reliability, service conditions, and quality control under various conditions, including seismic loading, sustained loading, reduced and elevated temperatures, and determination if anchors are acceptable for use in cracked and uncracked concrete.

### **2.2.4. AASHTO TP-84 (2013): Evaluation of Adhesive Anchors in Concrete Under Sustained Loading**

The AASHTO TP-84 provisional standard defines a specific test to evaluate anchors under sustained load and was intended to provide a better understanding of long term creep capacity of anchors beyond current provisions. AASHTO TP-84 directly references short-term testing procedures from ASTM E488 and ICC-ES AC308 to calculate the MSL of a test series at 110°F (43°C) to 120°F (48°C), as well as provides recommendations for concrete specimen dimensions, anchor embedment depth, specimen conditioning, and assembly of the test apparatus for static and creep testing at 110°F (43°C) to 120°F (48°C). The method results in a time to failure plot rather than only a pass/fail criterion of other long-term test methods.

## **2.3. Epoxy Behavior and Effect of Temperature**

An epoxy adhesive is a thermoset polymer that forms three-dimensional chemical bonds, or cross-links, with a curing agent and requires heat to cure (Cook et al., 1998). This heat is produced from an exothermic reaction between the epoxy resin and the curing agent (Cook et al., 1998). Epoxy adhesives for high performance anchor systems are

typically manufactured in dual-cartridge injection systems with premeasured portions of resin and hardener that are mixed in a proprietary mixing nozzle when dispensed.

When heat is applied, thermoset polymers usually decompose rather than melt and therefore irreversibly set after curing (Okba et al., 2017), unlike thermoplastic polymers which reversibly soften when heated beyond their glass transition point and harden when cooled (Rawn & Ouellette, 2018). Thermoset polymers form permanent chemical bonds, which eliminates the possibility of softening when additional heat is applied and greatly improves resistance to mechanical deformations. In addition, adhesives with a higher glass transition temperature ( $T_g$ ), or the temperature range at which glass transition occurs, typically have a higher tensile strength. The service temperature for polymers used in elevated temperatures should remain below the  $T_g$  in order to ensure the polymer remains in the high strength vitrified state.

Glass transition is the gradual process in which a polymer goes from a rubbery, viscous state to a rigid, glassy state, known as vitrification; or vice versa, known as gelation (Ellis, 1993). Three main types of curing can be identified: if a polymer is cured above its ultimate  $T_g$ , only gelation will occur, and will vitrify when cooled; if a polymer is cured below its  $T_g$  but above the temperature where gelation and vitrification occur simultaneously ( $_{gel}T_g$ ), the polymer will first gel and then vitrify; and if a polymer is cured below  $_{gel}T_g$ , the polymer will only vitrify (Lange et al., 1999). For construction materials and ambient temperatures, all materials are cured below  $T_g$ . As the polymer cures, its  $T_g$  increases and may surpass the curing temperature (May, 1987). The polymer is fully cured when it attains a critical degree of crosslinking at its optimum cure time, during which its flexural modulus significantly increases and plateaus, as seen in Figure 2-4.

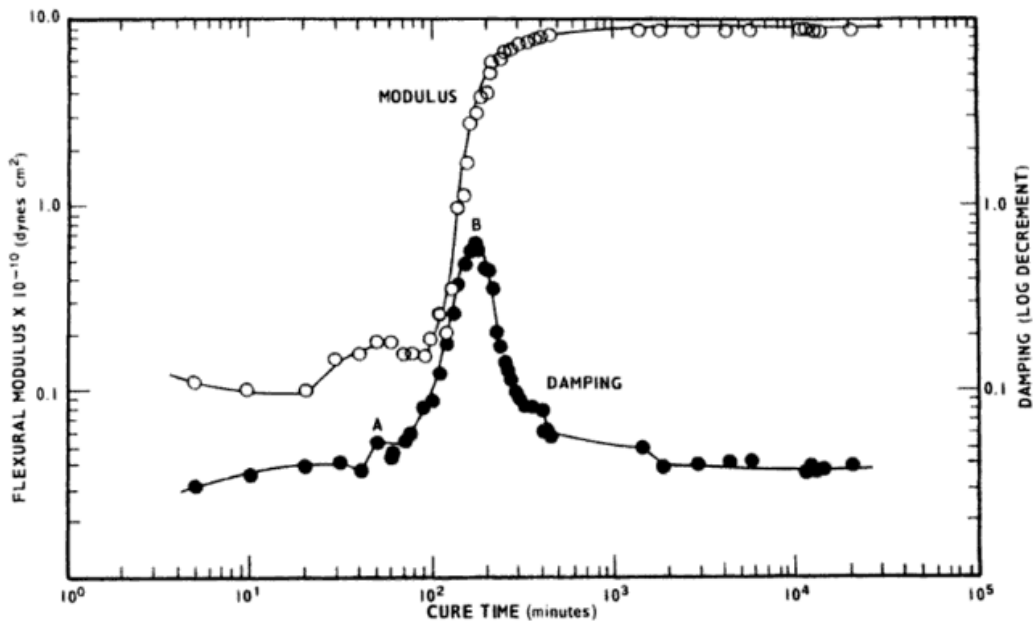


**Figure 2-4.** Dynamic mechanical properties of epoxy resin undergoing cure at 25°C (May, 1987).

Strength is developed in epoxy adhesive as the polymer is cured and is greatly affected by temperature and the rate at which it is loaded (Jordan et al., 2008). Cook et al. (1998) determined that bond strength in an anchorage system can also be affected by a number of other parameters besides the type of adhesive used, such as the cleanliness of the drilled hole, dampness of the hole, embedment depth, anchor diameter, and the duration of adhesive curing. It was observed that reduced temperatures during installation increases viscosity of the adhesive as well as retards its cure time. Under elevated temperatures around 104°F (40°C), the tensile load capacity of epoxy decreases substantially, as seen in Figure 2-5, in which three different hypothetical adhesive products underwent short-term tensile tests. According to Cook et al. (2013) and Dusel and Mir (1991), creep becomes a major concern for adhesives under sustained loading that are exposed to temperatures 18°F (10°C) above either its  $T_g$  or above its heat

distortion temperature, the temperature range at which a polymer begins to soften and deform under load (Gowariker & Viswanathan, 1986).

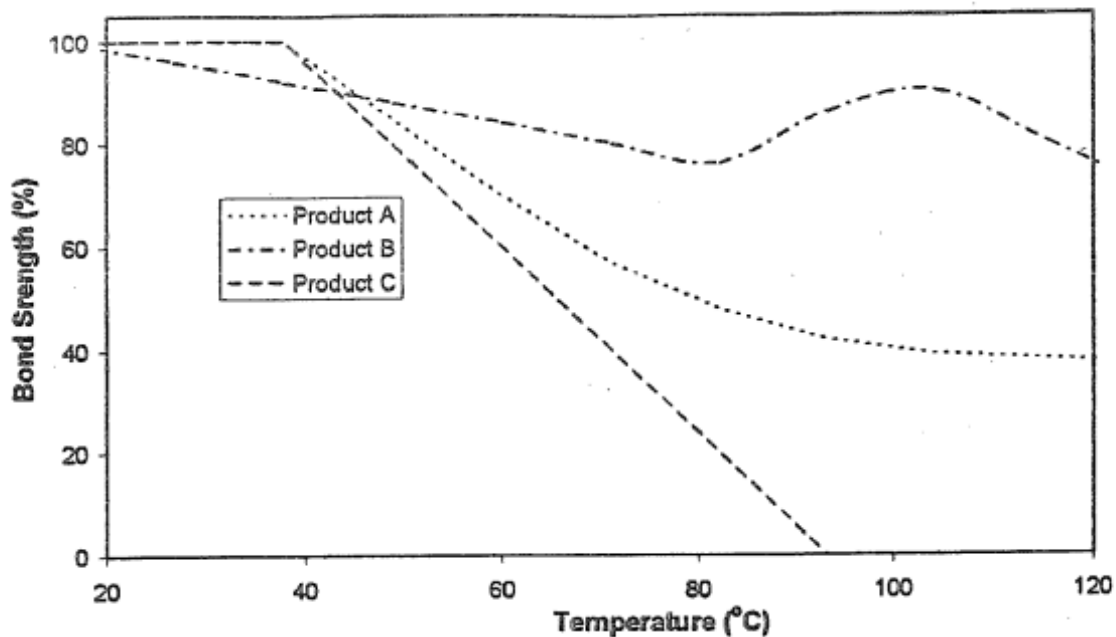


**Figure 2-5.** The effect of elevated temperatures on bond strength for three hypothetical adhesive products (Cook et al., 1998).

At temperatures above the glass transition range, polymers are in a rubbery state. Contrastingly, polymers become rigid and brittle at temperatures below the glass transition range due to restricted molecular movement. Impact resistance decreases, and brittleness becomes the main cause of failure. However, while lower temperatures reduce the ductility of the polymer, ultimate stress increases significantly, as evidenced in a study conducted by Fielder et al. (2005), whose results are shown in Figure 2-6.

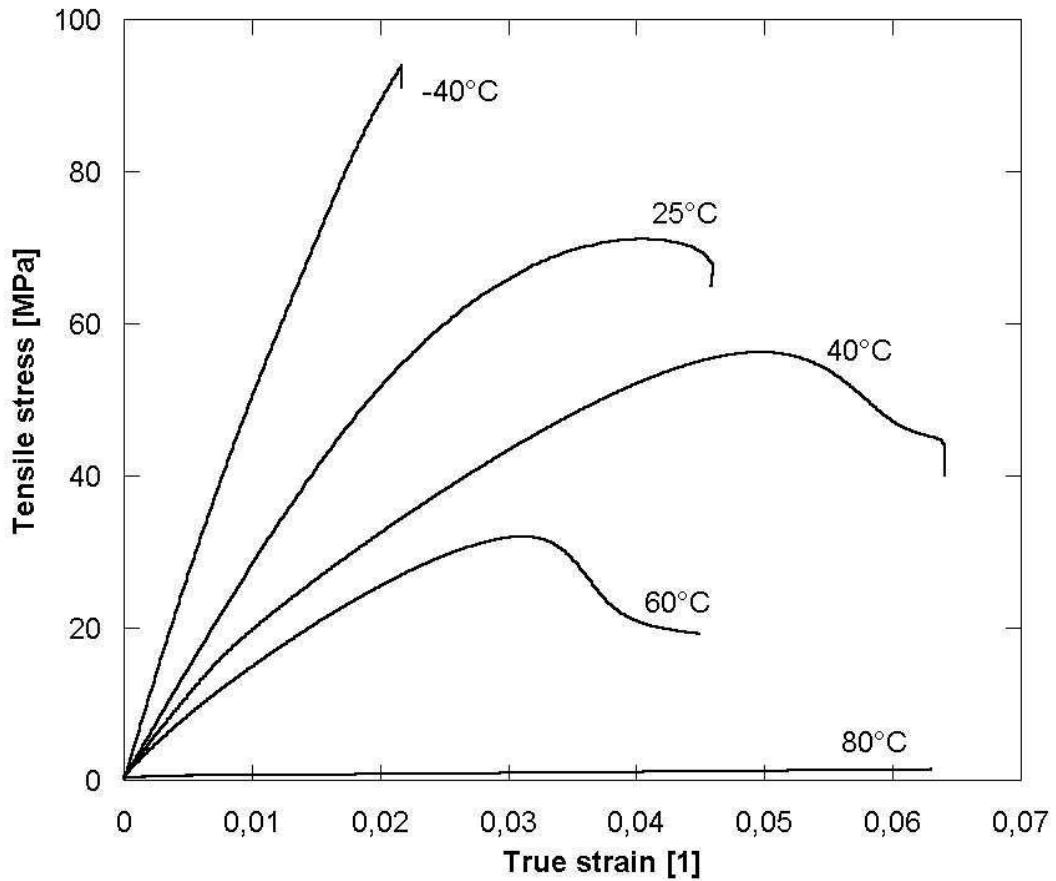


**Figure 2-6.** Stress-strain curve of amorphous neat epoxy resin (Fielder et al., 2005).

In addition, the data provided by Fielder et al. (2005) shows that as temperature increases, the tensile yield stress decreases while the ductility of the polymer increases. Other studies corroborate this finding: Okba et al. (2017) examined epoxy specimens that were cured at ambient temperature for 7 days in 28-day concrete before being subjected to 104°F (40°C), 212°F (100°C), 302°F (150°C), and 392°F (200°C) for up to 6 hours, and found that the mean bond strength, including the tensile bond strength, of the epoxy decreased as the thermal exposure level and exposure time increased in all cases.

For this thesis, Figure 2-6 will be used as a reference to evaluate epoxy resin behavior in ANSYS at different temperatures.

## 2.4. Effect of Temperature on Concrete Behavior

Concrete can be seriously damaged in high temperature conditions, predominantly due to fire. Factors such as specimen size, stressed and unstressed conditions, and hot/residual states all affect its mechanical properties, but only for elevated temperatures past 212°F (100°C) (Ma et al., 2015). In such cases, shown in Figure 2-7, the stress-strain curve of the concrete shows that the peak stress and modulus of elasticity of concrete decreases as temperature increases, while strain increases with temperature. Notably, however, the tests that have been performed utilized temperatures up to 1472°F (800°C). According to Ma et al. (2015), at the range from ambient to 572°F (300°C), the behavior of concrete remains largely unchanged.

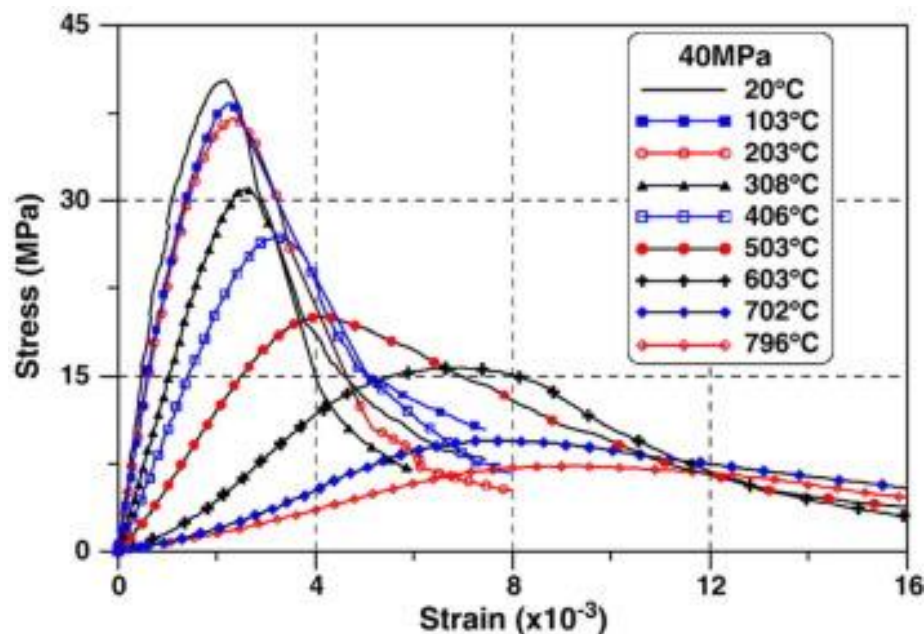


**Figure 2-7.** Stress-strain relationship of concrete at ambient and elevated temperatures. (Ma et al., 2015) Authorized reprint from Construction and Building Materials Volume 93.

Conversely, studies have been performed to determine the mechanical behavior of concrete under reduced temperature conditions. The compressive behavior of the

concrete specimens tested were significantly improved compared to those tested at ambient temperatures (Kim et al., 2017). A study conducted by Shoukry et al. (2009) also supports this result: as temperatures decreased from 122°F (50°C) to -4°F (-20°C), the compressive strength and modulus of elasticity of concrete specimens both increased, as seen in Figure 2-8; a change of approximately 23%.

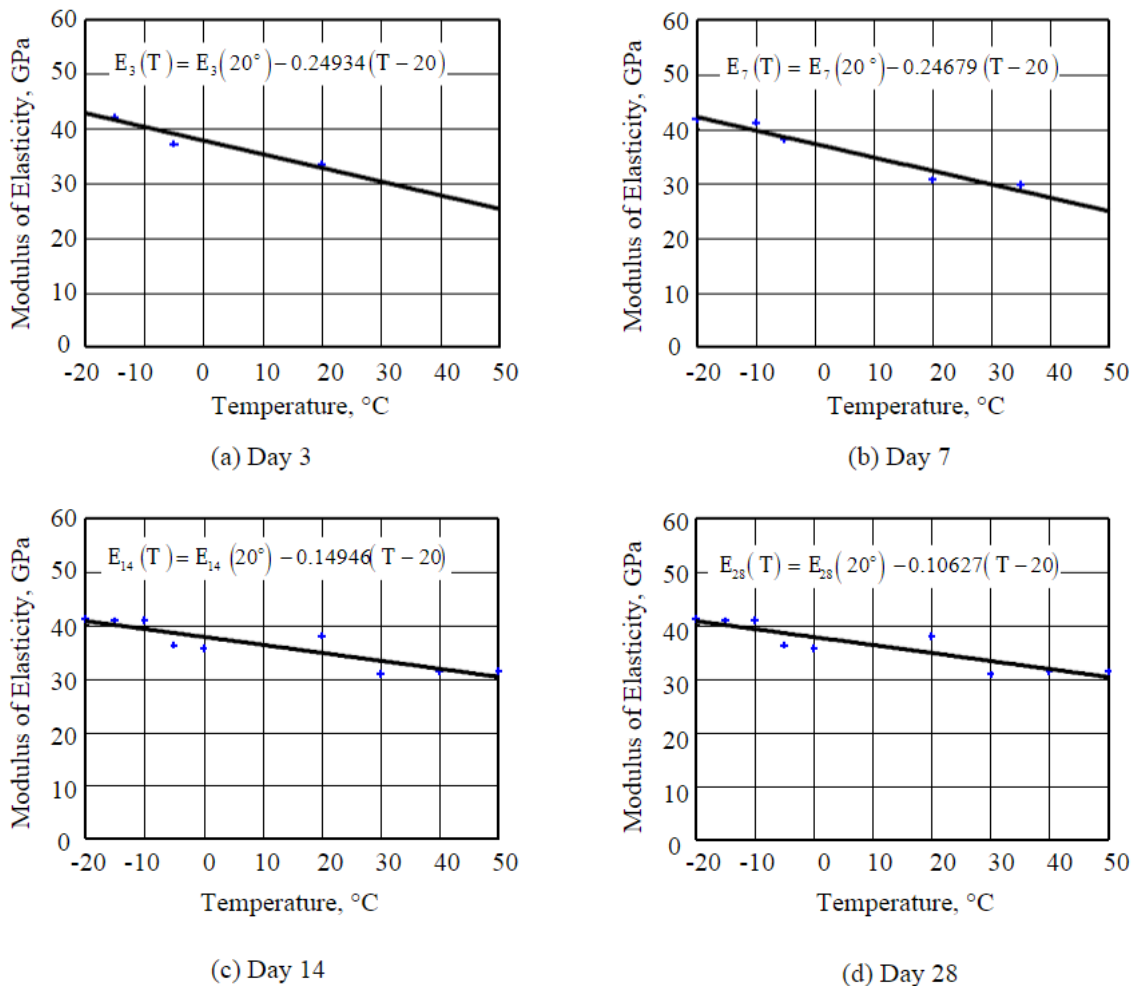


**Figure 2-8.** Modulus of Elasticity vs. Temperature at different concrete cure times (Shoukry et al., 2009). Authorized reprint from Construction and Building Materials Volume 25.

It can be assumed from the data that at 0°F (-18°C), the lowest temperature at which the concrete specimens used for this thesis were conditioned, the modulus of the

modeled concrete block would change approximately 725.19 ksi (5.00 GPa) compared to ambient temperature.

## **2.5. Effect of Temperature on Steel Behavior**

The susceptibility of steel to elevated temperatures has been studied extensively, specifically to address the effects of fire. Chen et al. (2006) performed a transient and steady-state test for an approximate equivalent of ASTM A514 high strength steel and determined that in temperatures ranging from 71.6°F (22°C) to 572°F (300°C), the ultimate strength of the steel specimens stayed largely the same with little variation, and only significantly began to drop around 770°F (410°C) as shown in Figure 2-9. On the other hand, the modulus of elasticity steadily decreased from  $3.03 \times 10^4$  ksi (209.2 GPa) at 71.6°F (22°C) to  $9.62 \times 10^3$  ksi (66.3 GPa) at 1112°F (600°C) (Chen et al., 2006). Similarly, Neuenschwander et al. (2017) found that the yield strength of cold formed ASTM A709 Grade 100 high strength steel initially decreases moderately as temperature increases, but rapidly drops when the temperature reaches 752°F (400°C). Additionally, the modulus of elasticity decreases as temperatures continue to increase, shown in Figure 2-10.

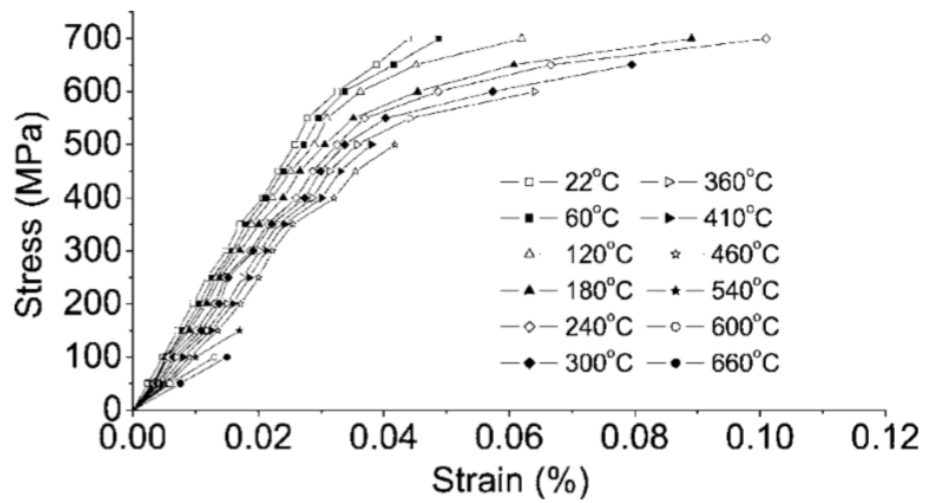


**Figure 2-9.** Stress-strain curve of ASTM A514 high strength steel at ambient and elevated temperatures (Chen et al., 2006).

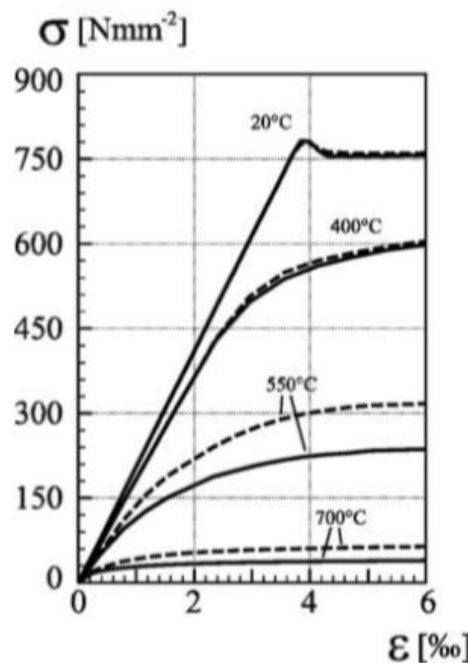


**Figure 2-10.** Stress-strain curves of ASTM A709 Grade 100 steel at ambient and elevated temperatures (Neuenschwander et al., 2017). Authorized reprint from Materials & Design Volume 136.

HRB335 (ASTM A572 Grade 65) high strength steel has also been tested under reduced temperatures ranging from -265°F (-165°C) to 68°F (20°C). A study has shown

that as temperatures decrease to -265°F (-165°C), the yield and ultimate strengths of the tested steel increased, while the ductility was reduced (Yan & Xie, 2017). In addition, the failure of reinforcing steel changes from ductile to brittle at -112°F (-80°C). It can be extrapolated from Figure 2-11 that at approximately -17.8°F (0°C), the lowest temperature tested in this thesis, there is only a slight rise in ultimate strength and negligible change to the elastic modulus; therefore, steel material properties remain unchanged from ambient conditions for the finite element model. Similarly, because specimens used for this thesis were tested only up to 120°F (48.9°C), it has been assumed that elevated temperature effects on the steel are also negligible.

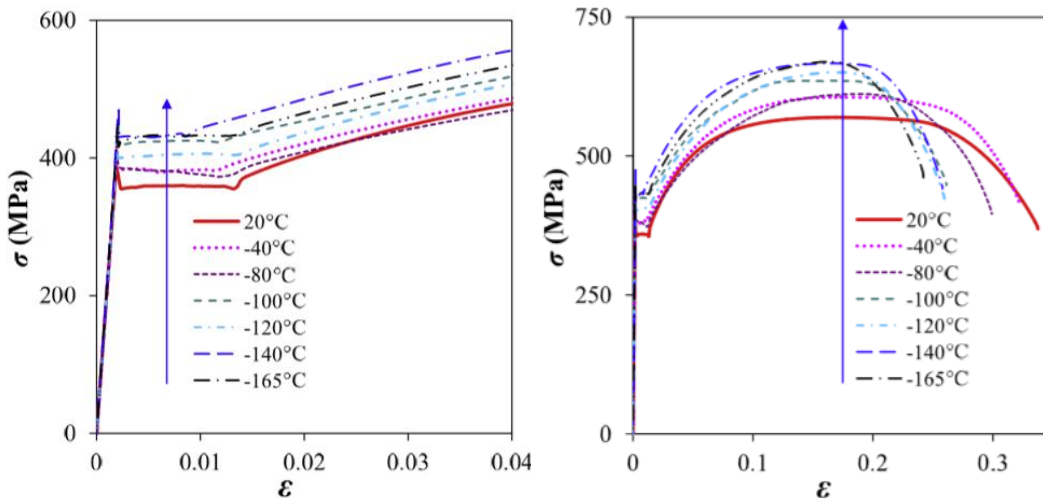


**Figure 2-11.** Stress-strain curve for steel reinforcement under ambient and reduced temperatures (Yan and Xie, 2017). Authorized reprint from Construction and Building Materials Volume 141.

## **CHAPTER 3**

### **PHYSICAL TESTING PREPARATION**

Physical testing of anchor specimens was conducted at the University of Massachusetts, Amherst. Cold chest freezers and a heat chamber were used to simulate different temperature conditions in a range of 20°F (-6.67°C) to 120°F (49°C), under which the specimens were installed, cured, and/or tested. All anchors were installed in accordance to manufacturer specifications and ensuing pullout tests were conducted with slight variations in accordance to ASTM E488.

#### **3.1. Test Specimens**

All test specimens were designed to meet the requirements of AASHTO TP-84. The specimens consisted of three components: the concrete base cylinder, steel anchor rod or steel reinforcement bar, and adhesive material.

##### **3.1.1. Concrete**

The concrete used in this study is standard MassDOT 4000 psi (27.60 MPa) strength concrete provided by a local ready-mix company. In accordance with the provisions set by Section 6 of AASHTO TP-84, which require sufficient dimensions so that the depth of the concrete member is at least 1.5 times the embedment depth of the anchor and the anchor placement is at least 2 times the embedment depth from any edge, specimens were cast in 16.00 inch (406.40 mm) diameter by 8.00 inch (203.20 mm) deep cylindrical sonotube cardboard forms sealed to a 0.5 inch (13 mm) plywood base board. Specimens were covered with wet burlap and plastic sheeting and moist cured for 14 days

before they were removed from the formwork, then left in ambient laboratory conditions for a minimum of 28 days.

In addition to the specimens, test cylinders were cast under the same conditions to be used for compressive strength testing in a Forney FX 500 compression machine in accordance with ASTM C39. Table 3-1 lists the concrete compressive strength of four cylinders from the same mixture at 28 days and at the end of testing.

**Table 3-1. Concrete Compressive Strength**

<b>28 DAYS (psi)</b>	<b>480 DAYS (psi)</b>
4904	5125
4875	5280
4912	5205
4880	5102



**Figure 3-1.** Concrete specimens with the center marked.

### 3.1.2. Anchor

Two types of anchor rods were used: ASTM A354 BD threaded rod and heat-treated Grade 60 reinforcing bar. ASTM 354 BD threaded rod was chosen to minimize the possibility of steel failure and has a nominal yield strength of 130 ksi (896 kPa) and an ultimate strength of 150 ksi (1034 kPa). Grade 60 reinforcing bar was sent to Industrial Steel Treating Co. and heat-treated to reach the same approximate yield strength and ultimate strength as ASTM A354 BD materials in order to similarly minimize steel failure in the anchor.

Each threaded rod anchor was 0.50 inches (12.70 mm) in diameter and cut to 6.00 inch (152.40 mm) lengths. The threaded rod anchors were installed into the concrete at a 2.75 inch (69.90 mm) embedment depth in accordance with the minimum embedment depth provisioned in AASHTO TP-84. This depth was chosen with the intent of ensuring bond failure.

The reinforcing bar anchors were also 0.50 inches (12.70 mm) (#4 bars) in diameter and cut to 9.00 inch (228.60 mm) lengths. One end of the reinforcing bar anchor was tapered and threaded by the supplier prior to heat treatment to enable the anchor rod to be connected to a Lenton Terminator D6 connector also provided by the supplier.

### **3.1.3. Bonding Material**

Three types of bonding material from different manufacturers were used for testing based on the observations made by Mendoza (2017). Both were adhesive materials whose material chemistries as listed in the Manufacturer Safety Data Sheet (MSDS) are briefly described below.

Material 1B : Epoxy resin with amine hardener (adhesive in cartridge format)

Material 2 : Bisphenol epoxy resin with amine hardener (adhesive in cartridge format)

Material 7 : Urethane methacrylate resin with dibenzoylperoxide hardener (adhesive in cartridge format)

### **3.2. Testing Program**

Post-installed adhesive anchors used in transportation structures are exposed to a wide range of temperatures throughout their service life, assumed in this thesis to be from 0°F (-18°C) to 120°F (49°C). As noted in Chapter 2, adhesive behavior is susceptible to variations in temperature, which may affect bond strength. Concrete properties also exhibit change under temperature variation, while steel properties can be assumed constant through this temperature range. In order to investigate such conditions, Material 1B and Material 2 were installed and at a minimum temperature of 23°F (-5°C) and maximum temperature of 105°F (41°C). Testing temperatures were chosen between 0°F

(-18°C) and 120°F (49°C) to represent the extreme in-service temperatures an anchoring system may undergo throughout its service life.

### **3.3. Specimen Preparation**

All test specimens were prepared in accordance with AASHTO TP-84 and their respective manufacturer's recommendations with slight modifications as specified.

#### **3.3.1. Condition Prior to Drilling**

Concrete specimens were stabilized at a temperature between 65°F (18°C) and 85°F (29°C) and 50 ± 10% relative humidity prior to drilling as specified by AASHTO TP-84.

#### **3.3.2. Drilling**

A Hilti TE-72 hammer drill with carbide-tipped hammer drill bits was used to drill anchor holes into the concrete specimens. A 0.56 inch (14.22 mm) diameter hole was drilled for Material 1B and a 0.63 inch (15.89 mm) diameter hole for Material 2 as per the manufacturer recommendations. All specimens were drilled in the downward direction and each specimen was checked for the correct depth and verticality.



**Figure 3-2.** Concrete specimens with drilled anchor holes and thermistor holes.

### **3.3.3. Hole Cleaning**

Anchor holes were cleaned as specified by the manufacturer's instructions before the adhesive material and anchors were installed. For Material 1B and Material 2, compressed air was blown into the hole before a wire brush was used to dislodge additional concrete dust particles. The hole was then blown again. The number of cleaning cycles varied by manufacturer and are specified in Table 3-2.

**Table 3-2: Hole Cleaning Procedure for All Materials**

MATERIAL	HOLE CLEANING PROCEDURE
1B	<ul style="list-style-type: none"><li>• Blow with compressed air (2x)</li><li>• Brush with rounded wire brush (2x)</li><li>• Blow with compressed air (2x)</li></ul>

2	<ul style="list-style-type: none"> <li>• Blow with compressed air (4x)</li> <li>• Brush with rounded wire brush (4x)</li> <li>• Blow with compressed air (4x)</li> </ul>
7	<ul style="list-style-type: none"> <li>• Blow with compressed air (2x)</li> <li>• Brush with rounded wire brush (2x)</li> <li>• Blow with compressed air (2x)</li> </ul>

### **3.3.4. Anchor Installation**

All anchors were installed in accordance to the manufacturer's installation instructions.

Material 1B, Material 2, and Material 7 adhesives are two-part chemical systems packaged in side-by-side cartridges and were installed using the manufacturer's specified installation guns and instructions. Prior to installation, a minimum of three strokes of the adhesive were dispensed through the mixing nozzle until the adhesive became a consistently uniform color.

Anchors were cleaned with a disposable rag prior to being installed to remove any dust and grease that may hinder the bond of the adhesive to the anchor. Duct tape was wrapped around the anchor at a depth of 2.75 inches (69.85 mm) to ensure that only the specified length of the rod would be bonded to the concrete, as seen in Figure 3-3. The cleaned and taped anchors were installed through a plastic support with a nut placed at the correct height in order to ensure both vertical placement and the correct embedment depth during curing.



**Figure 3-3.** Threaded rod anchor.

The adhesive was dispensed into the hole to fill approximately two-thirds of the hole depth and the fastened anchors were immediately inserted. As the anchor was inserted, it was rotated in the clockwise direction to eliminate air gaps and to ensure the threads of the anchor were fully coated with the adhesive. The anchors were left undisturbed for the duration of the adhesive's cure time as listed in the manufacturer's MSDS, or cure time specified for the tests, which varied according to the temperature of the environment, unless otherwise noted in the test results. Manufacturer required cure times for each material can be seen in Table 3-3.

**Table 3-3: Cure Times For Material 1B, Material 2, and Material 7**

MATERIAL	TEMPERATURE (°F)	CURE TIME (hr)
1B	23	168
	32	36
2	50	72
7	14 - 23	7
	32	4

Once curing was completed, any excess hardened adhesive surrounding the anchor above the concrete surface was sawed off and chipped away. This allowed a steel confining plate to bear flat against the concrete surface to be used for testing.

### **3.3. Environmental Conditioning**

#### **3.3.1. Freezers**

A 22 cubic foot moderate cold chest freezer was used to condition and test specimens at low temperatures. The freezer was equipped with a digital temperature controller which enabled the internal temperature of the freezer to be set between -29°F (-34°C) to 50°F (10°C). Preliminary tests using thermistors embedded in a concrete specimen were conducted prior to the testing program to determine the conditioning time required for specimens to reach the desired temperatures; it was determined that for a temperature of 20°F (-7°C) the specimens reached and stabilized at the freezer temperature approximately 21 hours after being placed in the freezer (Mendoza, 2017).



**Figure 3-4.** Cold chest freezer with one specimen inside.

### **3.3.2. Heat Chamber**

A temperature controlled and humidity-monitored chamber was used to condition and test specimens at elevated temperature. As per AASHTO TP-84, specimens were placed in the chamber to reach testing conditions of 110°F (43°C) to 120°F (49°C) and lower than  $50 \pm 10\%$  percent relative humidity. The chamber is powered by commercial heaters controlled by a thermostat which maintained chamber temperature between 110°F (43°C) and 120°F (49°C). Thermistors inserted into holes drilled in the specimens at a depth of 1.40 in (35.56 mm) and covered with rubber stoppers were used to verify specimen temperatures.

### **3.5. Short-Term Test Components**

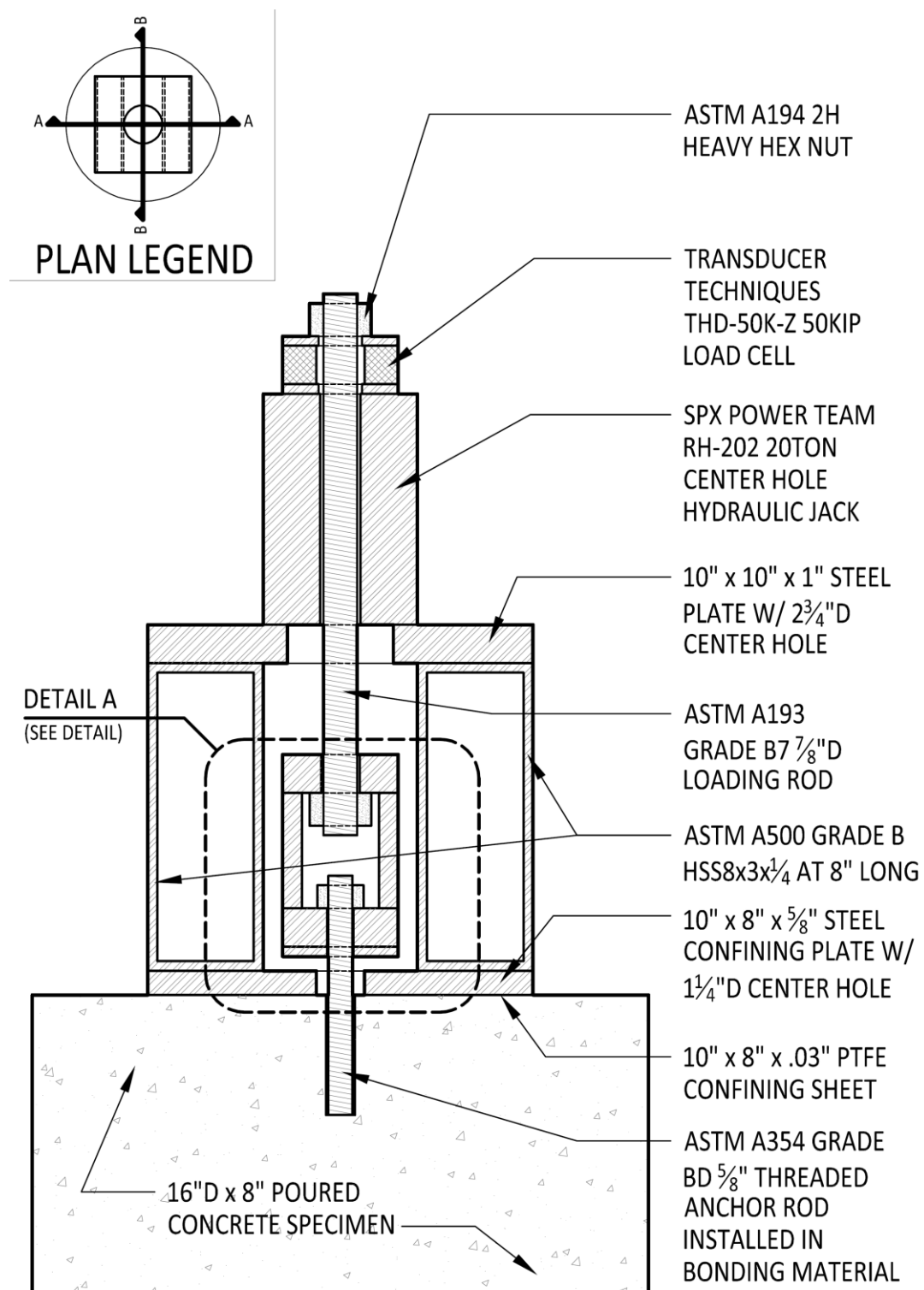
The test apparatus was designed according to the requirements of ASTM E488 and replicated from NCHRP Report 757. The assembled setup can be seen in Figure 3-5; section cuts of the setup during its design process can be seen in Figure 3-6 and Figure 3-7.

Once the anchor rod was installed and cured for the appropriate time and the excess adhesive or grout chipped away, a PTFE (polytetrafluorethylene) confining sheet and a steel confining plate were placed over the concrete. A non-rigid coupler was placed atop the steel confining plate and secured to the anchor using a high strength hex nut. A steel flat bar with aluminum angles, to which BEI 9610 Series Linear Position Sensors were attached, was inserted through the non-rigid coupler and secured to the anchor using an ASTM A194 2H high strength hex nut. Thus, the anchor rod being tested passed through the confining sheet, the confining plate, the non-rigid coupler, and the steel flat bar. An ASTM A500 Grade B HSS 8.00 x 3.00 x 0.25 inch (203.20 x 76.2 x 6.35 mm)

section was then placed on either side of the non-rigid coupler as a spacer in order to support a 10.00 x 10.00 x 1.00 inch (254.00 mm x 254.00 mm x 25.00 mm) steel plate with a 2.75 inch (69.85 mm) diameter hole in the center. An SPX Power Team RH-202 20-ton (178 kN) center hole hydraulic jack was set on top of the steel plate, followed by a Transducer Techniques THD-50K0Z model load cell on top of the hydraulic jack. Finally, a 0.89 inch (22.61 mm) loading rod was passed through the load cell, hydraulic jack, steel plate, and the non-rigid coupler and secured to the coupler with a heavy hex nut and washer on both ends.

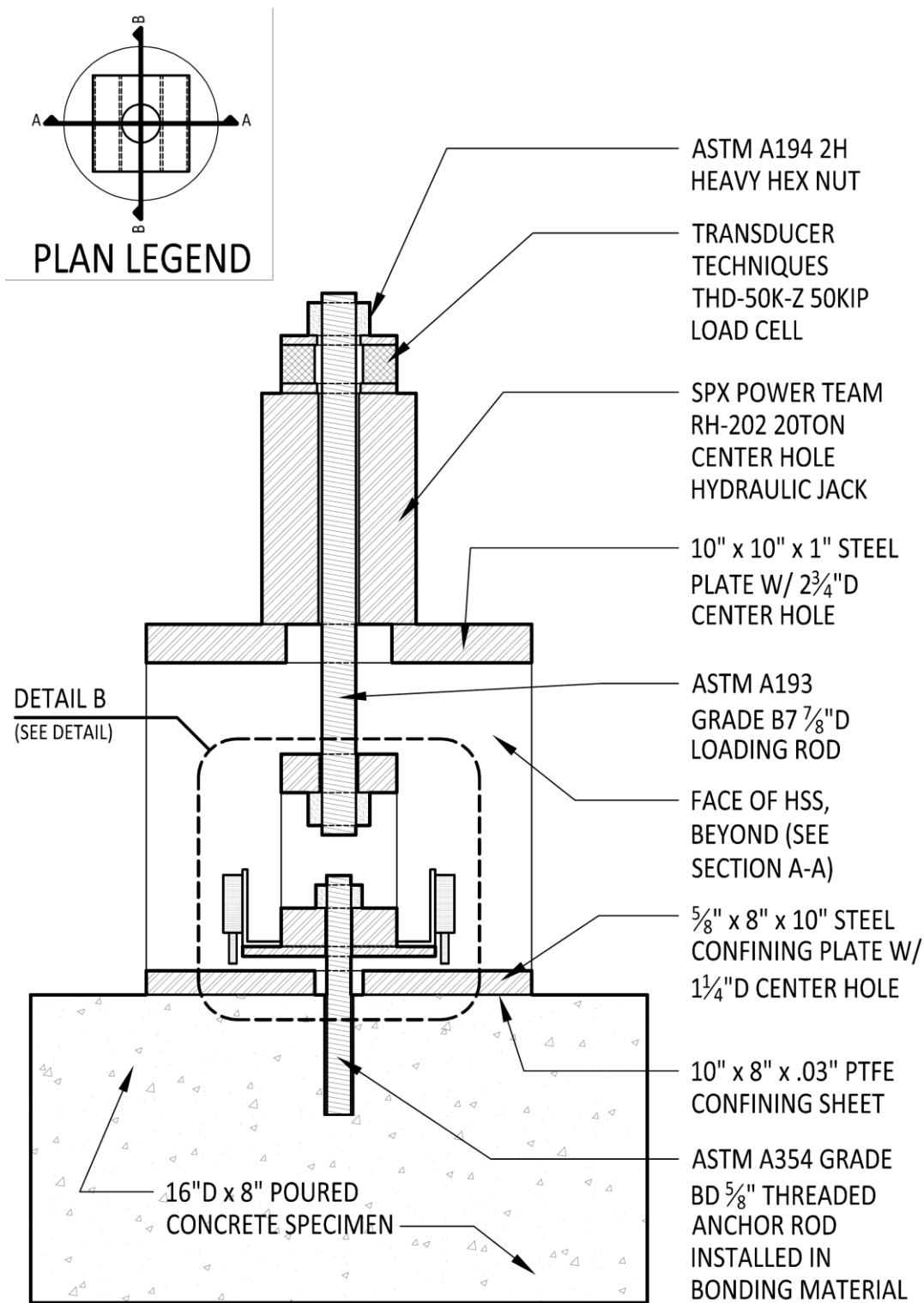


**Figure 3-5.** Short-term test setup.



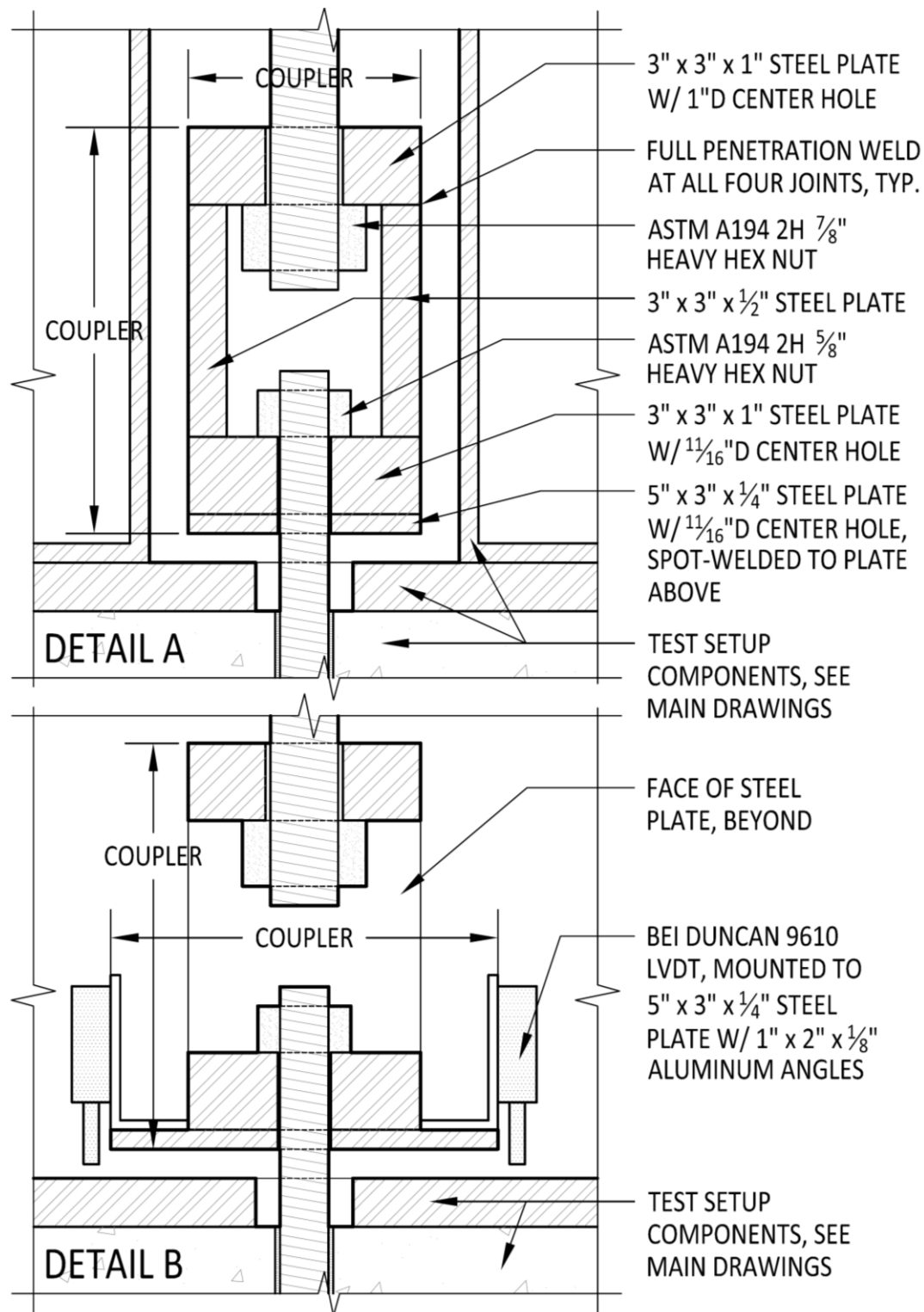
## SHORT-TERM TEST SETUP (SECTION A-A)

**Figure 3-6.** Short-Term Test Apparatus Section A-A. (Droesch, 2015)



## SHORT-TERM TEST SETUP (SECTION B-B)

Figure 3-7. Short-Term Test Apparatus Section B-B. (Droesch, 2015)



## TYPICAL NON-RIGID COUPLER DETAILS

Figure 3-8. Coupler details. (Droesch, 2015)

### **3.5.1. Loading Rod**

The capacity of the loading rod needed to be greater than the capacity of the anchor to ensure that the loading rod would not yield before the anchor. Therefore, a 0.88 inch (22.35 mm) diameter ASTM A193 Grade B7 Threaded Rod with a yield strength of 48.50 kips (215.70 kN) was used for testing.

### **3.5.2. Non-Rigid Coupler**

The steel non-rigid coupler serves to connect the anchor rod to the loading rod and is used to reduce bending moments applied to the anchor by allowing rotation at the connection points. The coupler consists of two 1.00 inch (25.40 mm) thick plates held apart by 0.50 inch (12.70 mm) thick plate sides. Because the full capacity of all the plates is required to carry loads of up to 40.00 kips (177.93 kN), full penetration welds were used to attach the top and bottom plates to the side plates. A 0.69 inch (17.5 mm) diameter hole at the bottom of the coupler allows the anchor rod to pass through and a 1.00 inch (25.40 mm) diameter hole at the top of the coupler allows the loading rod to pass through.

Both the anchor rod and the loading rod are secured with an A194 2H heavy hex nut.

### **3.5.3. Lenton Terminator D6**

To secure the reinforcing bar anchor rods to the non-rigid coupler, Lenton Terminator D6 connectors were used instead of heavy hex nuts. The connectors are cylindrical devices 1.38 inches (35.05 mm) in diameter and 0.56 inches (14.29 mm) thick with a hole in the center that tapers from one flat surface to the other. The hole is threaded to allow the fastening of the matching tapered end of the reinforcing bar.

### **3.5.4. Confining Plate**

A 0.63 inch (16.00 mm) thick 8.00 x 10.00 inch (203.20 mm x 254.00 mm) steel plate with a 1.25 inch (31.75 mm) diameter center hole was used to confine the tests in accordance with AASHTO TP-84, which requires the confining plate to be greater than or equal to the nominal anchor diameter  $\pm$  0.06 inch ( $\pm$  1.52 mm). Confining the tests prevents concrete failure, which allows for a more consistent measurement of bond failure.

### **3.5.5. Confining Sheet**

A confining sheet was placed on top of the concrete specimen underneath the confining plate as required by AASHTO TP-84 to correct surface irregularities. The confining sheet consists of 0.03 inch (0.76 mm) thick polytetrafluoroethylene (PTFE) that is roughly the same dimensions of the confining plate with a 1.25 inch (31.75 mm) diameter center hole.

### **3.5.6. Hydraulic Jack**

Load was applied to the loading rod using an SPX Power Team RH-202 20-ton (178 kN) center hole hydraulic jack. The pressure is applied to the jack with an SPX Power Team P450d hydraulic hand pump.

## **3.6. Instrumentation**

### **3.6.1. Temperature and Relative Humidity**

An Omega HX93B Series Temperature/Relative Humidity Transmitter was used to measure the air temperature and relative humidity when testing took place inside the hot chamber. QTI Sensing Solutions QTSSP Thermistors were used to measure the

internal temperature of each test specimen by inserting the thermistors into a hole located on the concrete surface. The holes were 0.50 inches (12.70 mm) in diameter and 1.40 inches (35.56 mm) deep and were sealed with a rubber stopper in order to more accurately measure the temperature of the concrete. The temperature of each specimen was constantly monitored to ensure compliance with the test method.

### 3.6.2. Displacement

BEI 9610 Series Linear Position Sensors were used to measure anchor displacement. The sensors were attached to aluminum angles secured to a steel flat bar, shown in Figure 3-9. A hole was drilled through the center of the flat bar to enable the anchor rod to pass through. Thin glass slides were placed underneath each transducer prior to testing to provide a smooth surface. Two sensors were used on either side of the steel flat bar and their values averaged to account for non-uniform readings on each side.



**Figure 3-9.** Displacement reading apparatus with two sensors attached to a steel flat bar, slipped through the non-rigid coupler atop the steel confining plate and polytetrafluoroethylene sheet.

### **3.6.3. Load**

Load on the specimen was measured using a Transducer Techniques THD-50K-Z donut 50 kip (222.40 kN) load cell for all tests.

## **3.7. Data Management**

### **3.7.1. Data Acquisition System and Sampling**

A LabVIEW 8.6 program developed by the University of Florida and modified by UMass was used to collect and record all data. Data acquisition was conducted with multiple National Instruments NI 9206 modules connected to a National Instruments NI cDAQ 9188 chassis. Each data sample included a timestamp, chamber temperature and relative humidity, concrete temperature, load, and anchor displacement. Readings were taken every 0.5 seconds for the duration of the test as per the test method.

## **3.8. Test Procedure**

Temperature was controlled for initial concrete temperature, curing temperature, and testing temperature. Specimens installed and cured at cold temperatures between 20°F (-7°C) to 30°F (-1°C) were conditioned in the freezer for 48 hours: 24 hours to reach the freezer temperature and an additional 24 hours to condition at that temperature. Specimens installed and cured at elevated temperatures were placed in the temperature and humidity-controlled heat chamber and allowed to stabilize at 110°F-120°F (43°C-49°C) for 24 hours before testing was initiated. Ambient specimens were stabilized at a temperature between 65°F and 85°F (18°C and 29°C) before drilling.

Once initially conditioned, anchors were installed and given the appropriate amount of time to cure per the manufacturer's instructions. Once cured, the specimen

underwent additional environmental conditioning to the final testing temperature for 48 hours in either the freezer or heat chamber.

For testing, an initial tensile load of 5% of the expected ultimate load capacity of the anchor was applied to bring all members into full bearing. The load was increased at a constant load rate that would cause the anchor to fail within  $2 \pm 1$  minutes. Data which included the load, temperature, and displacement readings was collected at a sampling rate of 0.5 seconds through the failure of the anchor.

A Load vs. Displacement plot was created using the data collected to determine the short-term load capacity of the anchor. The load capacity was defined as the peak of the curve, after which the anchor stiffness appeared to significantly decrease.

## **CHAPTER 4**

### **FINITE ELEMENT MODELING**

#### **4.1. Overview**

A great benefit in using finite element analysis to solve engineering problems is the ability to simulate and approximate solutions of complicated geometries without the necessity of expensive machinery and materials. The behavior of materials under different parameters can be observed and analyzed in a more flexible and convenient environment, including the effect of temperature on adhesive bond strength. However, the approximate nature of finite element modeling necessitates proper verification of results; for this study, verification was performed by comparing the results of the finite model with that from physical testing, as well by comparing the results to known behavior of adhesive anchor failure.

ANSYS 18.2 Workbench and its inbuilt geometry program SpaceClaim 18.2 were used to conduct this study. To compare the results of the finite model with that of the experimental model, parameters of the finite model were defined to resemble the parameters of the physical specimen as closely as possible. Factors such as proprietary properties of the adhesive require some assumptions in the finite element compared to the experimental tests; however, slight differences in material properties should not greatly alter the overall behavior of the specimen. Therefore, results should be comparable.

#### **4.2. Finite Element Model**

##### **4.2.1. Geometry**

The adhesive anchorage system finite element model is a full 3D model constructed in the ANSYS 18.2 inbuilt geometry program, SpaceClaim 18.2. The

geometry consists of four components: the concrete member, the steel threaded rod or reinforcing bar anchor, the adhesive layer, and the steel confining plate. The geometry of the reinforcing bar model is shown in Figure 4-1. A section cut of the same model is shown in Figure 4-2. Both the threaded rod model (TR) and reinforcing bar model (RB) were divided further into two versions: a version with adhesive coating the bottom of the anchor rod (-CB), and a version without (-NB).

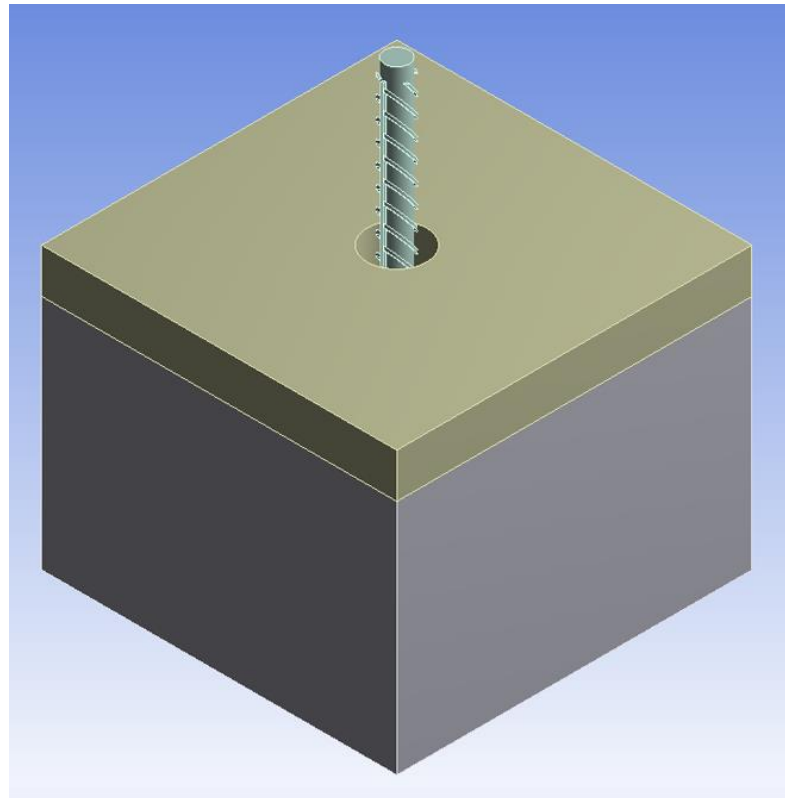


**Figure 4-1.** Full geometry with reinforcing bar anchor (RB).

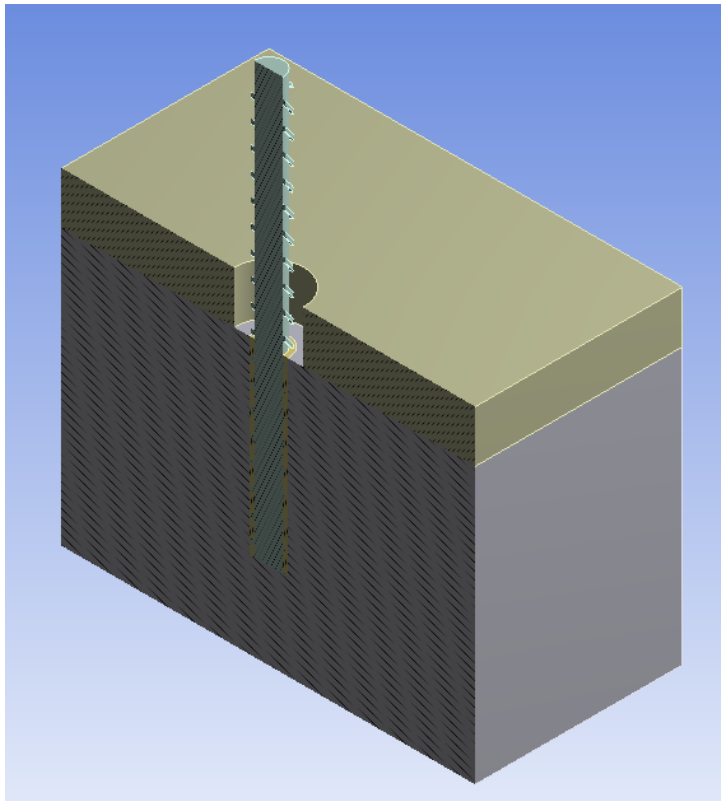


**Figure 4-2.** Section cut of the full geometry (RB-NB).

The geometry of the concrete consists of a 6 in x 6 in x 3 in (15.24 cm x 15.24 cm x 7.62 cm) block, shown in Figure 4-3. AASHTO TP-84, which references ASTM E488, prescribes the depth of the concrete member to be at least 1.5 times the embedment depth of the anchor. However, it was observed in preliminary models that the behavior of the concrete member was found to be negligible upon the application of a confining plate and a tensile force to the anchor. Thus, the depth of the concrete member was shortened in order to reduce the size of the mesh and optimize the runtime of the model. A hole 0.625 inches (1.58 cm) in diameter was cut out of the top face of the block to accommodate the anchor and the adhesive layer that envelops the anchor. The diameter size is in accordance to the adhesive manufacturer requirements of the physical specimen, referred to in Section 3.1. In further tests, a hole 0.875 in (2.22 cm) in diameter was cut out of the top

face of the concrete to assess the effect of a larger hole diameter on the behavior of the adhesive layer.

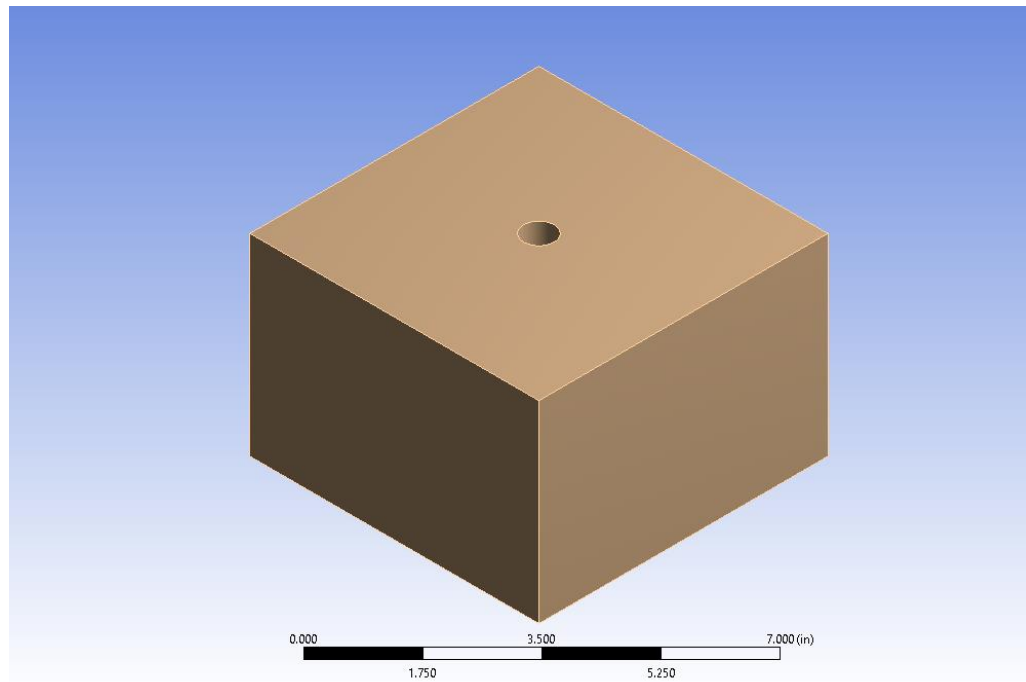


**Figure 4-3.** Concrete geometry.

The geometry of the #4 threaded rod shown in Figure 4-4 is modeled as a smooth cylinder with a diameter of 0.50 in (1.27 cm) and a length of 6 in (15.24 cm). The threaded rod anchor is embedded 2.75 in (6.99 cm) into the concrete block to be comparable to the physical specimen, which complies with the minimum embedment depth specified by AASHTO TP-84. The threads on the threaded rod were not modeled due to their profuse number, which was assumed to provide an equivalent transfer of force throughout the depth of the anchor, enough to emulate a fully bonded surface. Differences in results between fully modeled threaded rod and smooth threaded rod geometries are expected to be negligible.

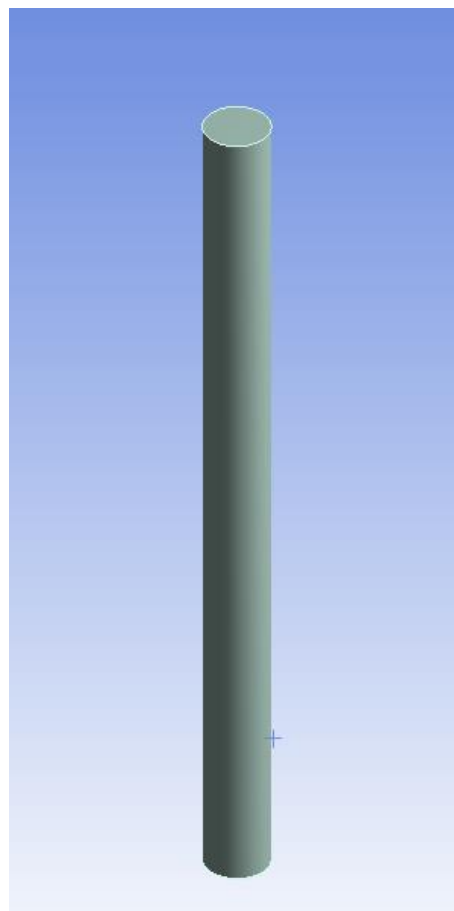


**Figure 4-4.** Model of #4 threaded rod anchor.

The geometry of the reinforcing bar shown in Figure 4-5 consists of a 0.50 in (1.27 cm) diameter rod with 0.125 in x 0.125 in (0.32 cm x 0.32 cm) lugs that spiral at 45 degrees from the x-axis along the surface length of the rod. Two longitudinal ribs extend down the rod from opposite sides. The reinforcing bar was initially modeled as a smooth cylinder before the lugs were added one by one, spaced 0.25 in (0.64 cm) apart. In order to suitably compare the reinforcing bar anchor with the threaded rod anchor, the reinforcing bar anchor is 6 in (15.24 cm) in length and embedded 2.75 in (6.99 cm) into the concrete block in accordance with AASHTO TP-84. The size of the lugs was taken from measuring a length of #4 rebar used for the physical testing.

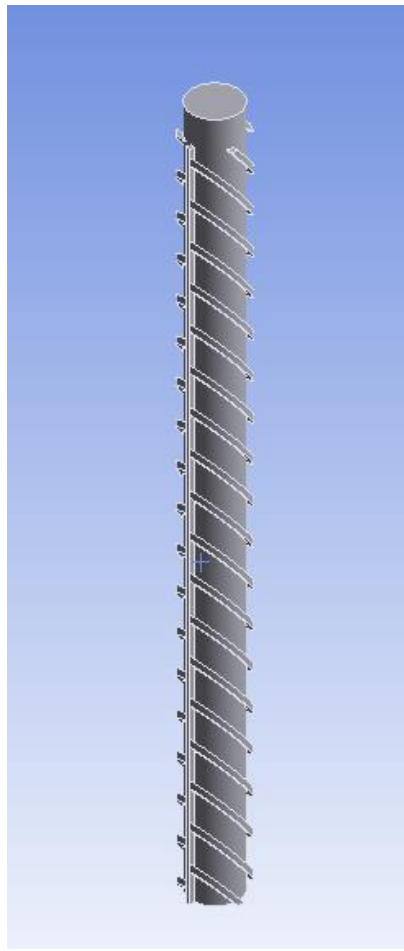


**Figure 4-5.** Model of #4 rebar anchor.

For both the threaded rod anchor model and the reinforcing bar anchor model, the adhesive layer is modeled to envelop the anchor at a depth of 2.75 in (6.99 cm). However, the thickness of the adhesive layer varies between the two models, due to the addition of lugs on the reinforcing bar. Furthermore, two versions of the adhesive layer were constructed for each model in order to further analyze the behavior of the adhesive: one without adhesive cover on the bottom of the anchor, and one with.

For the threaded rod anchor, the adhesive layer consists of a hollow cylinder that serves as a buffer between the anchor rod and the face of the hole drilled into the concrete block, shown in Figure 4-6. This thickness fills in the space between the concrete and

steel. The geometry of the adhesive layer for the reinforcing bar anchor, shown in Figure 4-7, is more complex; due to the lugs, perforations that match the shape and pattern of the lugs were removed from the hollow cylinder base. This ensured that the adhesive layer would fully envelop the reinforcing bar anchor without nodes or elements accidentally overlapping.

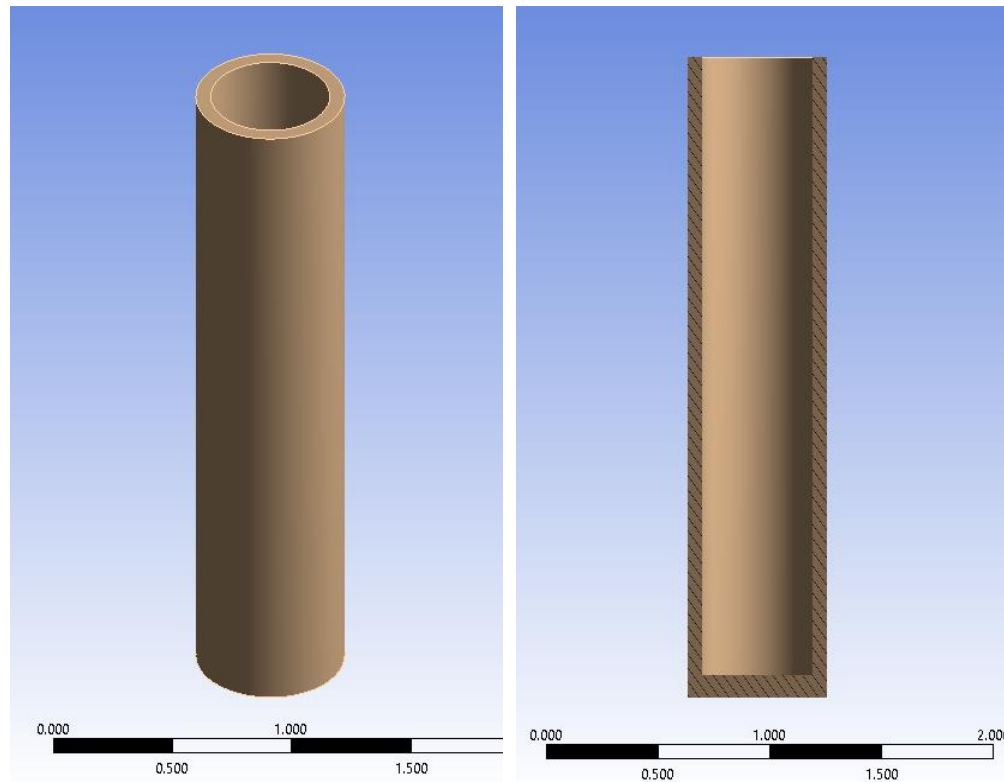


**Figure 4-6.** Geometry of the threaded rod adhesive layer (left). Section cut (right).

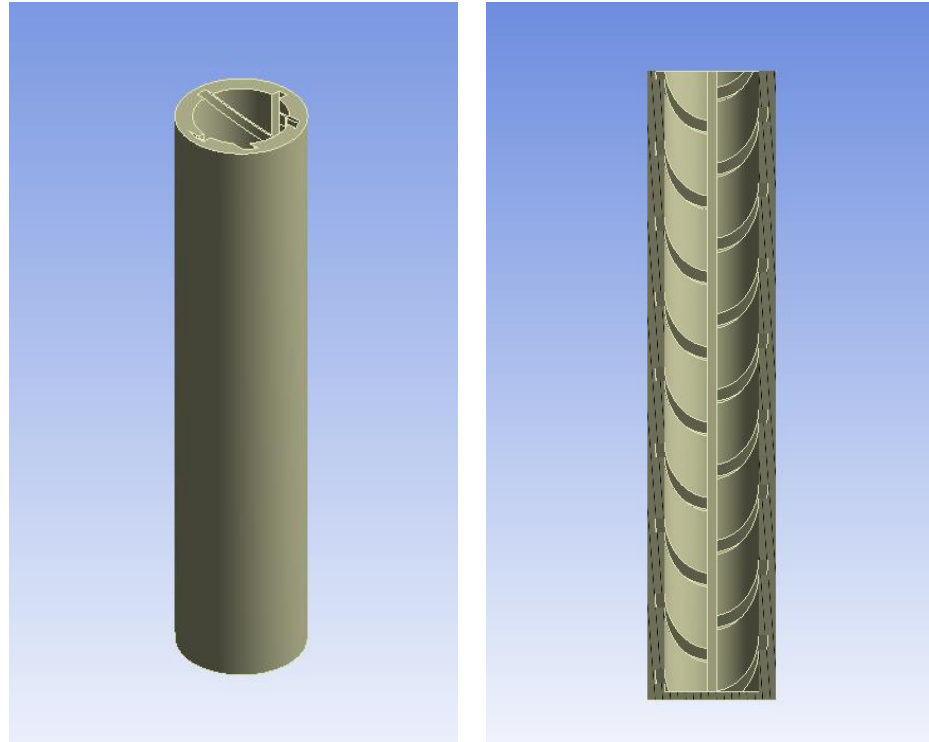


**Figure 4-7.** Geometry of the rebar adhesive layer (left). Section cut (right).

#### 4.2.2. Mesh and Element Type

Each component of the geometry utilized SOLID 185 elements with 8 nodes and 3 degrees of freedom, which allows plasticity, hyperelasticity, large deflections, and large strains. To optimize the run time of the simulation, each component was assigned a different element size, with the steel confinement plate assigned the largest elements and the adhesive layer assigned the smallest.

In all versions of the model, the mesh of the concrete block consists of tetrahedrons, as seen in Figure 4-8. Element size was set to 0.50 in (1.27 cm), which

resulted in a total of 13,122 elements, and was not further refined due to the insignificant difference in the concrete behavior between the coarser mesh size and finer mesh size.

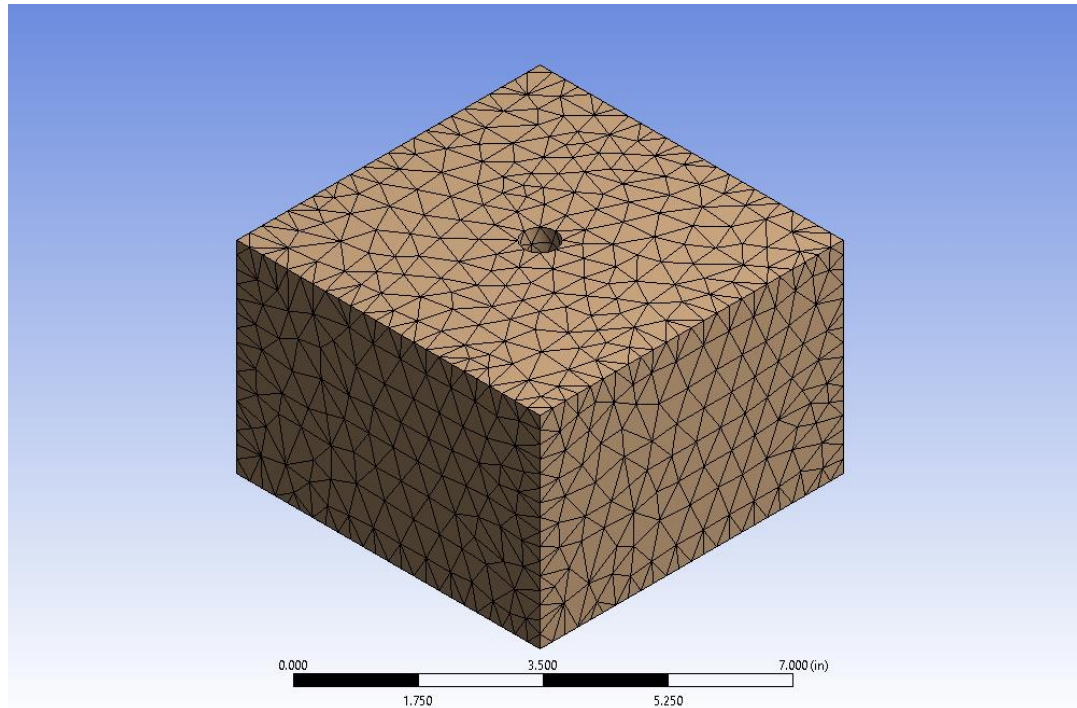


**Figure 4-8.** Concrete mesh.

The threaded rod and reinforcing bar anchors are meshed finer than the concrete due to their direct involvement in the application of the tensile force and stress distribution in the epoxy adhesive material, as seen in Figure 4-9. Tetrahedrons were used in both cases. The element sizes for each anchor were chosen and adjusted based on two conditions: that further refining the mesh would only result in a negligible difference in steel behavior, and that the number of elements in each anchor was relatively equivalent in order to be comparable. An element size of 0.1 in was assigned to the TR-CB model, resulting in 13,723 nodes and 3,756 elements, while an element size of 0.2 in was assigned to the reinforcing bar, resulting in 7,315 nodes and 3,802 elements.

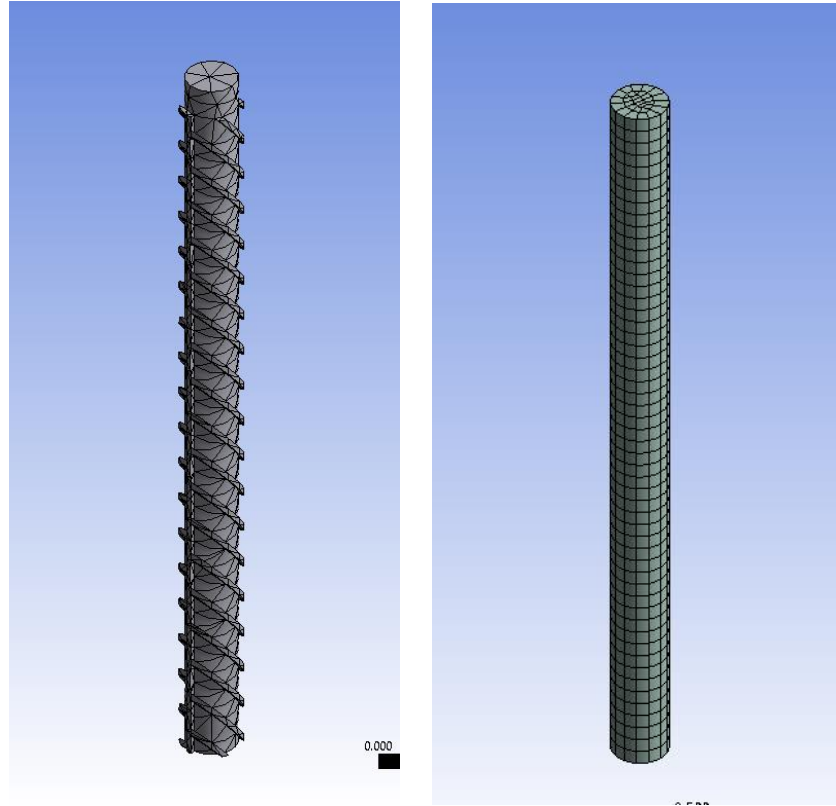


**Figure 4-9.** Rebar mesh (left) and threaded rod mesh (right).

The mesh of the adhesive layer, shown in Figure 4-10 and Figure 4-11 for the rebar and threaded rod anchors respectively, consists of the finest mesh size in the overall model. The material properties of the adhesive as well as the points of interest in the interface between the adhesive/anchor and adhesive/concrete necessitated a significantly finer element size to most accurately simulate the adhesive and interface behavior. Element sizes were adjusted until simulations showed equivalent stress and shear stress results within a 5% difference, and until the number of elements in all versions of the model were nearly equivalent. Table 4-1 shows the ultimate element sizes assigned to the adhesive layer in each model as well as the subsequent number of elements and nodes.

**Table 4-1. Adhesive Layer Element Sizes**

MODEL	ELEMENT SIZE (in)	# OF NODES	# ELEMENTS
TR-NB	0.03	63,642	11,811
TR-CB	0.06	22,611	11,943
RB-NB	0.07	18,308	9,439
RB-CB	0.075	18,094	9,329

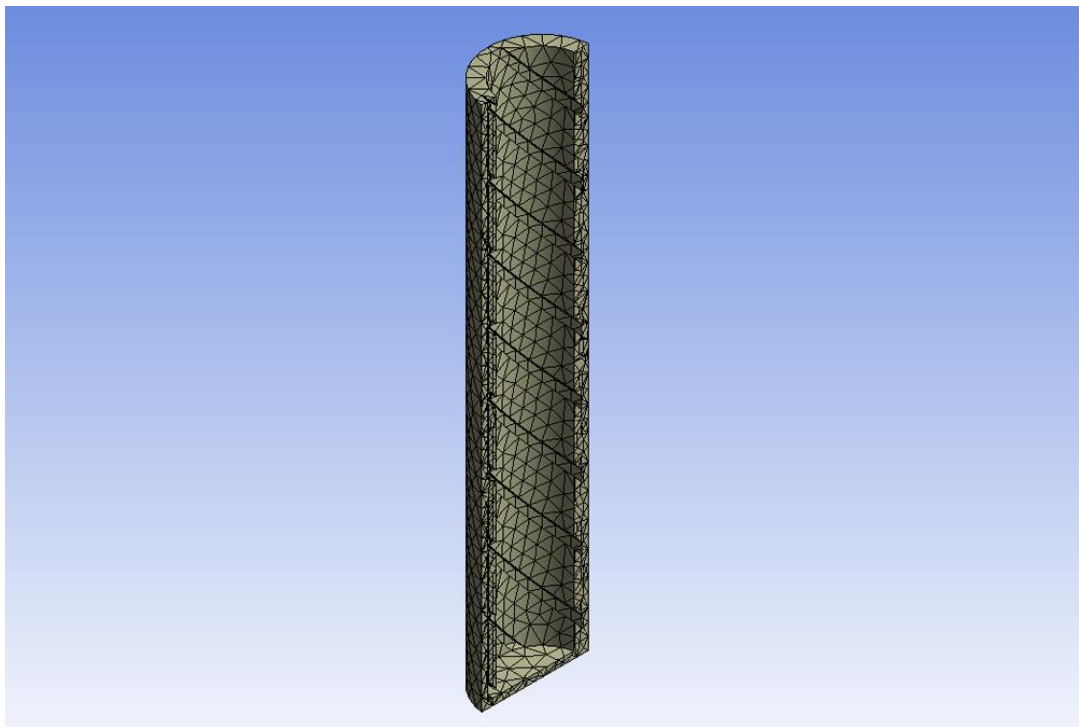


**Figure 4-10.** Section cut of mesh of the adhesive layer of the rebar anchor.

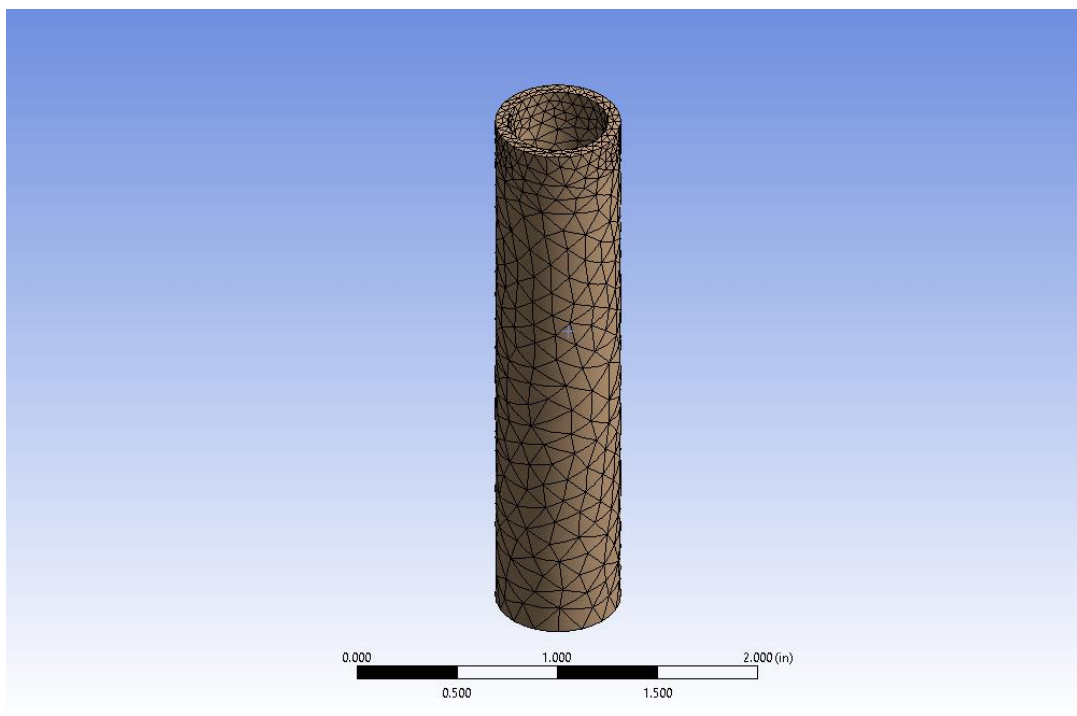


**Figure 4-11.** Mesh of the adhesive layer of the threaded rod.

#### 4.2.3. Material Properties

Each component of the model used a multilinear isotropic hardening model to simulate nonlinear behavior of the material.

The properties of the concrete block are based on 5000 psi (34.47 MPa) concrete, emulating the properties of the physical specimens described in Section 3.1.1. The concrete was further modeled with a density of 144 lb/ft<sup>3</sup> (1.85 kg/m<sup>3</sup>), a Poisson's ratio of 0.18, and a Young's Modulus of  $4.3 \times 10^6$  psi. Material properties for concrete under different temperatures were initially considered to change due to the change in modulus described in Section 2.4, but preliminary tests showed a negligible difference in the behavior of the system. Therefore, it was assumed that concrete properties remained constant under varying temperatures.

High strength steels were used for experimental testing with the intention of preventing steel failure in the specimens. The material properties of the threaded rod anchor were based on the properties of ASTM A354 Grade BD steel to match the properties of the experimental anchor and were assigned a nominal yield strength of 130 ksi (896.32 MPa) and an ultimate strength of 150 ksi (1034.21 MPa). The material properties of the reinforcing bar were based on the properties of A1035 Grade 120 steel and were thus given a nominal yield strength of 120 ksi (827.37 MPa) and an ultimate strength of 150 ksi (1034.21 MPa). Plastic strain values as defined by Equation 1 and true stress values as defined by Equation 2 were calculated from the engineering stress vs strain curves of each grade of steel, shown in Figure 4-12, Figure 4-13, and Figure 4-14, and inputted into multilinear isotropic plots to allow nonlinear behavior.

$$\text{Plastic Strain} = \varepsilon_{true\ total} - \left( \frac{\sigma_{true}}{E} \right) \quad \text{Eq. 1}$$

$$\text{True Stress} = \sigma_{eng} * (1 + \varepsilon_{eng}) \quad \text{Eq. 2}$$

Because the experimental rebar anchors were not originally Grade 120 steel and were instead heat-treated to a yield strength of 120 ksi (827.37 MPa), inaccuracies are possible in comparing the material properties of the simulated model with that of the actual specimen, though high strength steels were specifically used in experimental testing to preclude effects of steel components, so this should not affect the finite element model results. Material properties for different temperatures were not considered due to the assumption that the mechanical behavior of the steel would not change in the 0 °F (-18°C) to 120 °F (49 °C) temperature range, as explained in Section 2.5.

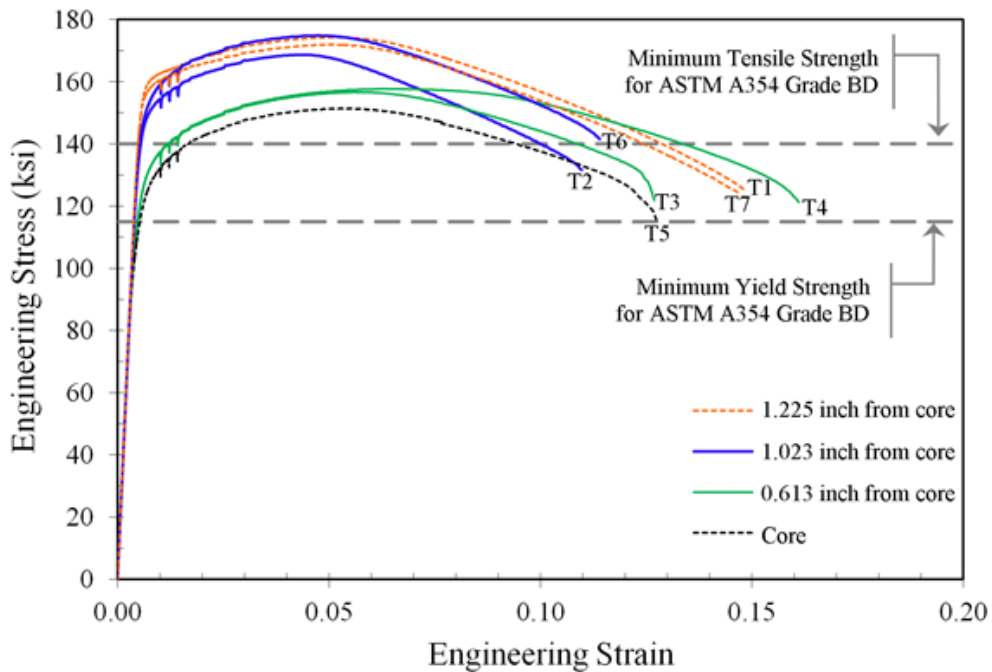


**Figure 4-12.** Engineering stress vs. engineering strain plot for ASTM A354 BD steel (Ocel & Provines, 2015). Authorized reprint by the Federal Highway Administration.

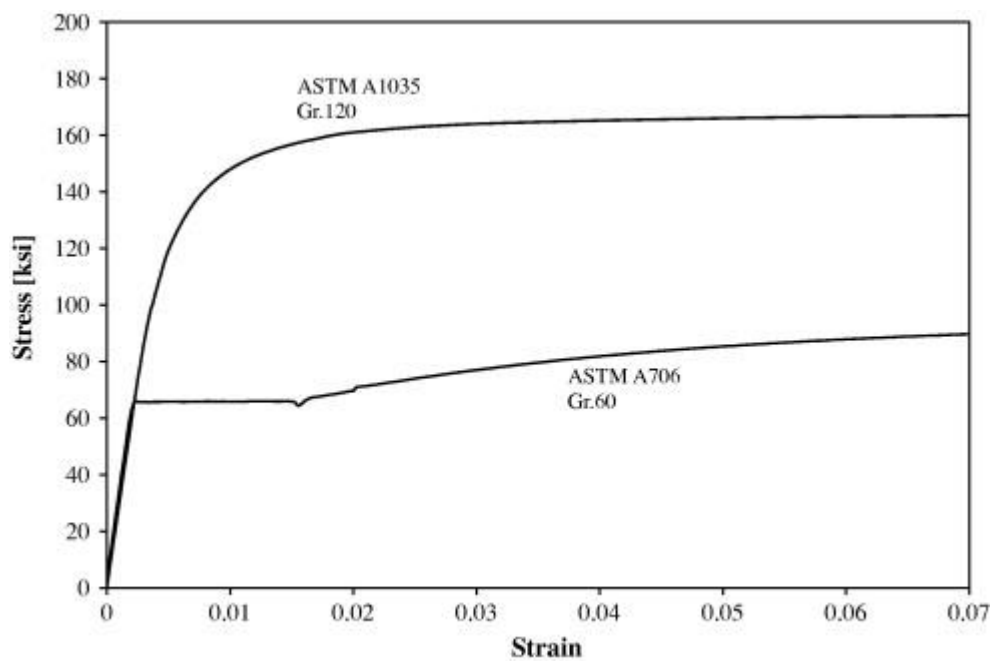


**Figure 4-13.** Engineering stress vs. engineering strain plot for A1035 Grade 120 steel (Rautenberg et al., 2012). Authorized reprint from Engineering Structures Volume 37.

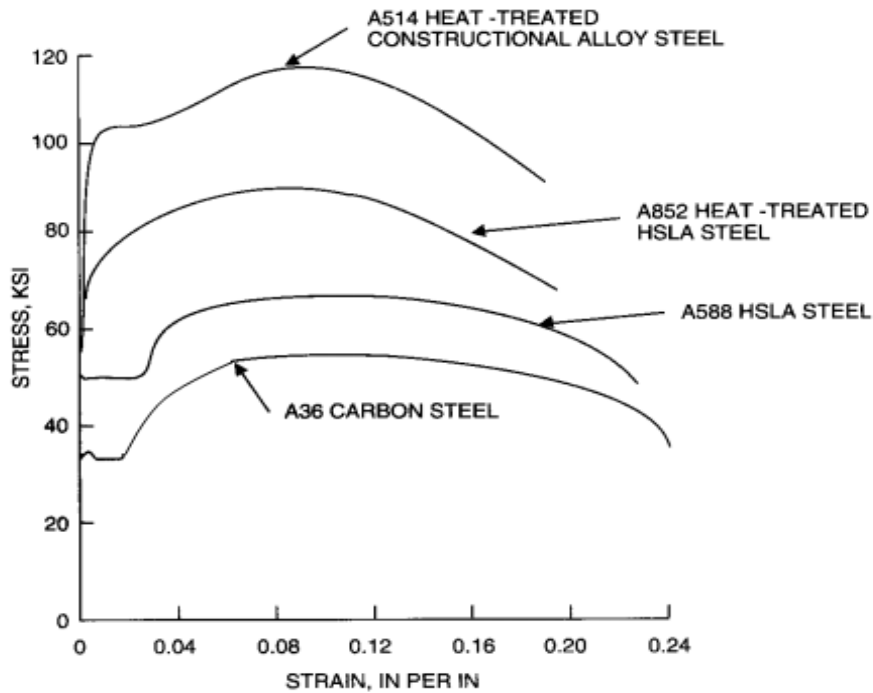


**Figure 4-14.** Engineering stress vs. engineering strain plot for A36 carbon steel.  
(Brockenbrough, 2006)

When the temperature of the environment changes, the behavior of the adhesive changes. Therefore, separate material properties were applied to the adhesive layer based on the behavior of the adhesive under the temperature fluctuation. Stress and strain values of general epoxy resin tested under different temperatures shown in Figure 2-6 were extrapolated and converted to plastic strain and true stress using Equations 1 and 2. The results were subsequently ratioed down to align with the ultimate stress of 6000 psi (41.37 MPa) given by Davis (2012) in a similar study and were input into a multilinear isotropic hardening model to allow for nonlinear analysis of the adhesive, shown in Figure 4-15, Figure 4-16, and Figure 4-17. A Poisson's ratio of 0.40 was applied to the adhesive as per the study conducted by Davis (2012). The Young's Modulus assigned to the adhesive varied based on the temperature conditions and were derived from Figure 2-6, the values of which are listed in Table 4-2.

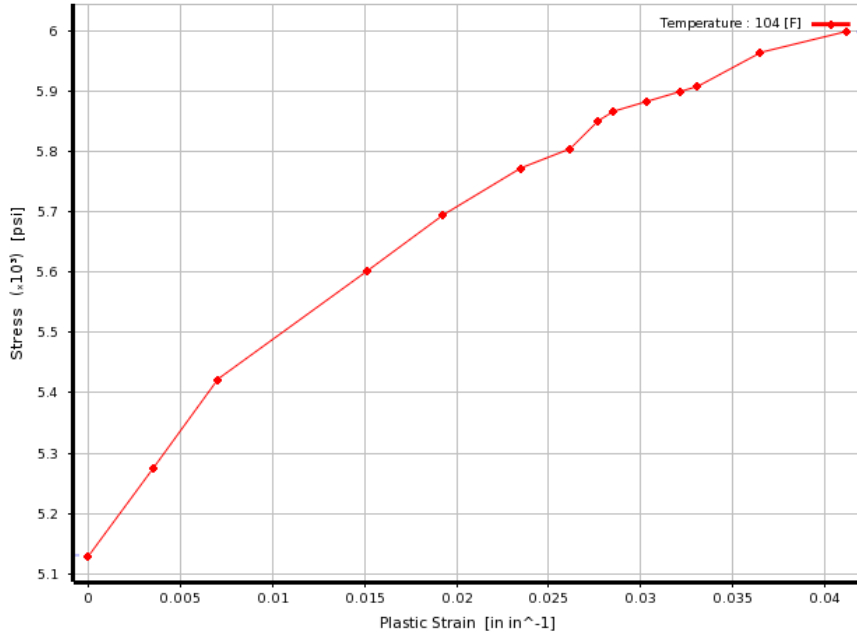


**Figure 4-15.** Plastic Strain vs. True Stress of the adhesive at 104°F (40°C).

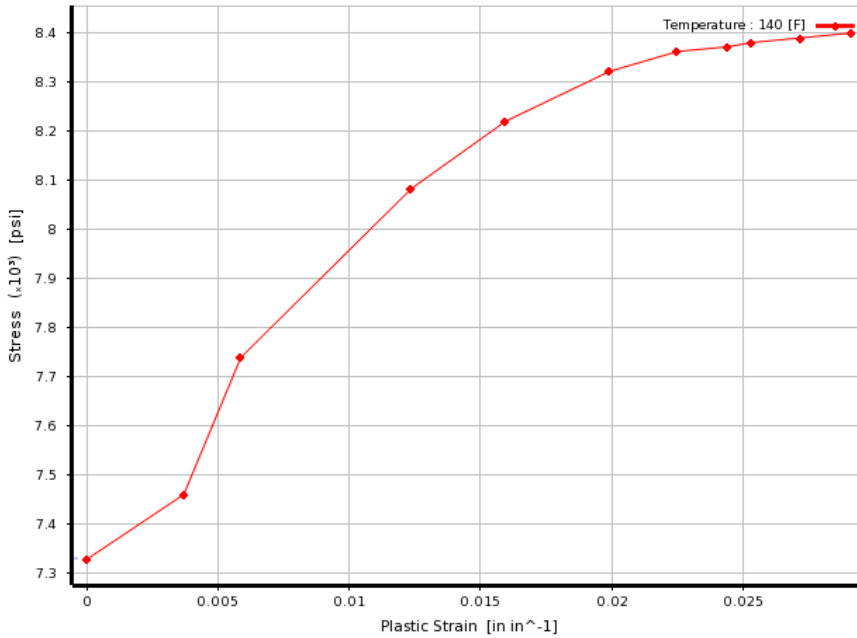


**Figure 4-16.** Plastic Strain vs. True Stress of the adhesive at 77°F (25°C).

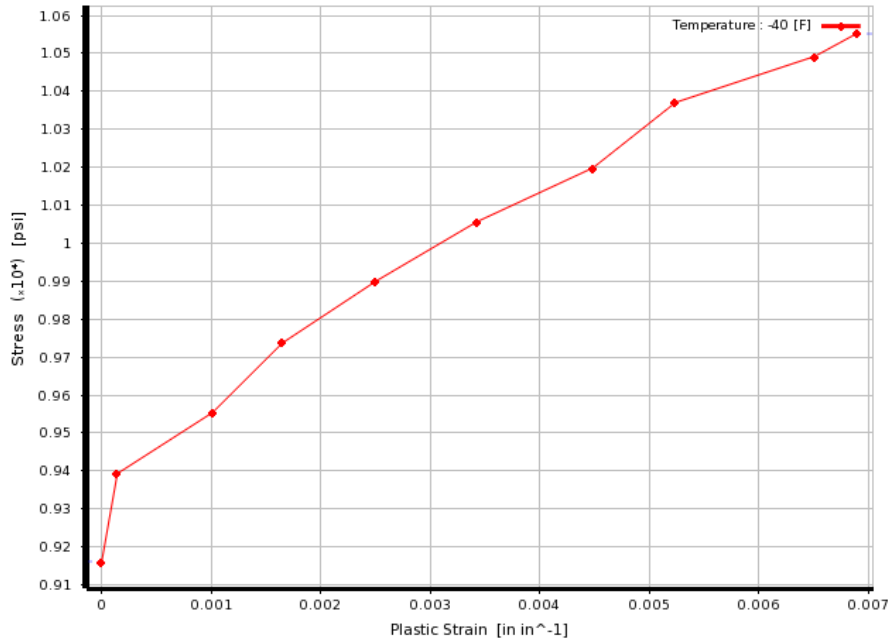


**Figure 4-17.** Plastic Strain vs. True Stress of the adhesive at -40°F (-40°C).

**Table 4-2. Young's Modulus for Adhesive at Various Temperatures**

TEMPERATURE	YOUNG'S MODULUS
-40°F (-40°C)	609 ksi (4200.29 MPa)
77°F (25°C)	360 ksi (2464.88 MPa)
104°F (40°C)	100 ksi (689.48 MPa)

#### 4.5. Contact Conditions

ANSYS program-controlled contact conditions were primarily used for analysis. This resulted in a bonded contact condition at both the steel/adhesive and adhesive/concrete interfaces. In the models without an adhesive-covered bottom, contact was manually removed at the interface between the bottom of the steel anchor and the bottom of the concrete hole to ensure the anchor was not directly attached to the concrete.

## 4.6. Parameters

### 4.6.1. Boundary Conditions

A steel plate with a thickness of 0.75 inch (1.91 cm) was set on top of the concrete block. A hole 1 inch (2.54 cm) in diameter was removed from the centroid of the steel plate, which allowed for the anchor to protrude through the plate as necessary. A fixed boundary support was then applied to the bottom of the steel plate, shown in Figure 4-18, which in turn fixed the concrete block in place and disallowed translation and rotation in the X, Y, and Z directions. The steel plate itself corresponds to the same plate that confines the experimental concrete specimen. All other surfaces remain unconstrained.

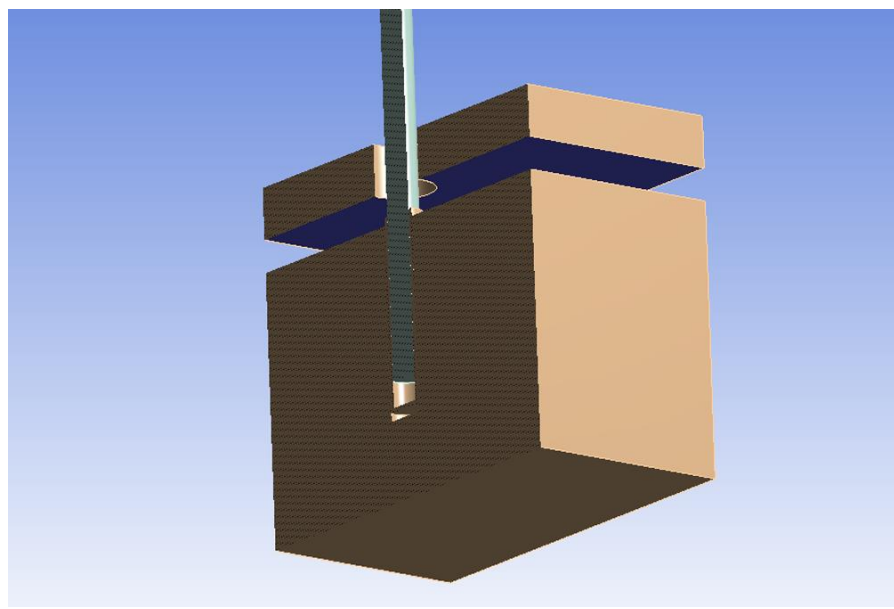


**Figure 4-18.** Section cut showing fixed support underneath the confining plate.

### 4.6.2. Applied Force

A ramped tensile force was applied to the top face of the anchor rod to simulate physical testing conditions, shown in Figure 4-19. A load capacity of approximately 18 kips was expected from data compiled by physical short-term load testing, which

complied with the provisions set by AASHTO TP-84. For the finite element models, a tensile force of 25 kips was applied to ensure total failure of the adhesive.

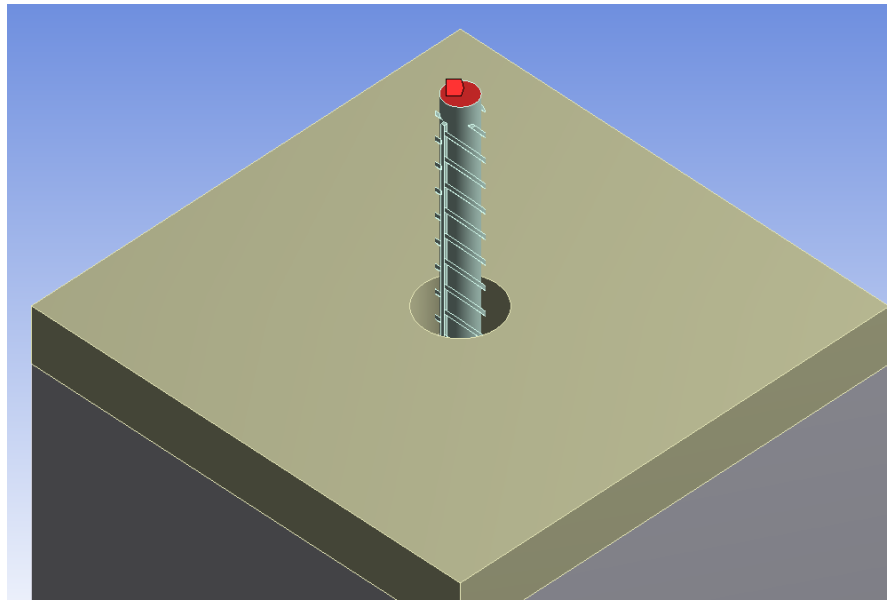


**Figure 4-19.** Force applied to the top surface of the anchor rod.

#### 4.7. Analysis Procedure

Non-linear analysis of the finite models was achieved through the implementation of multilinear isotropic hardening material models to the relevant components. True plastic strain and true stress values of concrete, ASTM A354 BD threaded rod, and Grade 120 A1035 reinforcing bar were inputted into the Engineering Data module for ANSYS Workbench 18.2. As stated in Section 4.3.3, temperature effects on the modulus of concrete were found to have no difference on the behavior of the overall model. Per Section 2.5, temperature was also expected to have an insignificant effect on the behavior of steel. Therefore, the non-linear material models for the concrete member, threaded rod, reinforcing bar, and steel confining plate remained constant throughout the changes in temperature. For the adhesive, true plastic strain and true stress were derived from the

curve provided by Fielder et al. (2005) shown in Figure 2-6 and ratioed to the chosen yield stress noted in Section 4.2.3.

A preliminary non-linear analysis study using a bilinear elastic perfectly plastic material model was also conducted for the adhesive layer to mimic the finite element study conducted by Davis (2012).

All versions of the model were assigned 60 2-second load steps. This simulated the ASTM E488 test procedure in which the load is applied to the anchor at a constant load rate for up to two minutes. 10 initial substeps were assigned with a minimum substep of 1 and a maximum substep of 50 to ensure that nonlinear calculations would run smoothly. However, because load rate effects were not included, ultimately the time increment assigned to the load steps did not affect the results.

#### **4.8. Nomenclature**

- TR: Threaded rod
- RB: Reinforcing bar
- NB: No adhesive on the bottom
- CB: Covered adhesive bottom

## **CHAPTER 5**

### **RESULTS OF PHYSICAL TESTING AND FEA**

This chapter includes the results of the anchor pullout tests under extreme temperatures and the results of the finite element analysis models.

#### **5.1. Nomenclature**

The nomenclature used to identify each of the test specimens is detailed below.

**M - T1 - T2 - T3 - #**

- M: Material (1B, 2, 7)
- T1: Initial concrete temperature
- T2: Installation and curing temperature
- T3: Testing Temperature
- #: Test number (1-3)

#### **5.2. Physical Testing Results**

All short-term anchor pullout tests were performed according to manufacturer specifications with several exceptions as noted. Three materials were tested, defined in Mendoza (2017) as Materials 1B, 2, and 7. Despite having accounted for the prevention of steel failure in the test design, during many of the tests of Material 1B the anchor failed before failure of the adhesive. This material is marketed as an improved version of Material 1 previously tested by Mendoza (2017) and caused the load capacity to increase to the point where the high strength steel was not adequate to prevent rod failure in many specimens. Only tests with failure of the adhesive are reported, but it is noted that anchors may have yielded in all specimens, so displacement measurements are a combination of

adhesive deformation and steel yielding. An anchor with failure of the adhesive is shown in Figure 5-1.

A summary of the extreme temperature testing results is shown in **Error! Reference source not found.**. Each plotted point represents an individual test unless performed by Mendoza (2017), whose results are plotted as a horizontal line at their MSL under AASHTO TP-84 test criteria of MSL for comparison. Results are listed in more detail in Table 5-1, Table 5-2, and Table 5-3, in which load capacity, standard deviation, and coefficient of variation for each test is provided. Also included is the failure mode in which the specimen failed.

The high strength steel anchors were expected to yield at 18 kips (80 kN). However, the load capacity of Material 1B surpassed the capacity of the anchor in many tests; as such, in many cases the displacements measured by the transducers are not solely of the adhesive but includes the yielding of the steel. Finally, displacements for several specimens could not be reported due to errors in instrumentation.



**Figure 5-1.** Adhesive failure in the anchor.

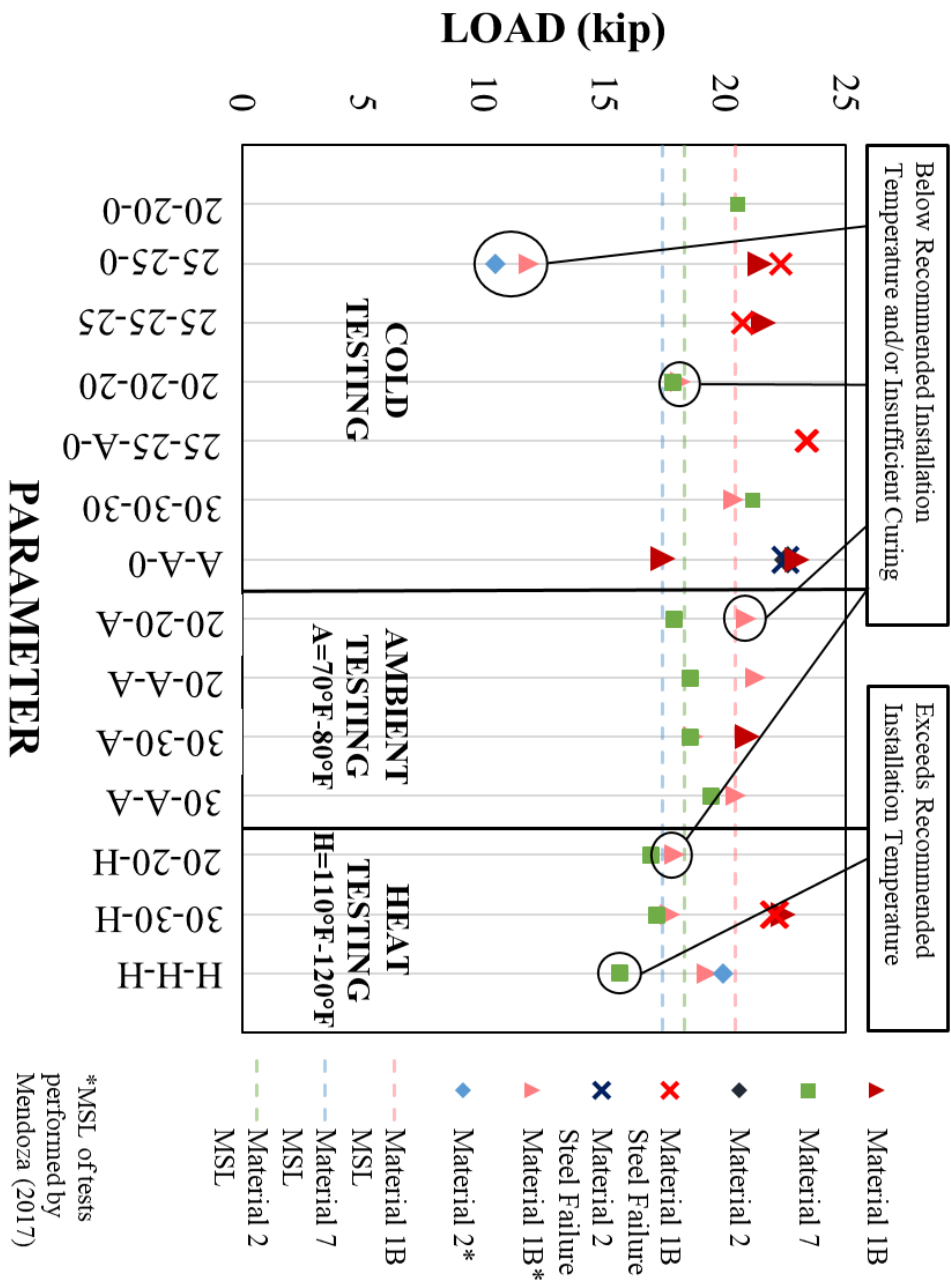


Figure 5-2. Summary of Extreme Testing Results.

**Table 5-1. Material 1B Results**

**MATERIAL 1B**

INITIAL CONCRETE TEMP.	INSTALLATION AND CURING TEMP.	TESTING TEMPERATURE	TEST NAME	LOAD (kip)	AVERAGE LOAD (kip)	STD. DEV.	COV	MIX	INSTALL	TESTED	FAILURE
A	A	0°F	1B-A-A-0-01	17.39	20.20	3.97	0.20	7	2-Aug-16	7-Aug-17	adhesive
A	A	0°F	1B-A-A-0-02	23				7	2-Aug-16	7-Aug-17	adhesive
25°F	25°F A	0°F	1B-25-25-A-0-01	23.37	23.40	0.04	0.00	7	22-Sep-17	2-Oct-17	steel
25°F	25°F A	0°F	1B-25-25-A-0-02	23.42				7	22-Sep-17	2-Oct-17	steel
25°F	25°F	0°F	** B-25-25-0-01	12.79				7	10-Nov-16	14-Nov-16	adhesive
25°F	25°F	0°F	** B-25-25-0-02	11.77				7	10-Nov-16	14-Nov-16	adhesive
25°F	25°F	0°F	** B-25-25-0-03	11.02				7	10-Nov-16	14-Nov-16	adhesive
25°F	25°F	0°F	** B-25-25-0-04	12.88	11.57	1.44	0.12	7	24-Aug-17	28-Aug-17	adhesive
25°F	25°F	0°F	** B-25-25-0-05	9.38				7	24-Aug-17	28-Aug-17	adhesive
25°F	25°F	0°F	1B-25-25-0-01	21.47				7	8-Jan-18	15-Jan-18	adhesive
25°F	25°F	0°F	1B-25-25-0-02	22.31	21.89	0.59	0.03	7	8-Jan-18	15-Jan-18	steel
25°F	25°F	25°F	1B-25-25-25-01	22.46	21.58	1.24	0.06	7	3-Jan-18	10-Jan-18	adhesive
25°F	25°F	25°F	1B-25-25-25-02	20.70				7	3-Jan-18	10-Jan-18	adhesive
30°F	30°F	30°F	1B-30-30-H-01	22.40				7	28-May-18	4-Jun-18	adhesive
30°F	30°F	30°F	1B-30-30-H-02	22.04	21.45	0.21	0.01	7	28-May-18	4-Jun-18	steel
30°F	30°F	30°F	1B-30-30-H-03	22.04				7	28-May-18	4-Jun-18	steel
30°F	30°F	30°F	1B-30-30-H-04	19.33				7	28-May-18	4-Jun-18	concrete
30°F	30°F	70°F - 80°F	1B-30-30-A	20.89	20.89	0.00	0.00	7	28-May-18	4-Jun-18	adhesive

\*A: 70°F - 80°F; H: 110°F - 120°F

\*\*Insufficient Cure Time

**Table 5-2. Material 7 Results**

**MATERIAL 7**

INITIAL CONCRETE TEMP.	INSTALLATION AND CURING TEMP.	TESTING TEMPERATURE	TEST NAME	LOAD (kip)	AVERAGE LOAD (kip)	STD. DEV.	COV	MIX	INSTALL	TESTED	FAILURE
20°F	20°F	0°F	07-20-20-0-01	19.72	20.55	0.72	0.03	6	3-Nov-16	7-Nov-16	adhesive
20°F	20°F	0°F	07-20-20-0-02	20.99	20.55	0.72	0.03	6	3-Nov-16	7-Nov-16	adhesive
20°F	20°F	0°F	07-20-20-0-03	20.94				6	3-Nov-16	7-Nov-16	adhesive
30°F	30°F	70°F - 80°F	07-30-30-A-01	19.25	18.56	0.98	0.05	6	30-Sep-16	4-Oct-16	adhesive
30°F	30°F	70°F - 80°F	07-30-30-A-02	17.86				6	19-Sep-16	23-Sep-16	adhesive
30°F	70°F - 80°F	70°F - 80°F	07-30-A-A-01	17.83	19.45	2.28	0.12	6	30-Sep-16	4-Oct-16	adhesive
30°F	70°F - 80°F	70°F - 80°F	07-30-A-A-02	21.06				6	30-Sep-16	4-Oct-16	adhesive
30°F	30°F	30°F	07-30-30-H-01	17.3				6	30-Sep-16	4-Oct-16	adhesive
30°F	30°F	110°F - 120°F	07-30-30-H-02	15.95	17.18	1.18	0.07	6	30-Sep-16	4-Oct-16	adhesive
30°F	30°F	30°F	07-30-30-H-03	18.3				6	30-Sep-16	4-Oct-16	adhesive
30°F	30°F	30°F	07-30-30-30-01	21.23				6	20-Oct-16	24-Oct-16	adhesive
30°F	30°F	30°F	07-30-30-30-02	21.07	21.13	0.09	0.00	6	24-Sep-16	28-Sep-16	adhesive
30°F	30°F	30°F	07-30-30-30-03	21.1				6	24-Sep-16	28-Sep-16	adhesive
20°F	20°F	70°F - 80°F	07-20-20-A-01	16.76	17.9	1.61	0.09	5	29-Jul-16	2-Aug-16	adhesive
20°F	20°F	70°F - 80°F	07-20-20-A-02	19.04				6	20-Oct-16	24-Oct-16	adhesive
20°F	70°F - 80°F	70°F - 80°F	07-20-A-A-01	19.54	18.59	1.34	0.07	5	29-Jul-16	2-Aug-16	adhesive
20°F	70°F - 80°F	70°F - 80°F	07-20-A-A-02	17.64				6	20-Oct-16	24-Oct-16	adhesive
20°F	20°F	20°F	07-20-20-H-01	15.44				5	29-Jul-16	2-Aug-16	adhesive
20°F	20°F	110°F - 120°F	07-20-20-H-02	16.63	16.93	1.67	0.10	5	29-Jul-16	2-Aug-16	adhesive
20°F	20°F	20°F	07-20-20-H-03	18.73				5	29-Jul-16	2-Aug-16	adhesive
20°F	20°F	20°F	07-20-20-20-01	18.71				5	10-Sep-16	14-Sep-16	adhesive
20°F	20°F	20°F	07-20-20-20-02	16.7	17.84	1.03	0.06	5	10-Sep-16	14-Sep-16	adhesive
110°F - 120°F	110°F - 120°F	07-H-H-H-01	16.15	15.61	0.77	0.05		5	10-Sep-16	14-Sep-16	adhesive
110°F - 120°F	110°F - 120°F	07-H-H-H-02	15.06					5	19-Aug-16	23-Aug-16	adhesive

\*\*Insufficient Cure Time

**Table 5-3. Material 2 Results**

MATERIAL_2										
INITIAL CONCRETE TEMP.	INSTALLATION AND CURING TEMP.	TESTING TEMPERATURE	TEST NAME	LOAD (kip)	AVERAGE LOAD (kip)	STD. DEV.	COV	MIX	INSTALL TESTED	FAILURE
A	A	0°F	02-A-A-0-01 02-A-A-0-02	22.51 22.62	22.57	0.08	0.00	7	24-Sep-16 24-Sep-16	28-Sep-16 adhesive
A	A	25°F	*02-25-25-0-01 **02-25-25-0-02	10.02 10.82	10.47	0.41	0.04	7	1-Dec-16 1-Dec-16	5-Dec-16 adhesive
25°F	25°F	0°F	**02-25-25-0-03	10.56	10.47	0.41	0.04	7	1-Dec-16 1-Dec-16	5-Dec-16 adhesive
110°F - 120°F	110°F - 120°F	110°F - 120°F	02-H-H-H-01	19.63	19.92	0.40	0.02	6	20-Oct-16 20-Oct-16	24-Oct-16 adhesive
110°F - 120°F	110°F - 120°F	110°F - 120°F	02-H-H-H-02	20.2				6	1-Dec-16 1-Dec-16	5-Dec-16 adhesive
70°F - 80°F	70°F - 80°F	70°F - 80°F	02-RB-S-01	18.57				7	13-Jan-17 13-Jan-17	17-Jan-17 adhesive
70°F - 80°F	70°F - 80°F	110°F - 120°F	02-RB-S-02	18.54	20.08	1.79	0.09	7	13-Jan-17 13-Jan-17	17-Jan-17 adhesive
70°F - 80°F	70°F - 80°F	70°F - 80°F	02-RB-S-03	21.21				7	13-Jan-17 13-Jan-17	17-Jan-17 adhesive
70°F - 80°F	70°F - 80°F	70°F - 80°F	02-RB-S-04	22.01				7	13-Jan-17 13-Jan-17	17-Jan-17 adhesive

\*\*Insufficient Cure Time

### **5.2.1. Material 1B**

Overall, Material 1B threaded rod anchorage systems were observed to have consistent high performance in both cold and elevated temperatures when cured to the manufacturer's specifications. Reinforcing bar tests with Material 1B were not conducted.

Previous short-term pullout tests in accordance with ASTM E488/AASHTO TP-84 have shown the MSL of Material 1B to be 20.10 kips (89.41 kN) with a coefficient of variation of 7% (Mendoza, 2017). To compare, when cured at 25°F (-4°C), Material 1B failed at an average load of 21.58 kips (95.99 kN) and 21.89 kips (97.37 kN) when tested at 25°F (-4°C) and 0°F (-18°C) respectively, shown in Figure 5-3. In addition, when cured at 30°F (-1°C), Material 1B failed at 21.45 kips (95.41 kN) and 20.90 kip (92.97 kN) when tested at 110°F to 120°F (43°C to 49°C) and ambient temperatures respectively, shown in Figure 5-4 and Figure 5-5 in which the results are overlaid overtop the Material 1B static tests. This shows that regardless of curing and testing temperature, Material 1B shows a load capacity that rarely goes below the MSL when cured to manufacturer specifications. An exception to this is when Material 1B was cured at ambient temperature and tested at 0°F (-18°C), at which one of the specimens failed at 17.39 kips (77.35 kN).

When cured and tested at lower temperatures, Material 1B exhibits an approximately 10% increase in strength, which is consistent with adhesive behavior in cold temperatures as per Section 2.3, while the load capacity suffers when cured at a cold temperature and tested at ambient and elevated temperatures. However, it should be noted that the steel anchor failed in almost 50% of the Material 1B tests as shown in Figure 5-2, implying that the load capacity of Material 1B is in fact greater than what was observed.

Failure in the steel also affected the displacement measurements taken, as seen in Figure 5-3, in which two of the specimens showed much higher displacements due to the transducers reading the yielding of the steel in addition to deformation of the epoxy. Failure in the steel in further tests are not reported.

Overall, Material 1B did not exhibit large changes in stiffness when subjected to changes in temperature as described in Section 2.3. Small changes in stiffness did occur in the data presented in Figure 5-7; however, more tests should be performed in order to better investigate the results.

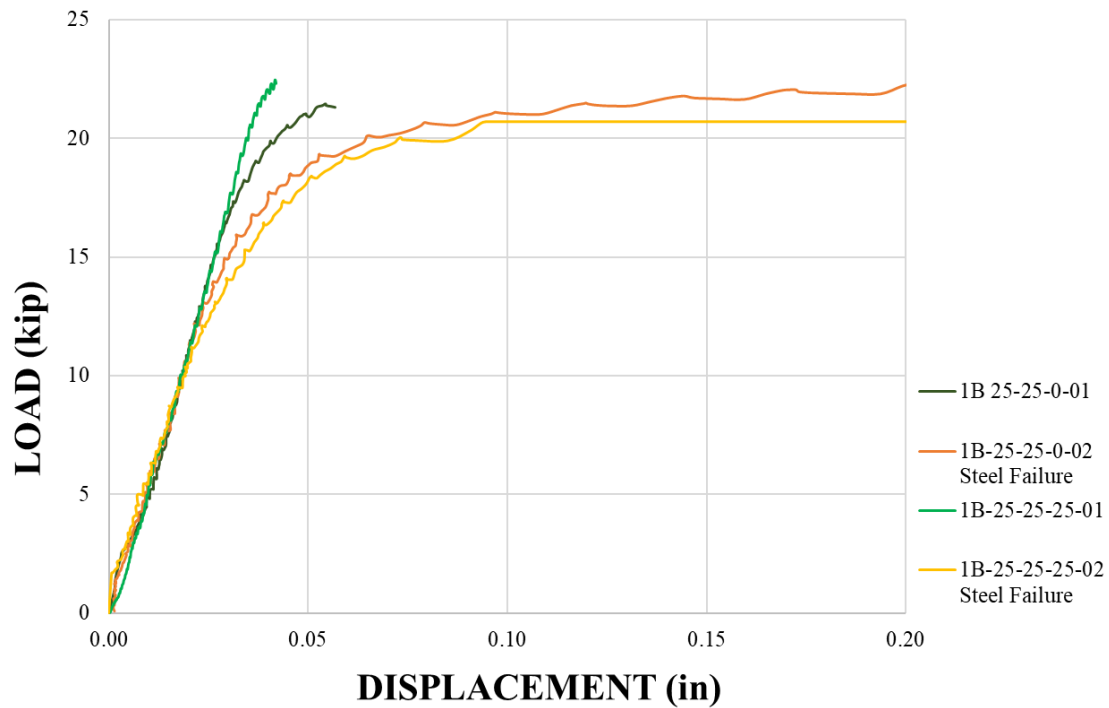


**Figure 5-3.** Material 1B Tested at 0°F (-18°C): Load vs. Displacement.

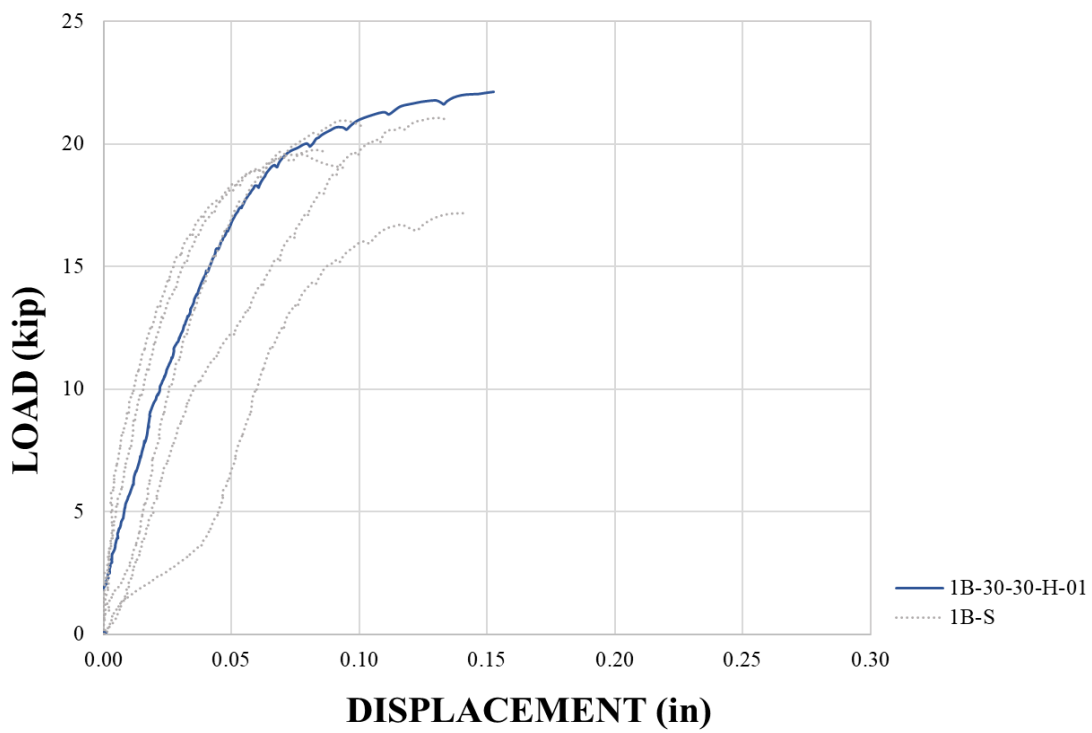


**Figure 5-4.** Material 1B Tested at 110°F to 120°F (43°C to 49°C): Load vs. Displacement.

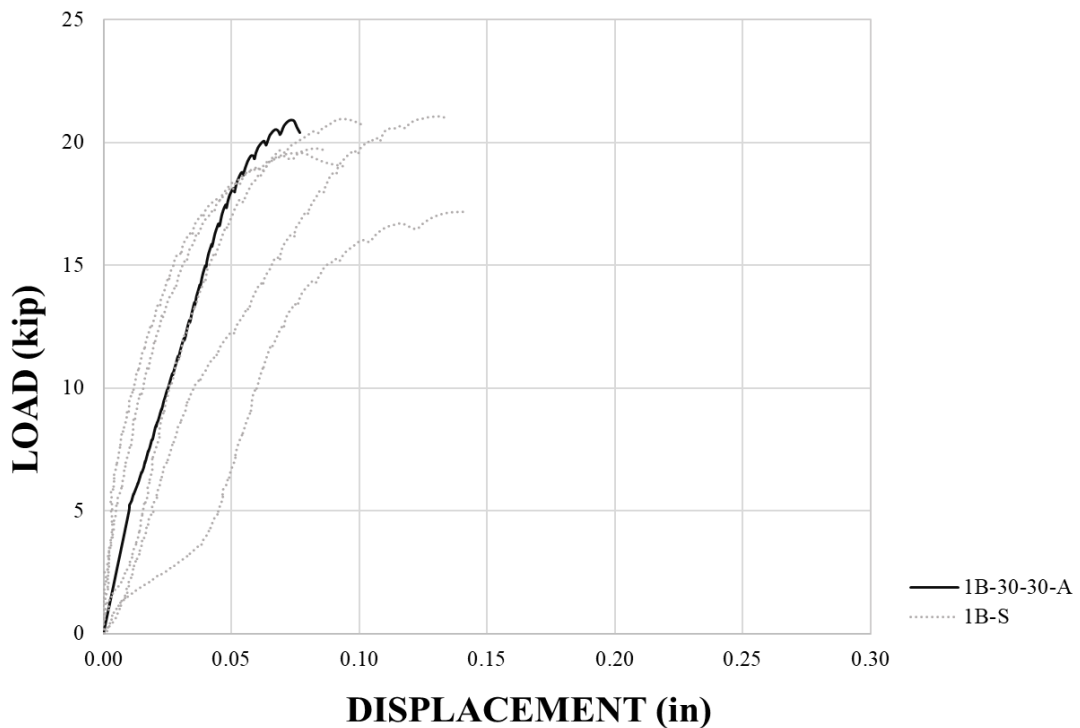


**Figure 5-5.** Material 1B Tested at Ambient: Load vs. Displacement.

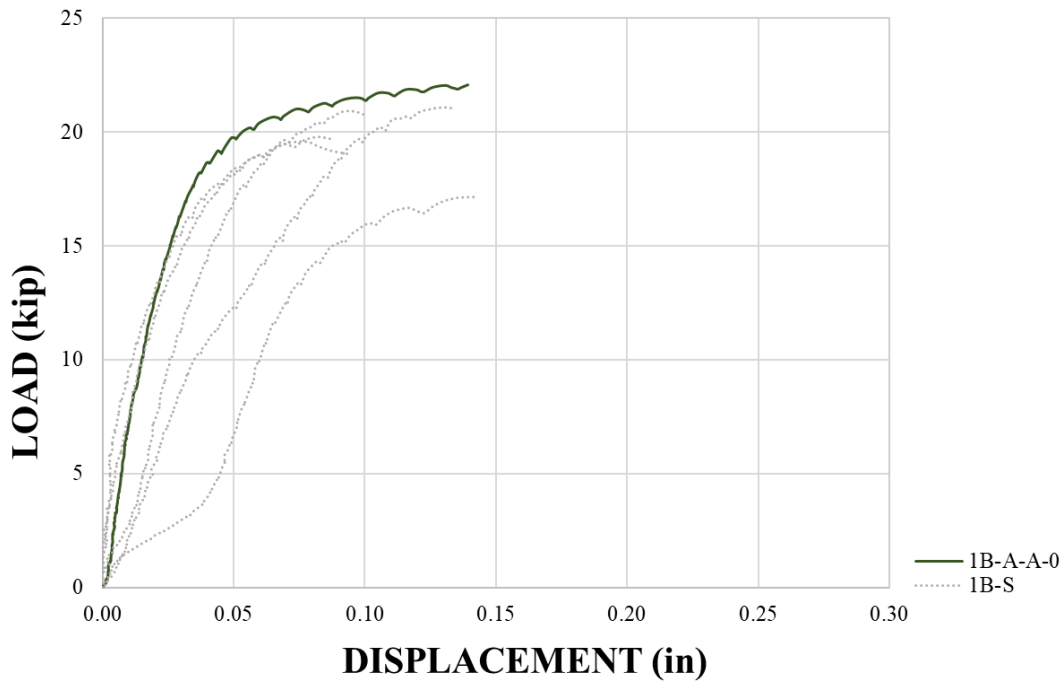


**Figure 5-6.** Material 1B Cured at Ambient and Tested at 0°F (-18°C): Load vs. Displacement.

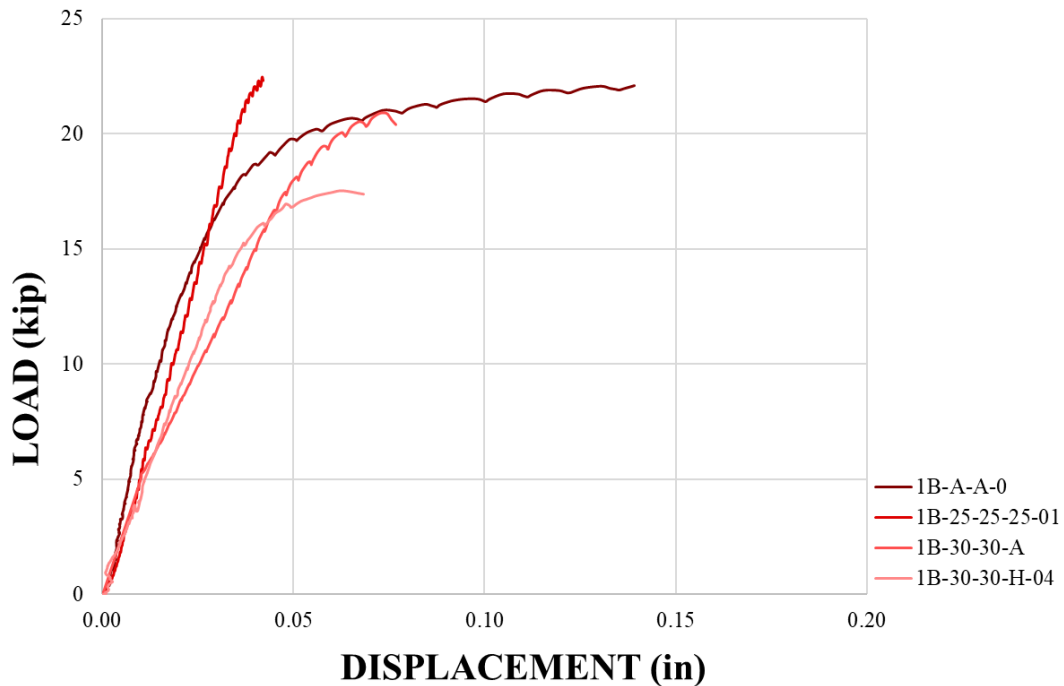


**Figure 5-7.** Material 1B Stiffness Tested Under Different Temperatures.

### 5.2.2. Material 7

Material 7, an adhesive formulated specifically for cold weather applications, performed well when cured and installed in cold temperatures, but performed significantly worse as temperatures increased. From static tests performed in compliance with ASTM E488/AASHTO TP-84 by Mendoza (2017), Material 7 was found to have an MSL of 17.42 kip (77.49 kN) and a coefficient of variation of 4%.

When cured at 20°F (-7°C) and tested at 0°F (-18°C), Material 7 failed at an average load of 20.55 kips (91.41 kN), a 15% increase in strength, shown in Figure 5-8. Material 7 also exhibited an increase in strength when cured and tested at 30°F (-1°C), failing at an average load of 21.13 kips (93.99 kN) as seen in Figure 5-9. When cured and tested at 20°F (-7°C), however, Material 7 failed at an average load of 17.84 kips (79.36 kN), close to its MSL, as seen in Figure 5-10. The displacements for Material 7 tested at cold temperatures averaged from 0.05 inches (1.27 mm) to 0.08 inches (2.03 mm).

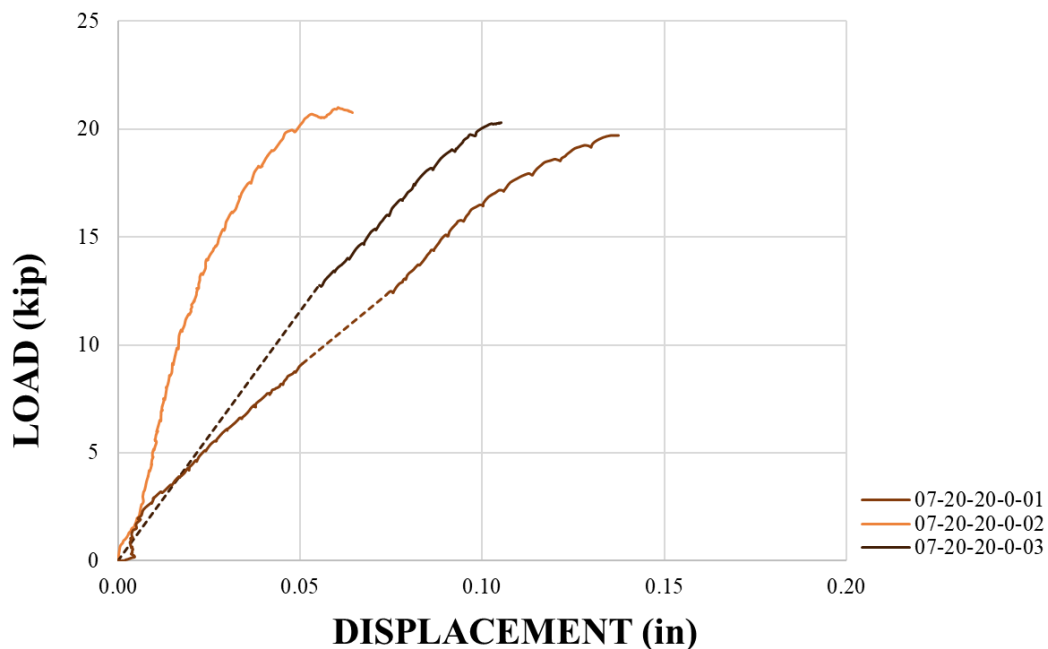


**Figure 5-8.** Material 7 Tested at 0°F (-18°C): Load vs. Displacement

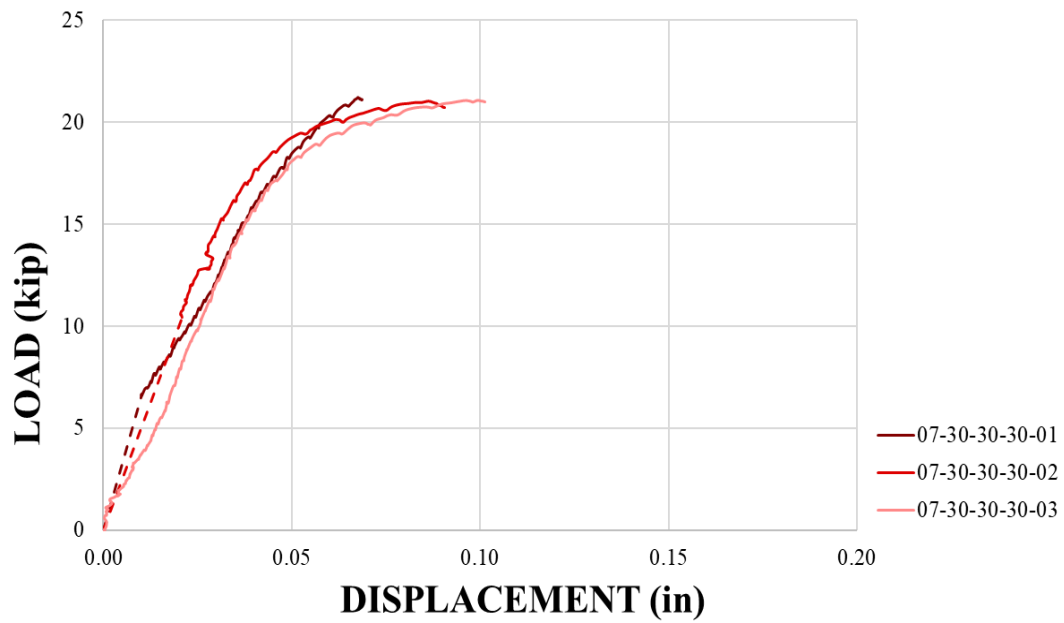


**Figure 5-9.** Material 7 Tested at 30°F (-1°C): Load vs. Displacement.

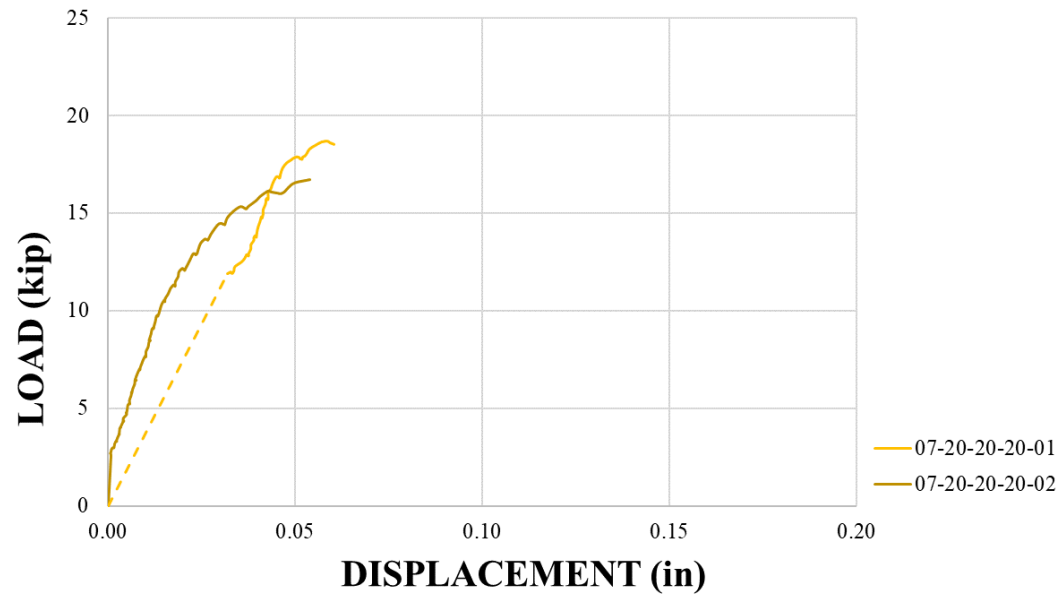


**Figure 5-10.** Material 7 Tested at 20°F (-7°C): Load vs. Displacement.

When cured and tested at ambient temperature, Material 7 in general exhibited a higher strength than its MSL but a lower strength than when cured and tested at a cold temperature. For instance, when cured and tested at ambient temperature with an initial concrete temperature of 30°F (-1°C), Material 7 failed at an average load of 19.46 kips (86.56 kN), shown in Figure 5-11. Likewise, included in Figure 5-11, when cured and tested at ambient temperature with an initial concrete temperature of 20°F (-7°C), Material 7 failed at an average load of 18.59 kips (82.69 kN). Curing temperature is observed to have little effect on the load capacity when tested at ambient temperature; Material 7 exhibited an average load of 18.56 kips (82.56 kN) and 17.90 kips (79.62 kN) when cured at 30°F (-1°C) and 20°F (-7°C) respectively, seen in Figure 5-12, still above the reported MSL but lower than the results of the cold temperature tests. Displacements for the Material 7 specimens tested at ambient temperature averaged 0.08 inches (2.03 mm) to 0.10 inches (2.54 mm). Overall, Material 7 exhibited less stiffness at ambient temperature tests than the cold temperature tests, which supports the behavior of adhesive materials under changing temperatures referred to in Section 2.3.

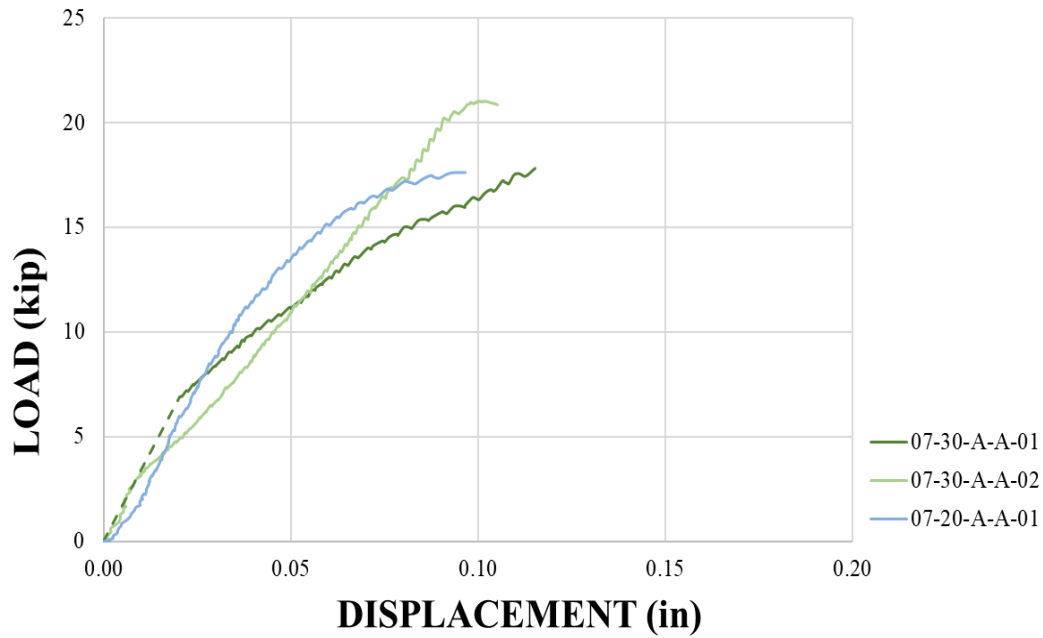


**Figure 5-11.** Material 7 Tested at Ambient: Load vs. Displacement.

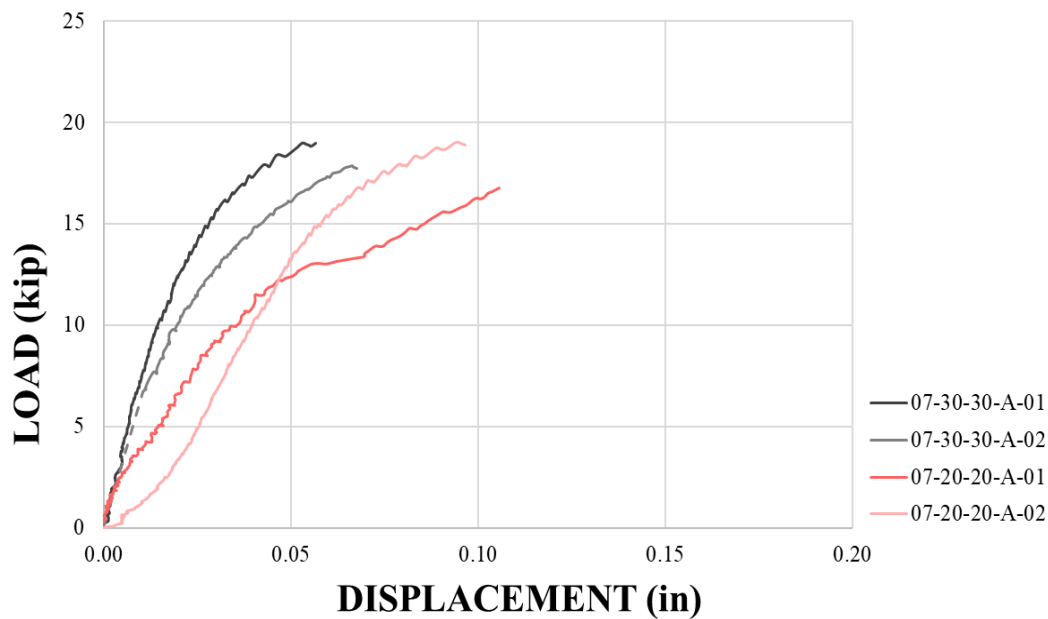


**Figure 5-12.** Material 7 Cured at 20°F (-7°C) and 30°F (-1°C) and Tested at Ambient: Load vs. Displacement

When cured at a cold temperature of 20°F (-7°C) and 30°F (-1°C) but tested at an elevated temperature of 110°F to 120°F (43°C to 49°C), as shown in Figure 5-13, Material 7 exhibited reduced strength in both cases, failing at 16.93 kips (75.31 kN) and 17.18 kips (76.42 kN) respectively. The results are expected due to the fact that Material 7 is specifically formulated for curing at colder ambient temperatures. A displacement of 0.08 inches (2.03 mm) was observed as well as reduced stiffness than that of both the cold temperature testing and ambient temperature testing, further supporting the expected behavior of adhesives described in Section 2.3.

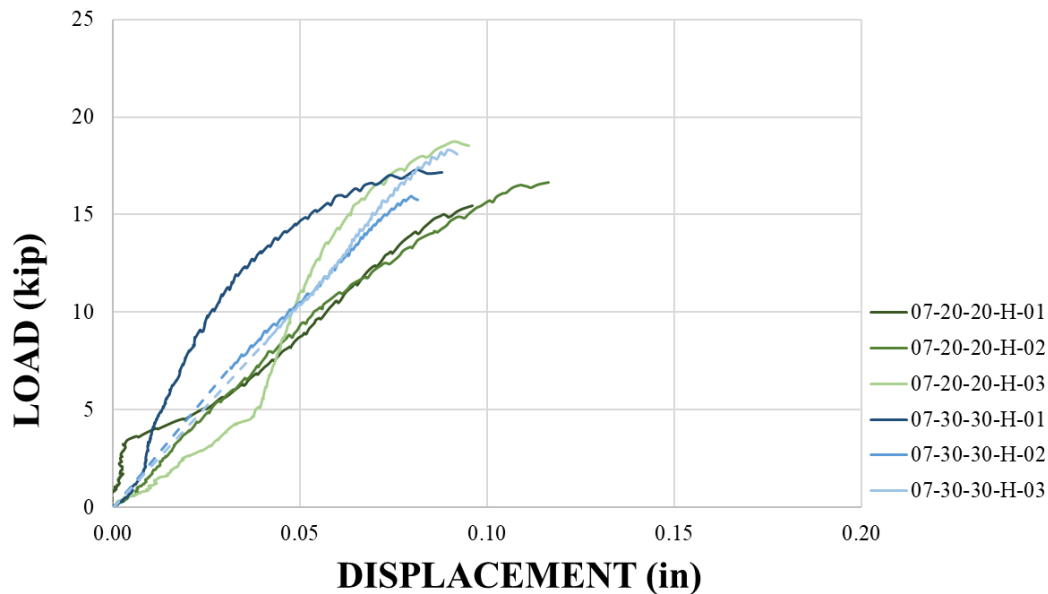


**Figure 5-13.** Material 7 Tested at 110°F to 120°F (43°C to 49°C): Load vs. Displacement

### 5.2.3. Material 2

Material 2, an epoxy adhesive with amine hardener, was observed to have an MSL of 18.33 kips (81.54 kN) and a coefficient of variation of 5% as per the short-term pullout tests defined by ASTM E488 and AASHTO TP-84 and conducted by Mendoza (2017).

To compare, Material 2 specimens were cured at ambient temperature and tested at 0°F (-18°C). One of the two specimens failed the anchor and therefore is not reported. The other specimen failed at 22.51 kips (100.13 kN), shown in Figure 5-14, in which the result is overlaid overtop the Material 2 short-term pullout tests performed by Mendoza (2017). A displacement of 0.14 inches (3.56 mm) is observed; however, it should be noted that the specimen that failed the anchor failed at approximately the same load, so the large displacement may have been incurred from yielding of the steel. While the 18% increase in load capacity is as expected, contrary to adhesive behavior described in Section 2.3, no changes were found in stiffness when comparing the cold temperature test to the results given by the test standard.

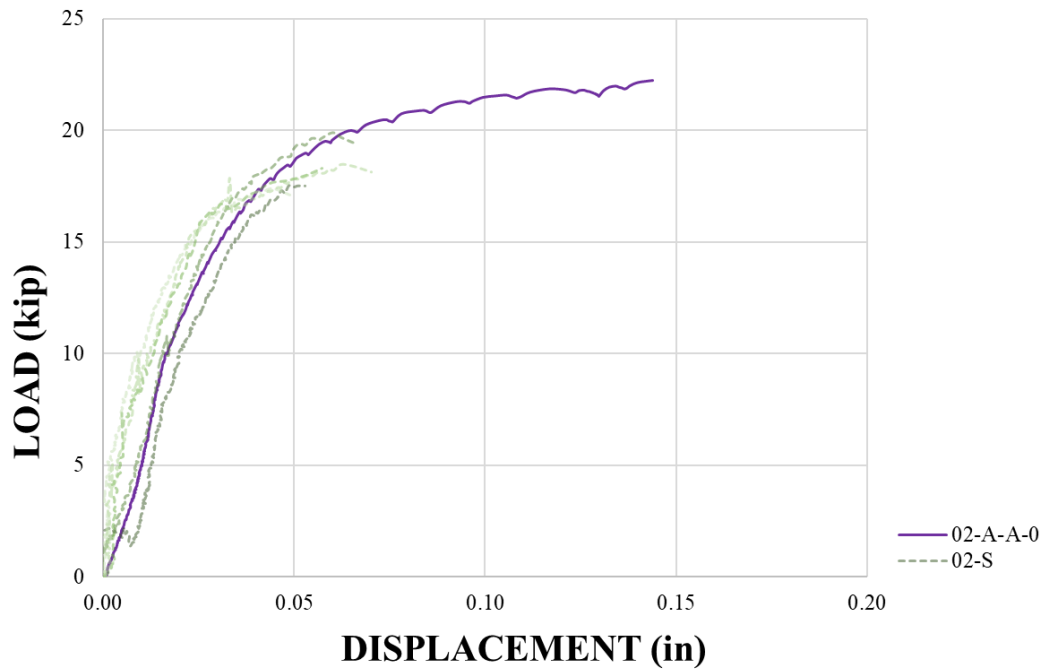


**Figure 5-14.** Material 2 Tested at 0°F (-18°C): Load vs. Displacement.

When cured and tested at an elevated temperature of 110°F to 120°F (43°C to 49°C), Material 2 failed at a load of 19.92 kips (88.51 kN), a 10% increase over the MSL,

at a displacement of 0.12 inches (3.048 mm). Results are shown in Figure 5-15. The increase in load capacity is incongruous with the adhesive behavior described in Section 2.3; however, Material 2 tested at an elevated temperature exhibits less stiffness than the test conducted in cold temperature, which is expected. Overall, more tests should be performed at both cold temperature and elevated temperature in order to gather more data to better investigate Material 2 behavior.

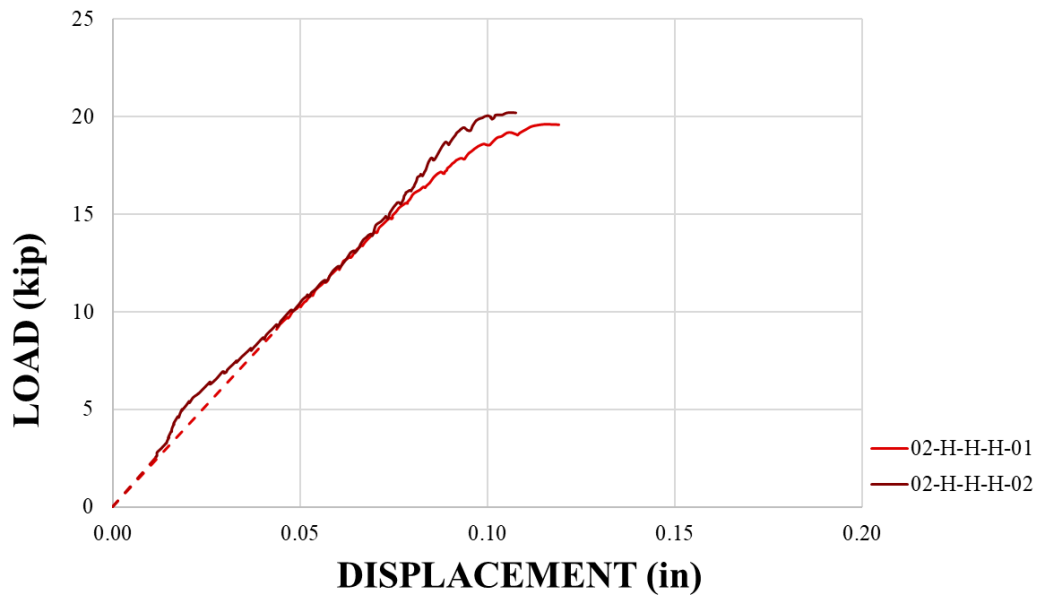


**Figure 5-15.** Material 2 Tested at 110°F to 120°F (43°C to 49°C): Load vs. Displacement.

#### 5.2.4. Reinforcing Bar Pullout Tests

Material 2 was tested with reinforcing bar anchors and compared with the short-term pullout tests conducted with threaded rod anchors by Mendoza (2017). In the tests performed by Mendoza (2017), it was found that the MSL of Material 2 for threaded rod was 18.33 kips (81.54 kN) with a standard deviation of 1.00 and a coefficient of variation of 5%. For the reinforcing bar tests, Material 2 was found to have an MSL of 20.08 kips

(89.32 kN) with a standard deviation of 1.56 and a coefficient of variation of 7%, shown in Figure 5-16 overlaid overtop the threaded rod results.

Overall, the reinforcing bar tests displayed a higher load capacity but more variation than the threaded rod tests. The lugs on the reinforcing bar may have had an effect on the bonding of the adhesive to the steel, providing the bar a 10% increase in capacity. In addition, the high displacements given by the reinforcing bar tests possibly indicate yielding of the anchor, which did not occur in the threaded rod tests; this may be due to the heat treatment undergone by the reinforcing bar, for which there is no guarantee that the strength of the bar matches the high strength of the threaded rod.

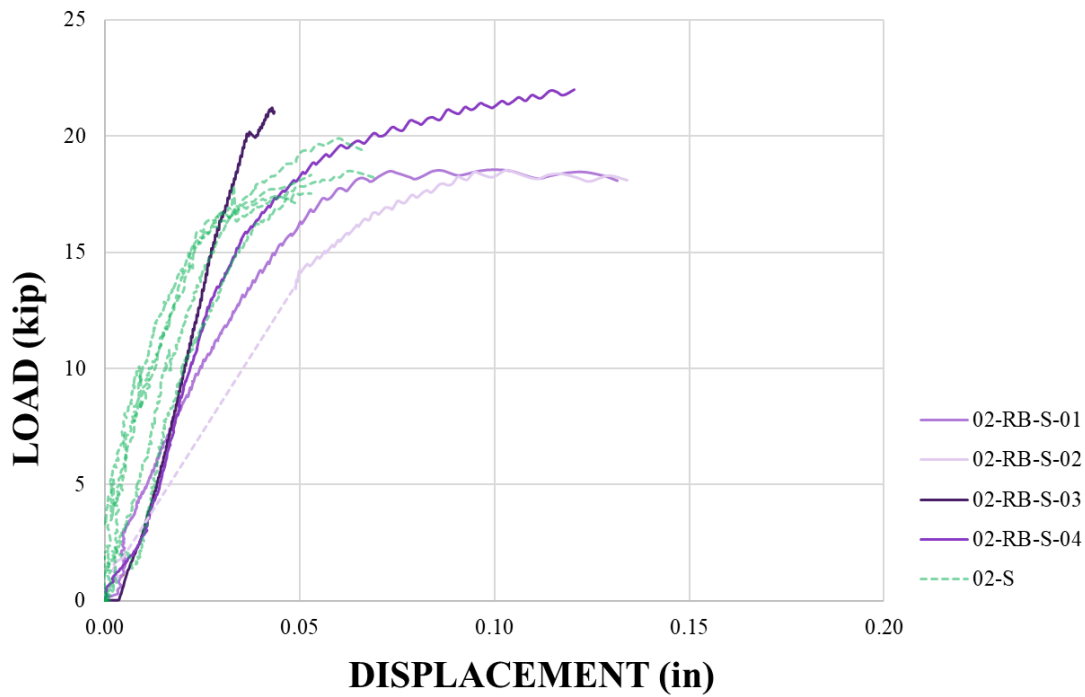


**Figure 5-16.** Material 2 Reinforcing Bar and Threaded Rod Results: Load vs. Displacement.

### **5.2.5. Exceptions to Manufacturer Specifications**

Several tests were performed outside of manufacturer specifications to observe the load capacity and displacement of the adhesives under extreme in-service temperature conditions in which the adhesive was not allowed enough time to fully cure. In addition, several anchors were cured at a temperature below or above the manufacturer specified temperatures. Material 1B and Material 2 exhibited a significant decrease in capacity in both cases.

Material 1B specimens cured at 25°F (-4°C) for 36 hours less than the manufacturer specifications and tested at 0°F (-18°C) gave an average load of 11.57 kips (51.47 kN), a reduction of 45% below MSL. These specimens failed at a displacement of 0.03 inches (0.76 mm) as seen in Figure 5-17 and show approximately the same stiffness as the other Material 1B tests, but at a significantly lower load capacity.

Material 2 specimens cured at 25°F (-4°C) and tested at 0°F (-18°C) were cured below the manufacturer recommended temperatures. These specimens failed at an average load of 10.46 kips (46.53 kN) or 44% below MSL, at a 0.03 inch (0.76 mm) displacement, shown in Figure 5-18.

Material 7 specimens cured and tested at an elevated temperature of 110°F (43°C) to 120°F (49°C) were cured above the manufacturer recommended temperature. Material 7 displayed a significant loss in capacity, failing at an average load of 15.61 kips (69.44 kN) or 12% less than the MSL, shown in Figure 5-19, which coincides with the overall observation that Material 7 has the highest performance in cold temperature and loses strength as temperatures increase.

Overall, not allowing materials time to sufficiently cure as well as curing outside manufacturer specified temperatures can severely degrade the performance, as expected. This highlights the importance of inspection in the field of not just the installation temperatures, but also the temperatures throughout the entire curing time, which can be as long as 7 days for temperatures at the low end of the recommended installation temperature for materials tested.

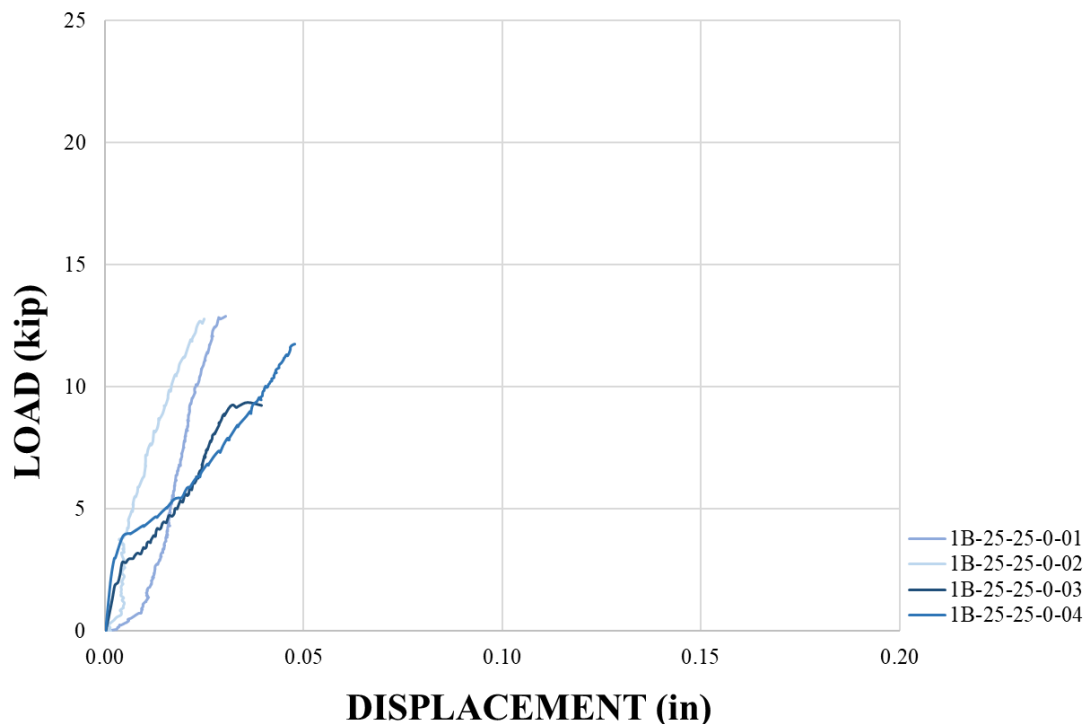


**Figure 5-17.** Material 1B Insufficiently Cured and Tested at 0°F (-18°C): Load vs. Displacement.

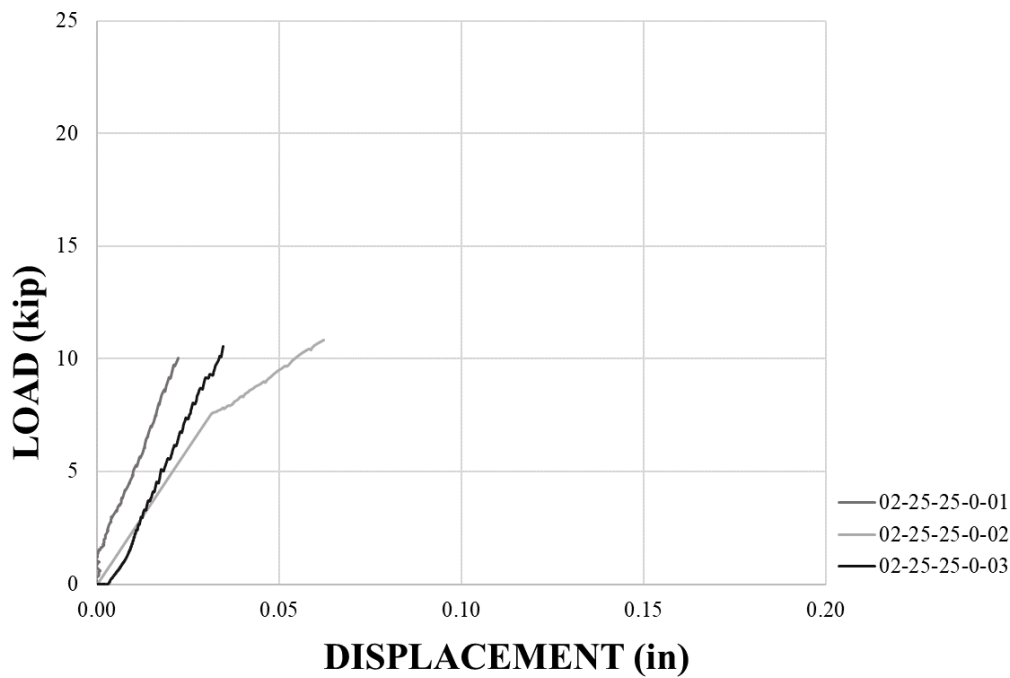


**Figure 5-18.** Material 2 Cured Outside Manufacturer Specifications and Tested at 0°F (-18°C): Load vs. Displacement.

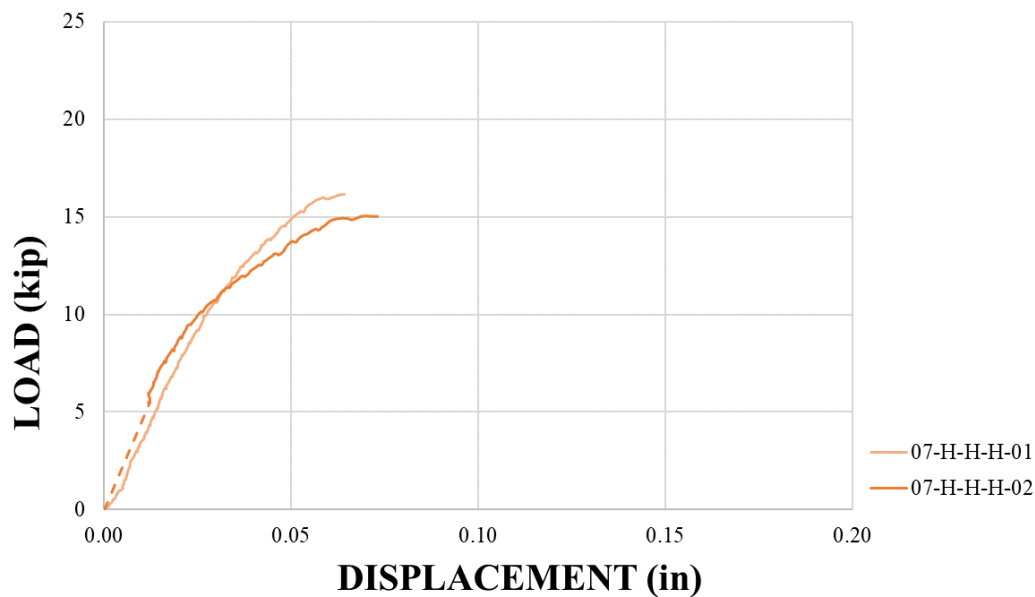


**Figure 5-19.** Material 7 Cured Outside Manufacturer Specifications and Tested at 110°F to 120°F (43°C to 49°C): Load vs. Displacement

### **5.3. Finite Element Analysis Results**

Four types of finite element models were assessed: two threaded rod models and two reinforcing bar models. Each model is subcategorized into whether a layer of adhesive is included at the bottom of the hole, then further subcategorized for variations in temperature, for which the material properties of the adhesive change. Displacement is measured from a selected node in the anchor 0.25 inches (0.64 cm) above the surface of the steel confining plate, which replicates the positioning of the displacement transducers on the physical specimens. A summary of the results is listed in Table 5-4.

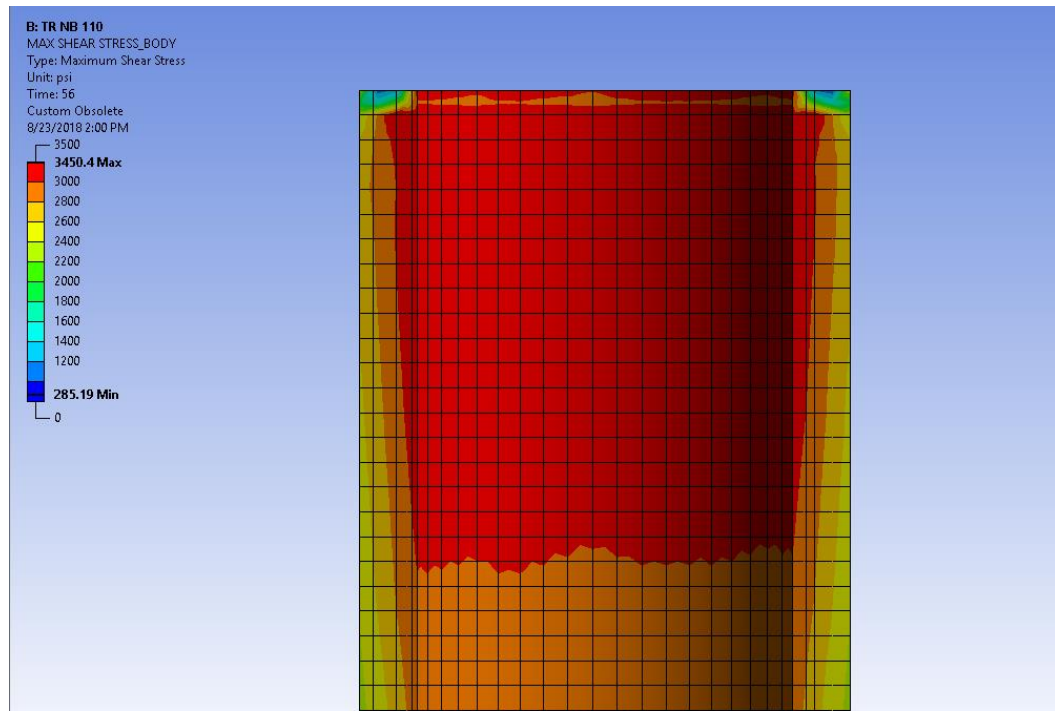
**Table 5-4. Summary of Finite Element Results**

MODEL	TEMPERATURE (°F)	LOAD (kip)	DISPLACEMENT (in)
TR-NB	77	21.67	0.02
	104	17.46	0.04
TR-CB	77	25.00	0.01
	104	19.17	0.03
RB-NB	77	23.50	0.03
	104	16.67	0.03
RB-CB	104	20.42	0.03

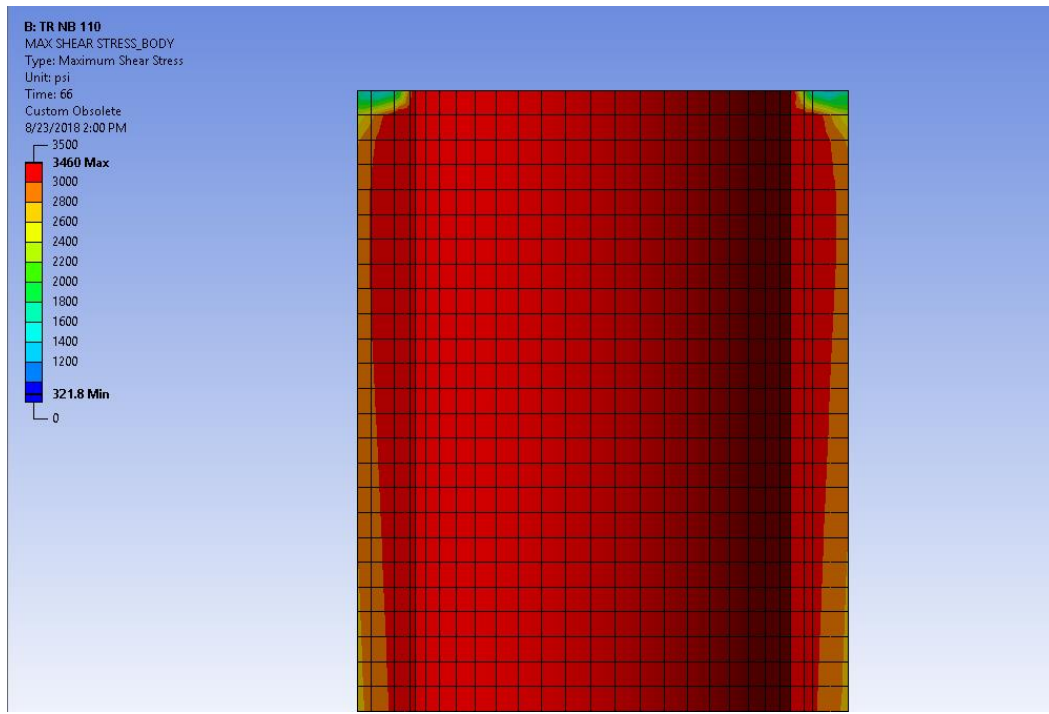
#### **5.3.1. TR-NB**

Upon applying a tensile force to the TR-NB model with assumed adhesive properties at 104°F (40°C), the adhesive layer reaches a maximum shear stress of 3464 psi (23.88 MPa) and a maximum equivalent stress of 6000 psi (41.37 MPa), the latter of which matches the ultimate stress of the adhesive at 104°F (40°C) provided by the stress-strain curve in Section 4.2.3. Shear stress is defined as the force per unit area acting parallel to the surface of the hole, and in the following figures, refers to the shear between

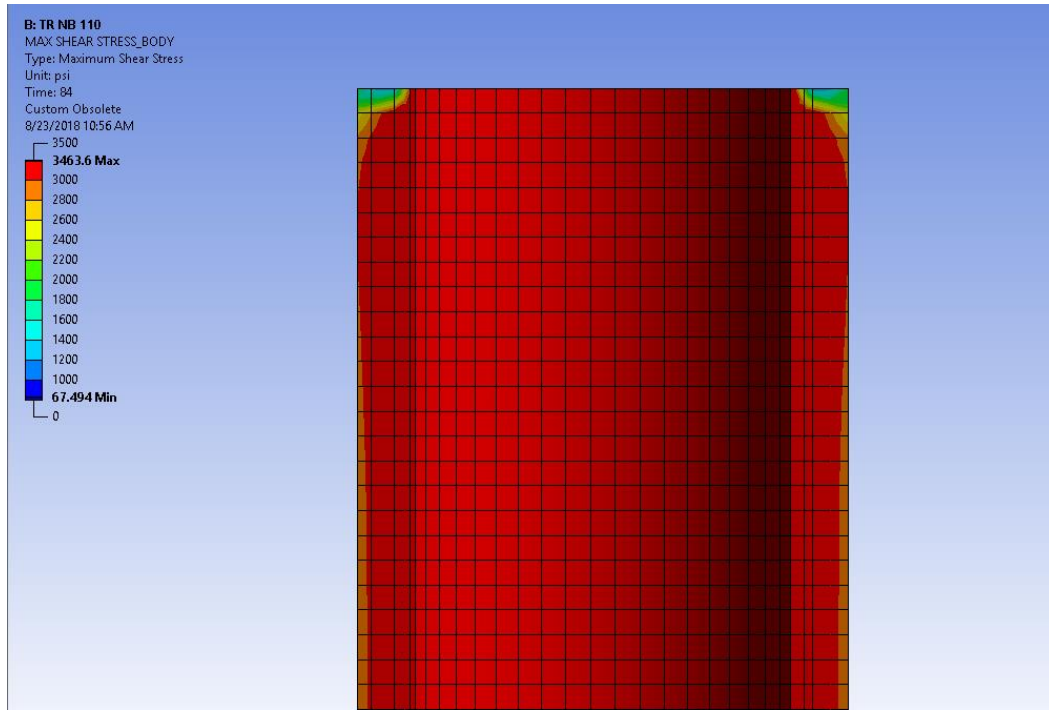
the anchor rod, adhesive, and concrete interfaces. From further studying of the results, it was found that as time steps advanced and the load increased, the adhesive reached peak shear stress first at the steel/adhesive interface, before spreading down the length of the adhesive and through to the outside surface, or the concrete/adhesive interface, as seen in Figure 5-20. From this behavior, failure in the adhesive layer is assumed to occur at the point at which the peak shear stress of the adhesive has distributed evenly along the inner face and penetrates through the adhesive layer to the outer face.



(a)



(b)

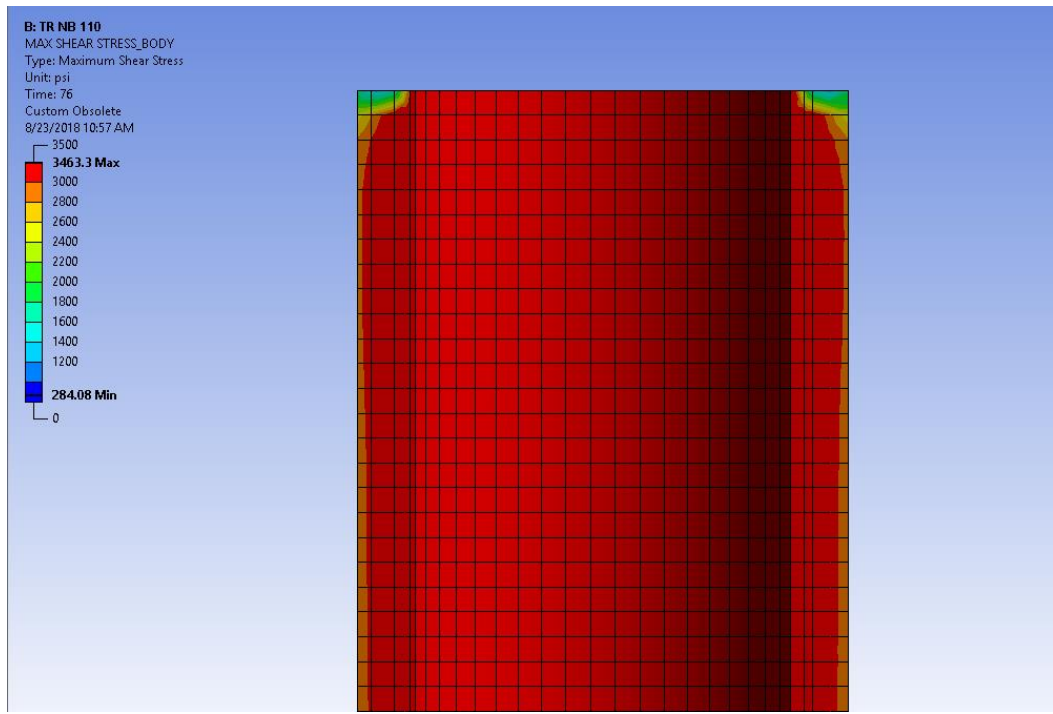


(c)

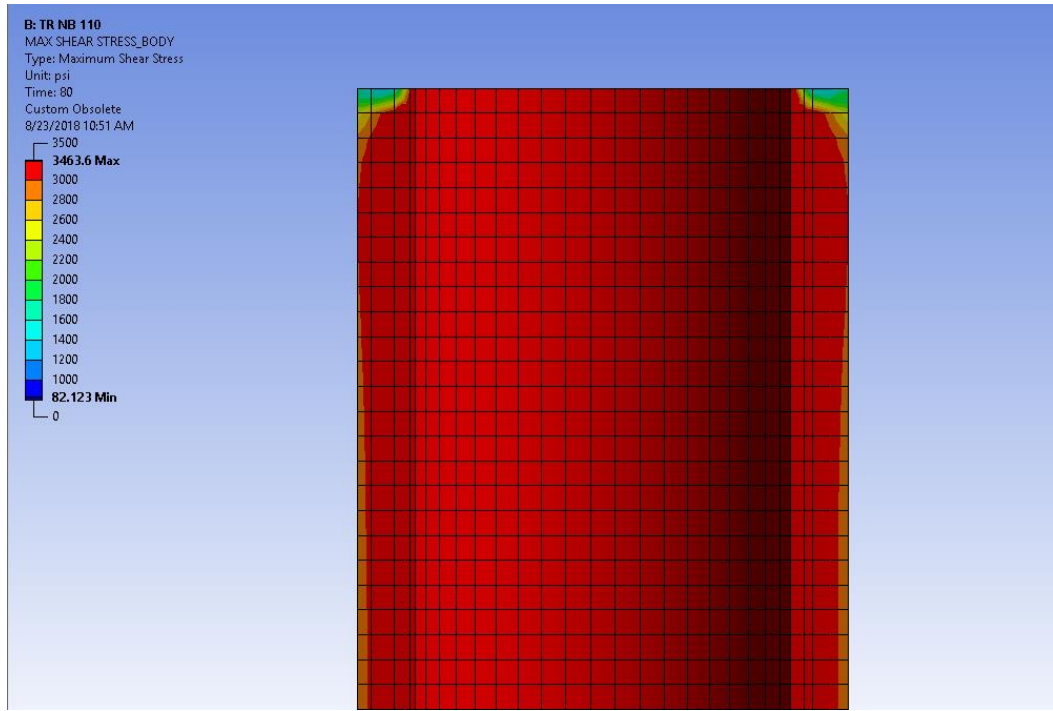
**Figure 5-20.** Shear stress contour plot of the adhesive layer at time 12 kips (53 kN) (a), 14 kips (62 kN) (b), and 18 kips (80 kN) (c).

From the defined failure criterion, the TR-NB model with assumed adhesive properties at 104°F (40°C) was found to reach failure at 17.46 kips (77.67 kN), which will thus be referred to as STL. Progression of shear stress in the contour plot for the time step before failure, at failure, and after failure is shown in Figure 5-21. Figure 5-22 shows an isometric section cut of the TR-NB model at failure, in which spots of peak shear stress are visible on the outside surface of the adhesive layer. Figure 5-23 shows the contour plot of the equivalent stress. Figure 5-24 shows the contour plot of Y-direction normal stress, or the force per unit area acting normal to the applied surface, in the adhesive at the failure load.

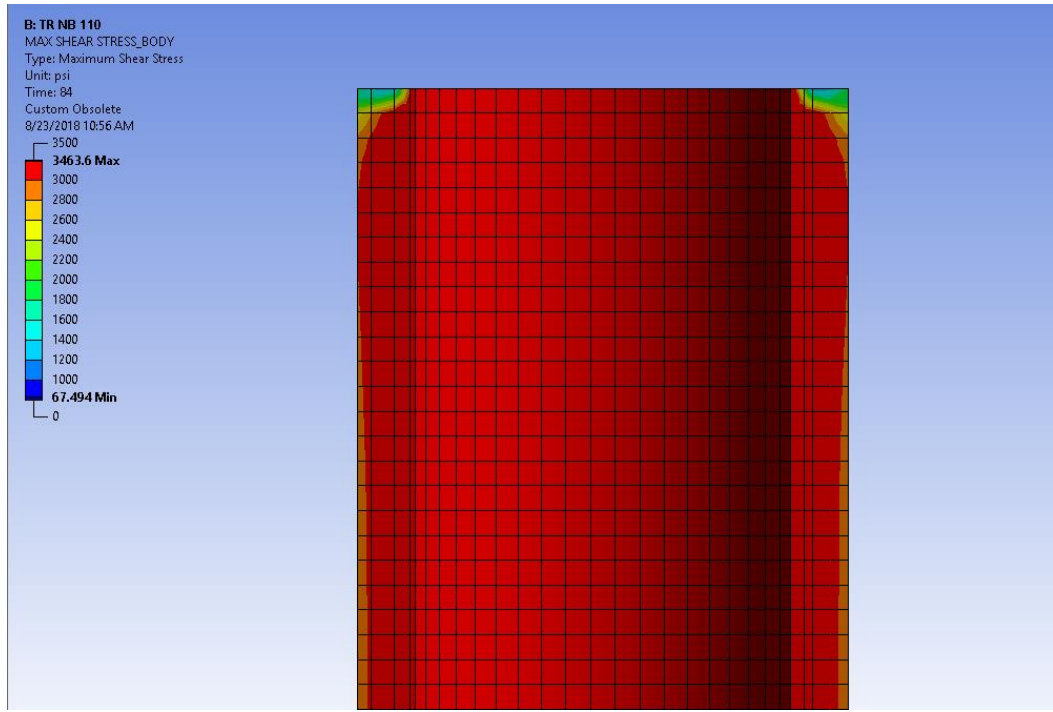
A displacement of 0.04 in (1.02 mm) was observed in the anchor node at STL. This coincides with the Material 2 physical testing specimens tested at 110°F to 120°F (43°C to 49°C), for which an MSL of 18.33 kips (81.54 kN) and failure at 0.04 inches (1.02 mm) of displacement was determined. Shown in Figure 5-25 are the load vs. displacement results for Material 2 compared with the load vs. displacement result given by TR-NB at 104°F (40°C), as well as the point at which failure in the TR-NB model is assumed. This point matches closely with the results of Material 2 physical testing and provides confidence in the defined failure criteria for threaded rod anchors. In addition, as loading decreases to 80% STL, 60% STL, and 40% STL, the distribution of shear stress at the hole diameter decreases drastically from the surface to the bottom of the hole, shown in Figure 5-26. At 100% STL, the stress distribution is constant, indicating that the adhesive has an even distribution of stress along the outside face.



(a)



(b)



(c)

**Figure 5-21.** Shear stress contour plot of the adhesive layer of the TR-NB model at 104°F (40°C) before failure (a), at failure (b), and after failure (c) as load increases.

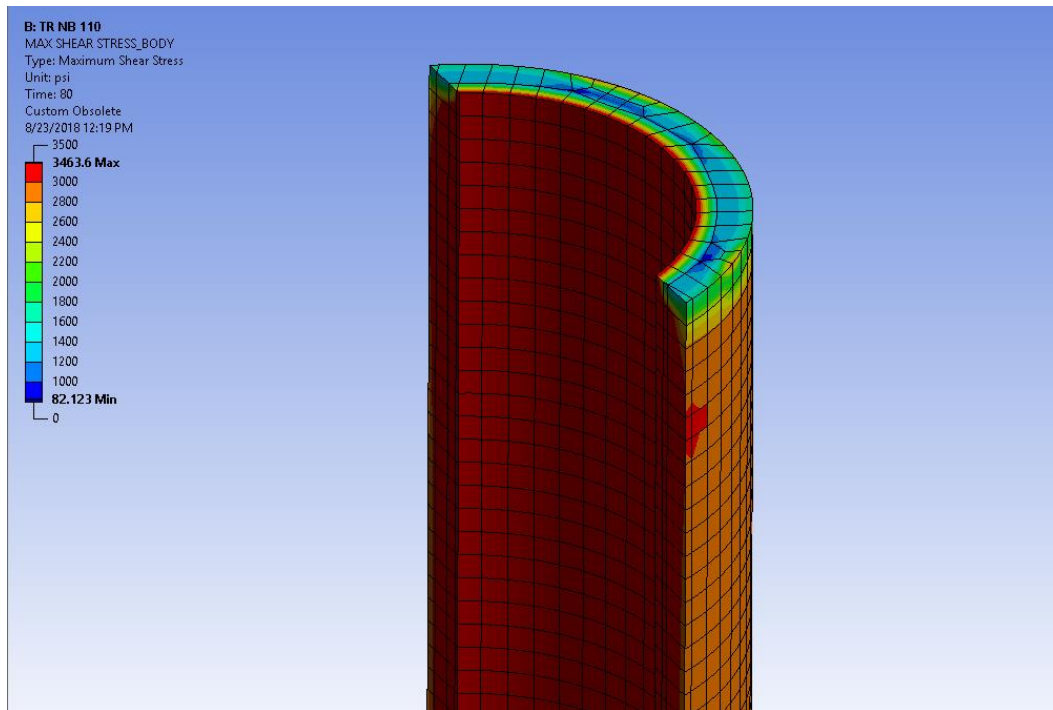


**Figure 5-22.** Section cut of the adhesive layer of the TR-NB model at 104°F (40°C).

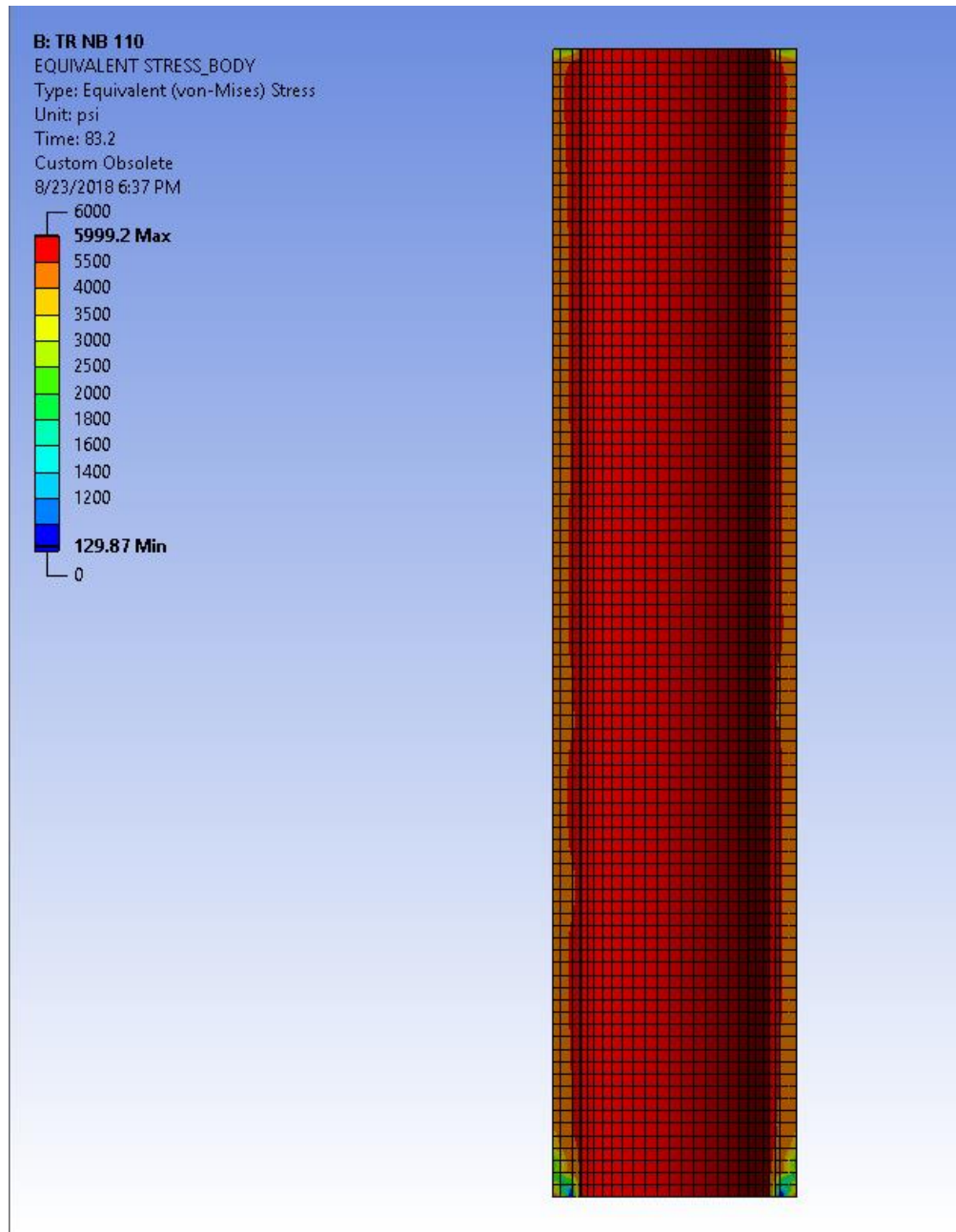


**Figure 5-23.** Contour plot of the equivalent stress in the adhesive layer at 104°F (40°C) at failure.

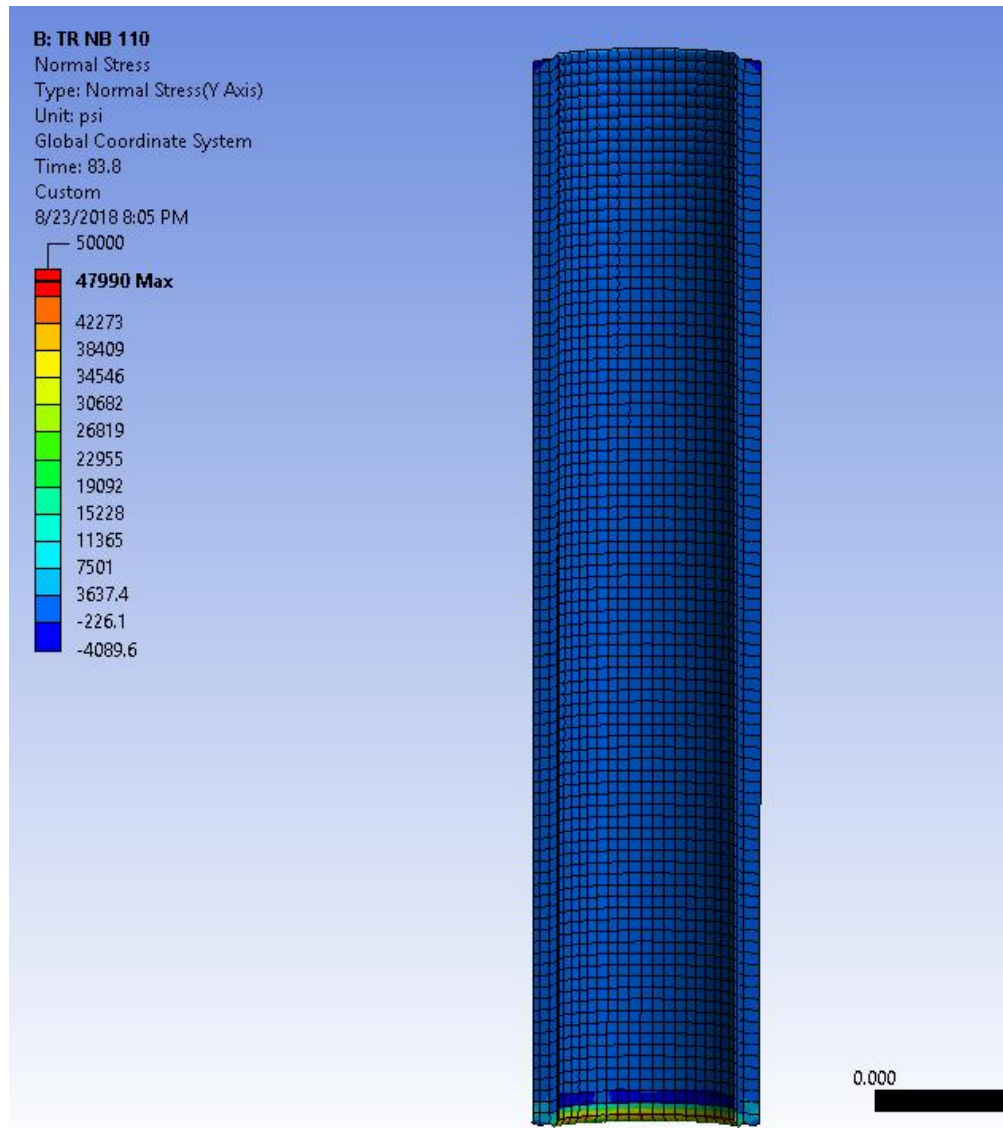


**Figure 5-24.** Contour plot of the normal vertical-direction stress in the adhesive layer at 104°F (40°C) at failure.

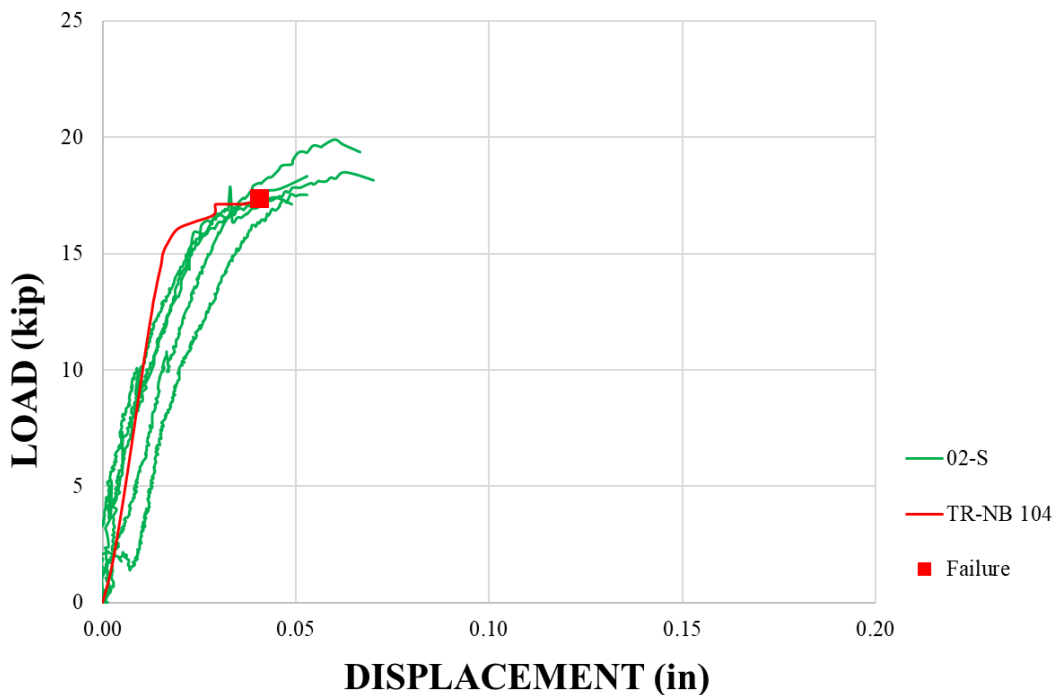


**Figure 5-25.** Material 2 Threaded Rod Results and the TR-NB Model Results with assumed adhesive material properties at 104°F (40°C): Load vs. Displacement.

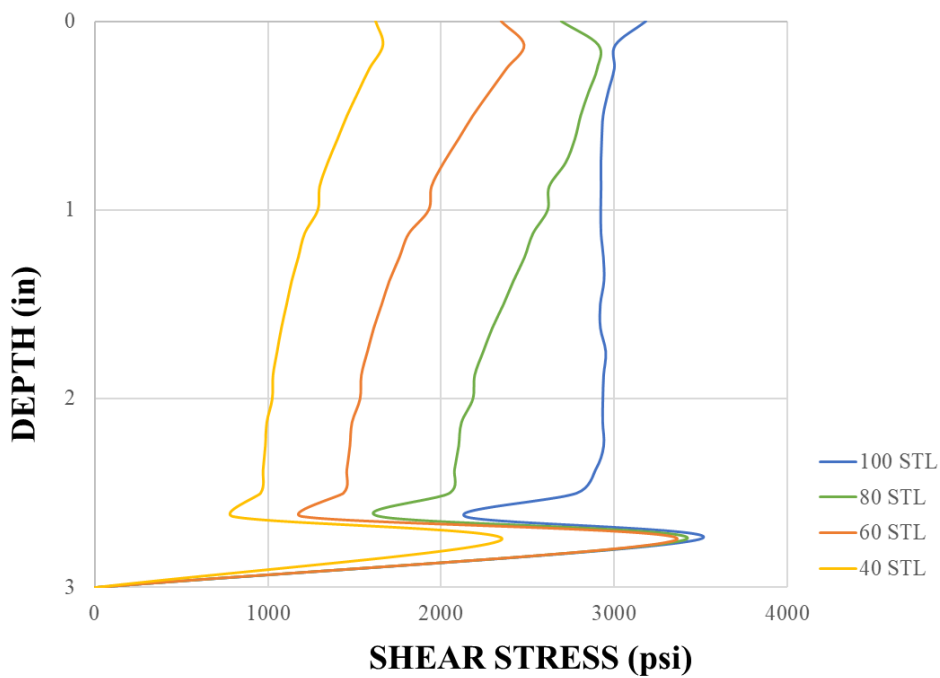


**Figure 5-26.** Shear Stress Distribution at the hole diameter for TR-NB at 104°F (40°C).

Upon applying a tensile force to the TR-NB model with assumed adhesive material properties at 77°F (25°C), the maximum shear stress in the adhesive was observed to be 4850 psi (33.44 MPa) and the maximum equivalent stress was observed to be 8400 psi (57.92 MPa), which coincides with the material properties defined in Section 4.2.3. The adhesive exhibits failure at 21.67 kips (96.39 kN) with an observed displacement of 0.02 inches (0.58 mm). A contour plot of the failure is shown in Figure 5-27.

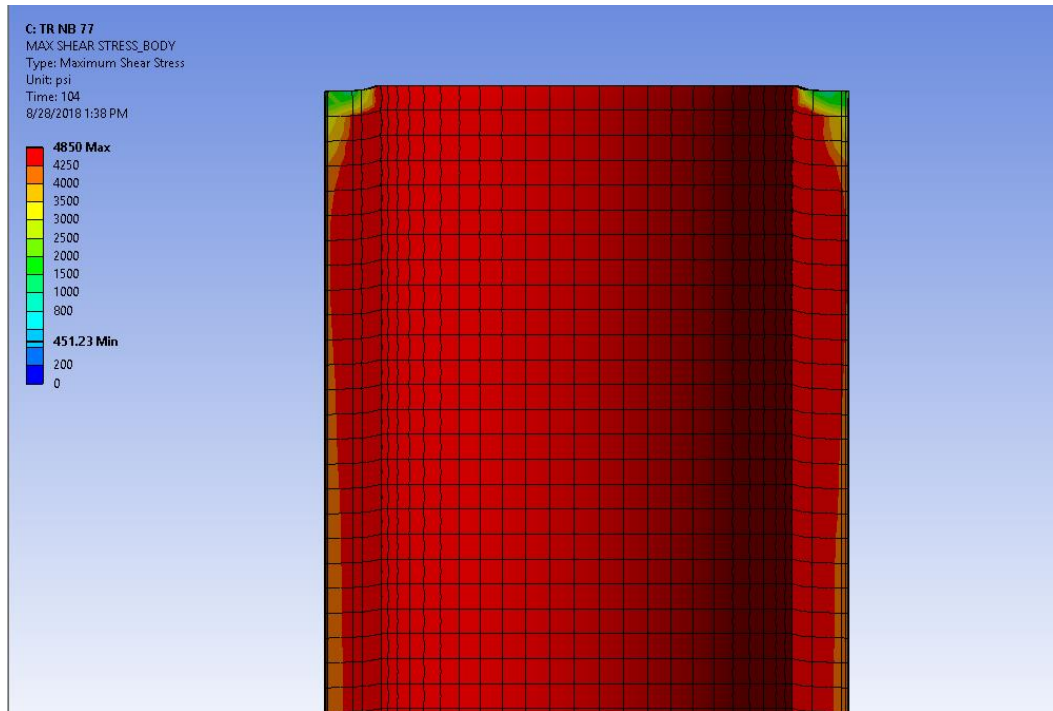


**Figure 5-27.** Shear stress contour plot of the adhesive layer of the TR-NB model at 77°F (25°C) at failure.

The TR-NB model run with assumed adhesive material properties at -40°F (-40°C) gives a maximum shear stress of 6092 psi (42 MPa) and a maximum equivalent stress of 10533 psi (72.62 MPa) for the adhesive, which adheres to the material properties

calculated in Section 4.2.3. However, failure in the adhesive could not be observed in this model based on the defined failure criteria because the shear stress distribution did not extend through the full length of the adhesive before the steel anchor exhibited failure, rendering the system unsolvable under further load. This implies that the adhesive fails beyond 25 kips, which coincides with the adhesive material properties under different temperatures defined in Section 2.3, in which a 25% increase in strength is observed in adhesives as temperatures decrease from 77°F (25°C) to -40°F (-40°C). In the physical tests, Material 2 failed at a 18% higher load capacity when the testing temperature decreased from 110°F to 120°F (43°C to 49°C) to 0°F (-18°C), following a similar trend, while Material 1B experienced steel failure in 50% of the cold temperature tests.

### **5.3.2. TR-CB**

Upon applying a tensile force to the TR-CB model with assumed adhesive material properties at 104°F (40°C), the adhesive layer was observed to reach failure at 19.17 kips (85.27 kN) of force. A maximum shear stress of 3462 psi (23.87 MPa) and a maximum equivalent stress of 5997 psi (41.35 MPa) was determined, and a displacement of 0.03 in (0.76 mm) is observed in the anchor node at this point. The stress contour plot at failure is shown in Figure 5-28. Compared to the TR-NB model at 104°F (40°C), the TR-CB model exhibits 10% more capacity following the failure criterion defined in Section 5.3.1. This implies that the additional layer of adhesive at the bottom of the hole contributes to further distributing the stress in the adhesive body, enabling the adhesive to take more load. The shear stress distribution plot is shown in Figure 5-29.

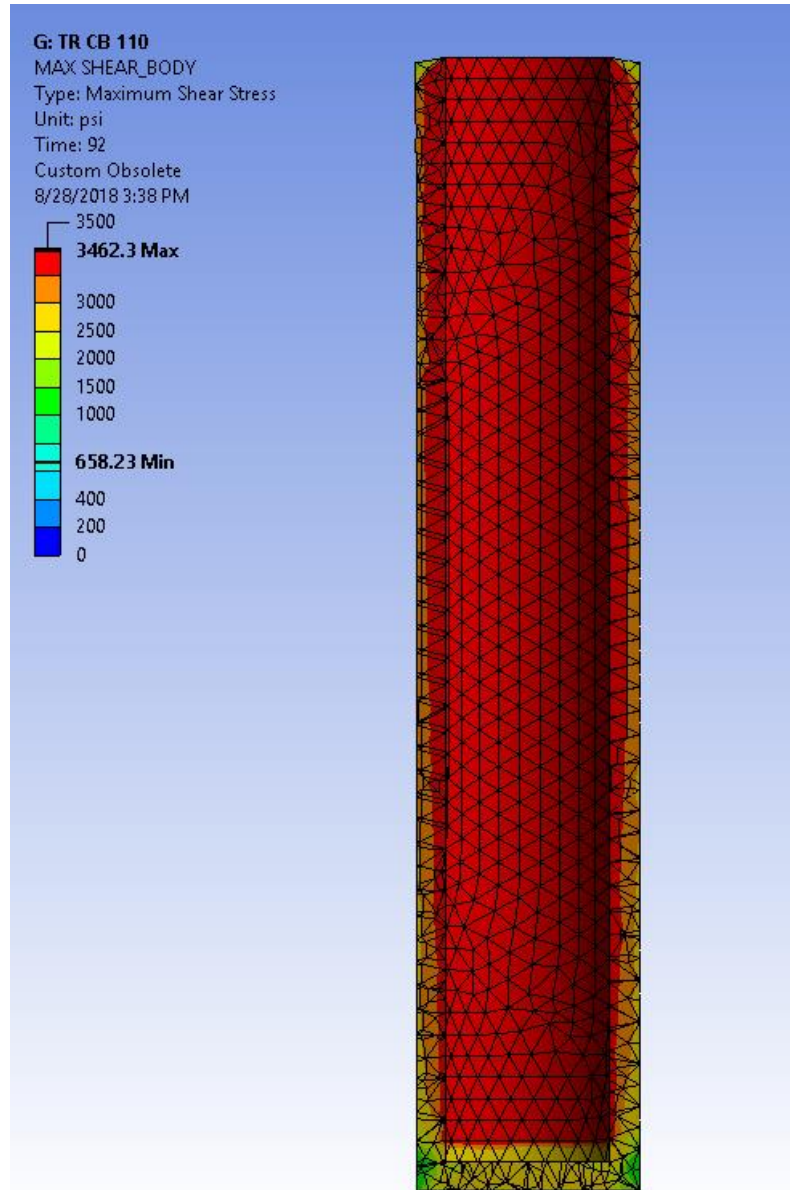


**Figure 5-28.** Shear stress contour plot of the adhesive layer of the TR-CB model at 104°F (40°C) at failure.

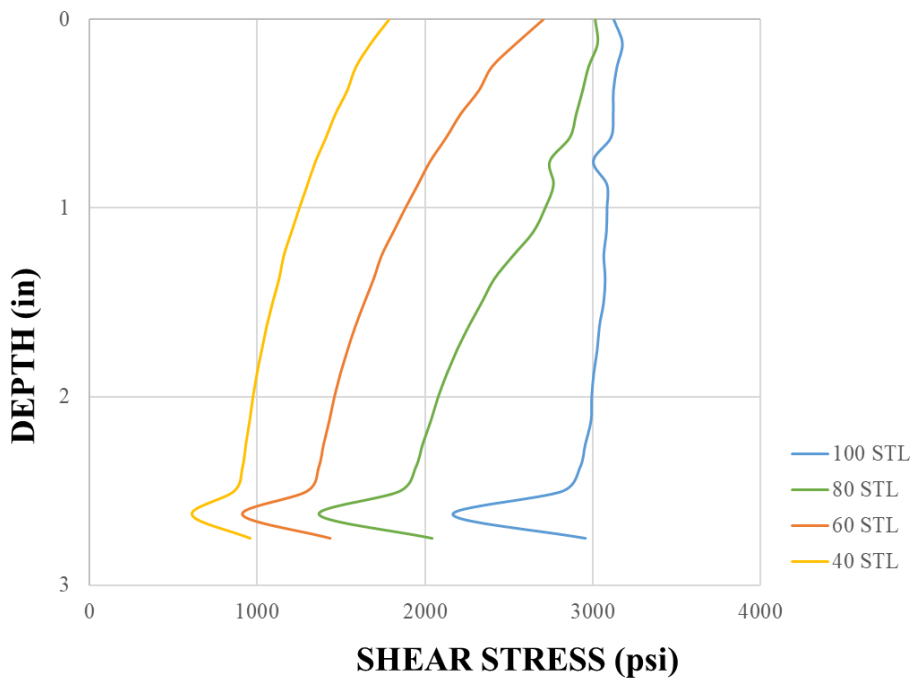


**Figure 5-29.** Shear Stress Distribution at the hole diameter for TR-CB at 104°F (40°C)

At 77°F (25°C), failure occurs at 25 kips (11.21 kN), a 20% increase in load capacity from the TR-NB model. The maximum shear stress and maximum equivalent stress at this point was found to be 4848 psi (33 MPa) and 8397 psi (57 MPa) respectively, and the displacement was observed to be 0.01 in (0.25 mm). The stress contour plot at failure, defined in Section 5.3.1, is shown in Figure 5-30.

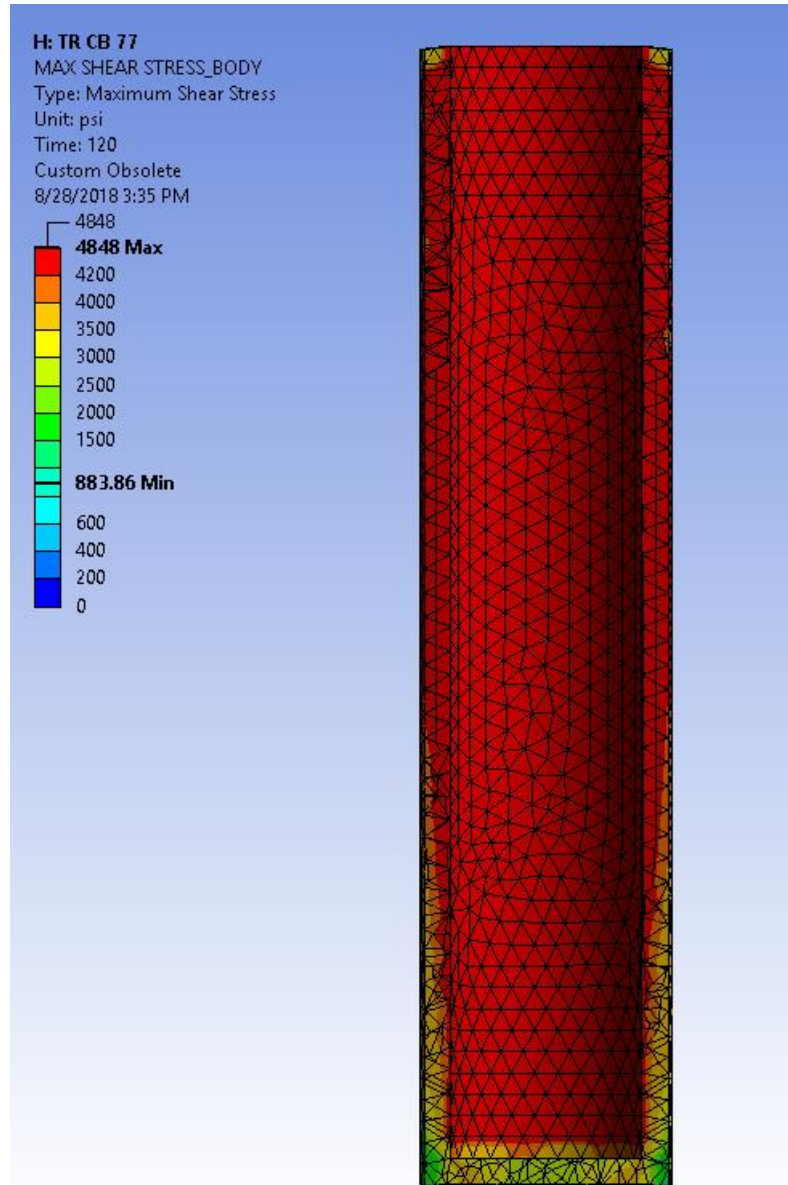


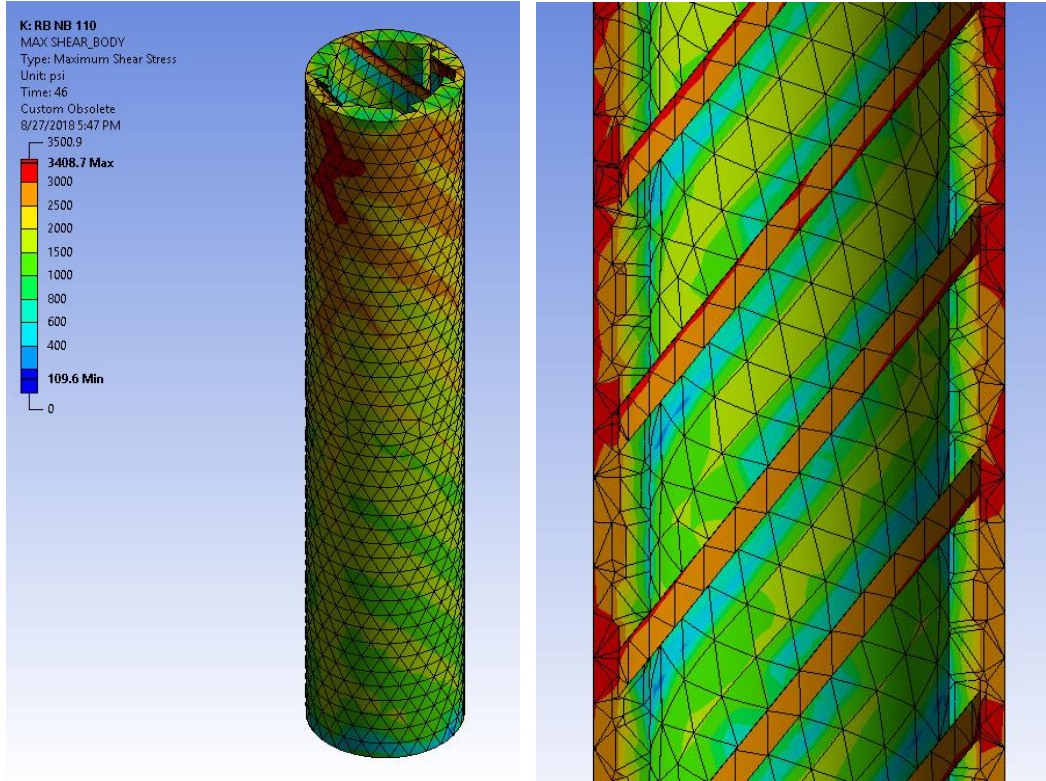
**Figure 5-30.** Shear stress contour plot of the adhesive layer of the TR-CB model at 77°F (25°C) at failure.

At -40°F (40°C), the TR-CB model reaches a maximum shear stress and maximum equivalent stress of 6090 psi (42 MPa) and 10550 psi (73 MPa) respectively. Similarly to the TR-NB model, failure could not be observed based on the defined failure criteria due to the anchor failing before the peak stress could distribute evenly along the

inner surface of the adhesive. The Material 1B pullout tests reflect this in that steel failure occurred before adhesive failure in 50% of the cold temperature tests.

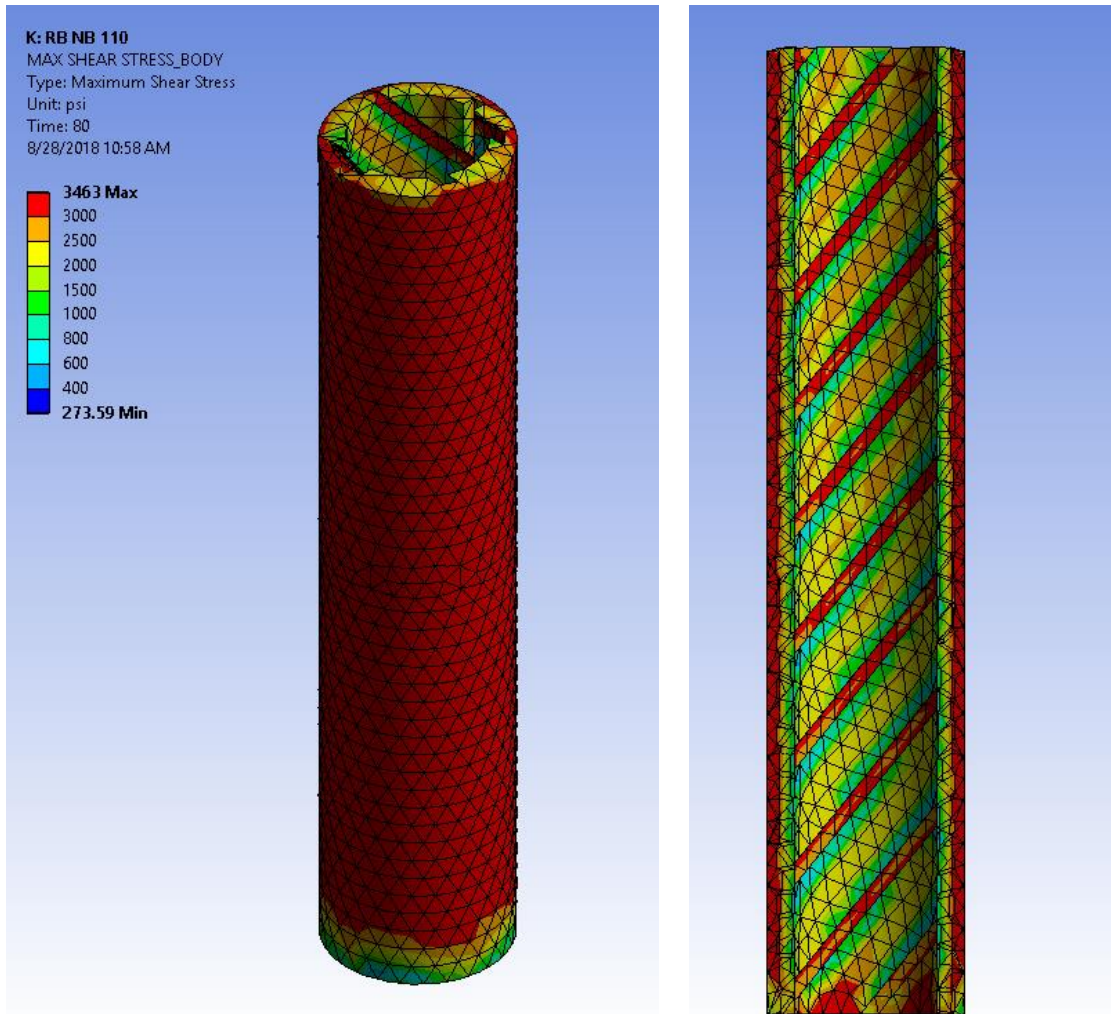
### **5.3.3. RB-NB**

The reinforcing bar finite element model results show a significant change in shear stress distribution compared with the threaded rod results. While the threaded rod models display the highest shear stress initially on the steel/adhesive interface that gradually spreads down the length of the adhesive as well as laterally to the adhesive/concrete interface, the reinforcing bar models display the highest shear stress initially alongside the adhesive/concrete interface and around the reinforcing bar lugs before gradually spreading throughout the rest of the adhesive, following the contours of the lugs. The force applied to the anchor is transferred through the lugs into the adhesive, creating pockets of high stress at the edge of the lugs and pockets of low stress between the lugs. This can be seen in Figure 5-31.

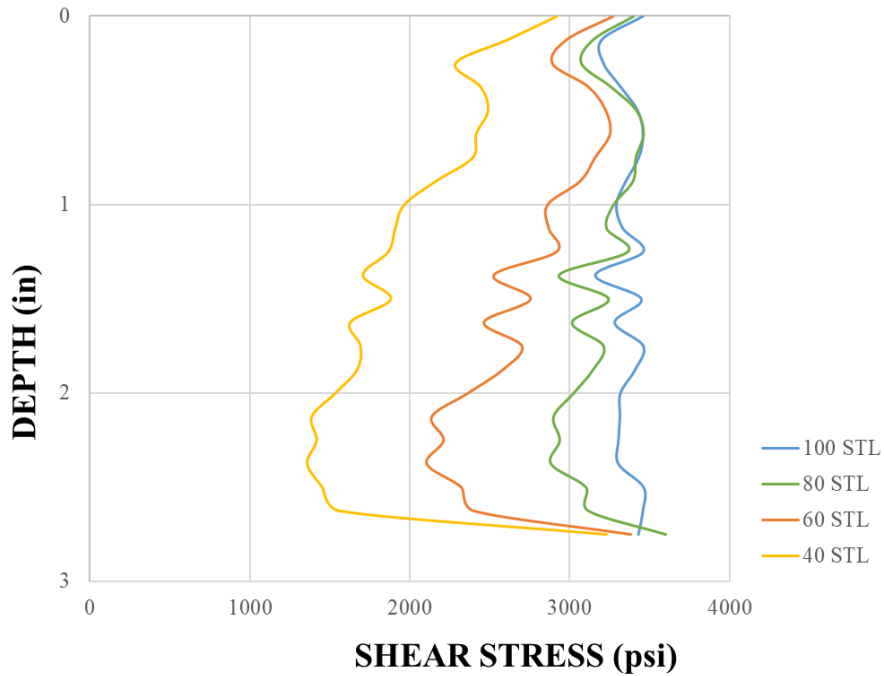


**Figure 5-31.** Shear stress pattern, which follows the shape of the reinforcing bar lugs (left), and the pockets of high stress at the lugs and low stress between the lugs (right).

Because of the differences in behavior, adjustments to the failure criterion were made for the reinforcing bar models. It was found that as the applied load increased, the high shear stress at the adhesive/concrete interface would eventually spread down the entire length of the adhesive, as seen in Figure 5-32, and create a consistent patterned distribution of stress on the inner face at 100% STL, seen in Figure 5-33. From this observation, it was assumed that failure occurs in the reinforcing bar models at the point at which the peak stress in the adhesive has spread consistently across the outer surface of the layer.



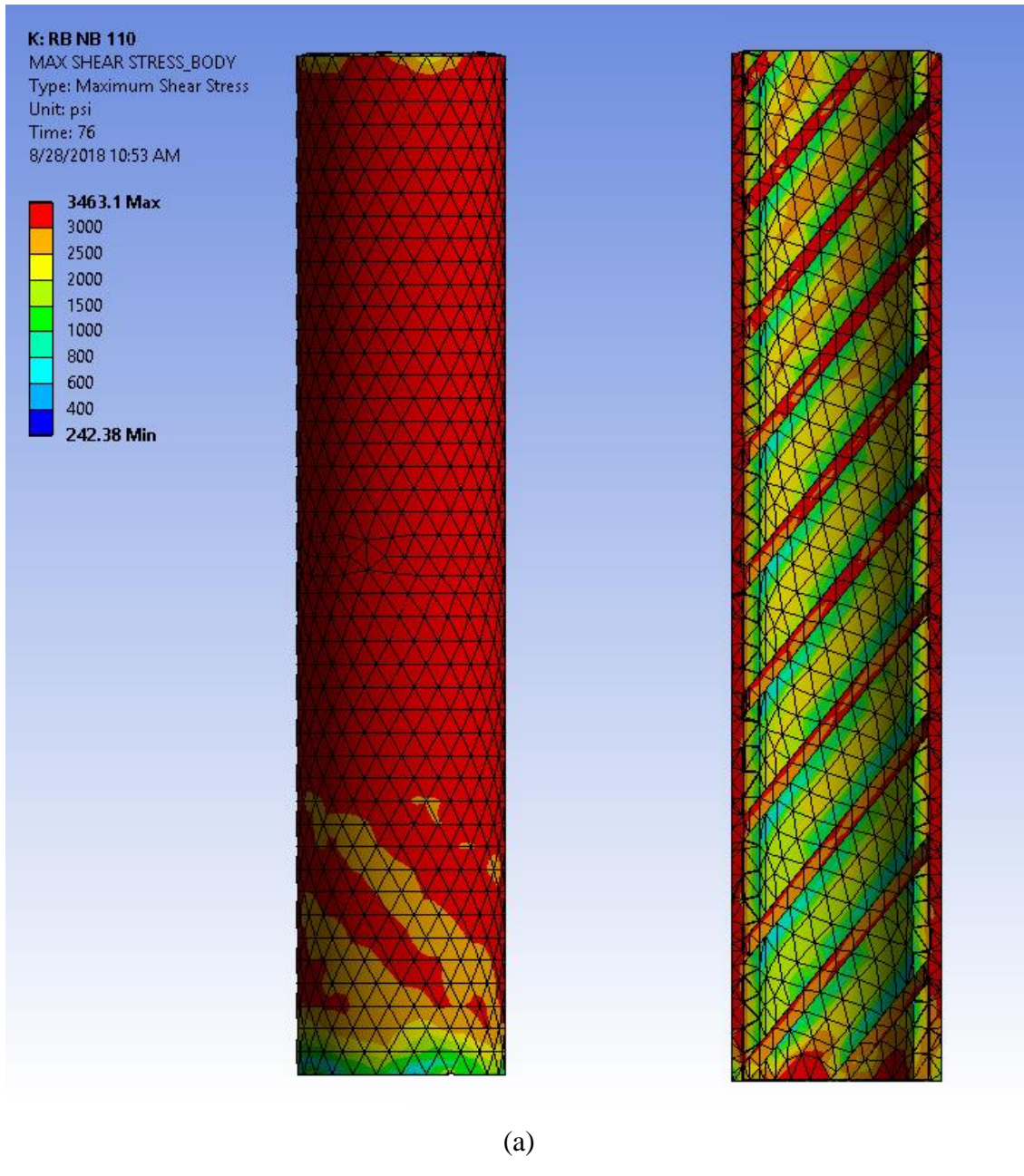
**Figure 5-32.** Evenly distributed shear stress on the outside face of the adhesive (left) and consistently distributed shear stress on the inside of the adhesive (right).

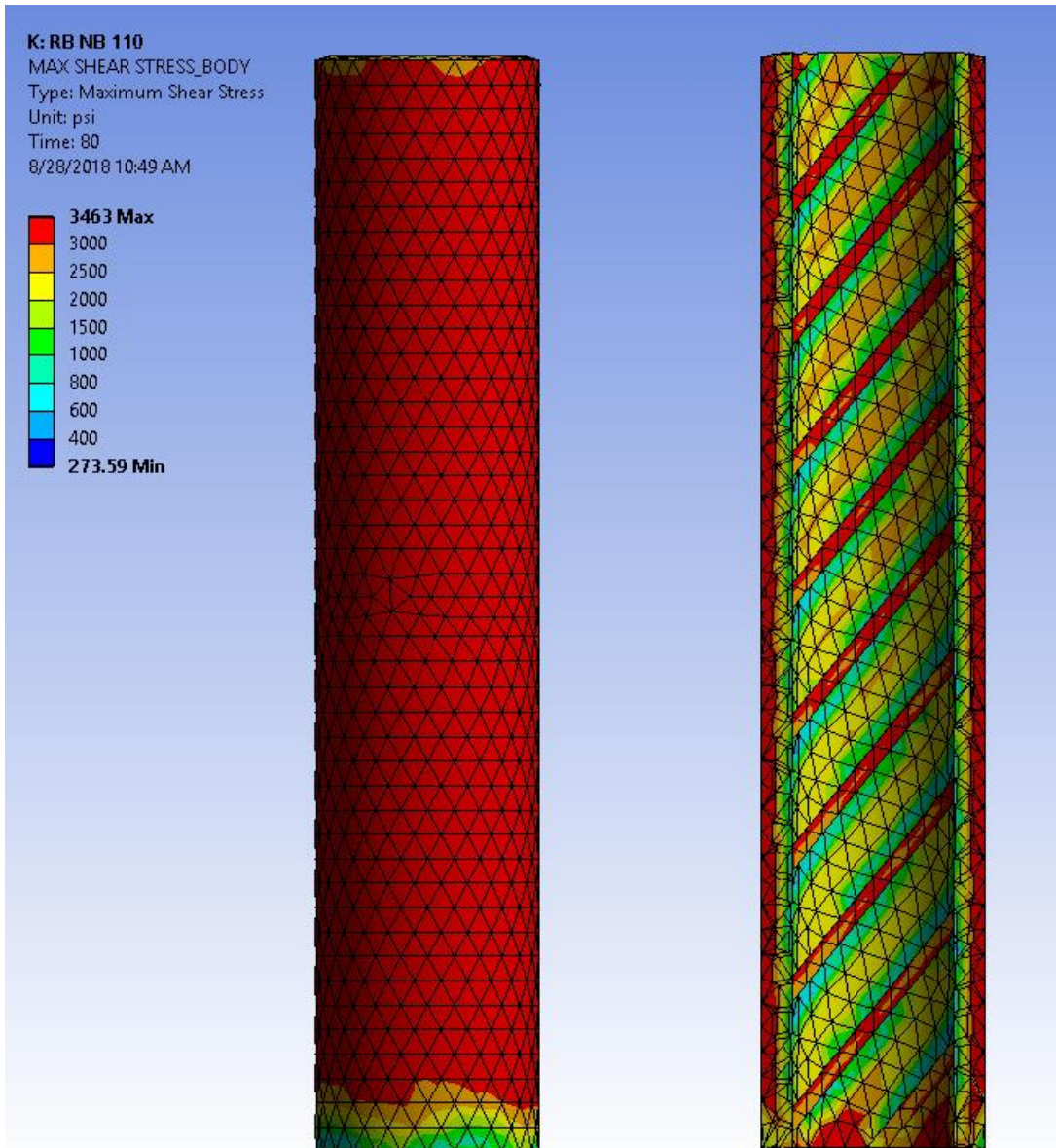


**Figure 5-33.** Shear Stress Distribution at the steel/adhesive interface for RB-NB at 104°F (40°C).

The RB-NB model run with assumed adhesive properties at 104°F (40°C) exhibits failure at 16.67 kips at a displacement of 0.03 in (0.76 mm). A maximum shear stress of 3463 psi and a maximum equivalent stress of 6085 psi was observed. Shown in Figure 5-34 are the contour plots of the RB-NB adhesive layer before failure, at failure, and after failure. Compared with the TR-NB model, the RB-NB model shows a reduced load capacity as well as a reduced displacement. Compared with the Material 2 reinforcing bar pullout tests, the load vs. displacement curve of the RB-NB model falls between the plots of the pullout tests and fails along the same trajectory, shown in Figure 5-35. Included in Figure 5-35 is the assumed failure point of the RB-NB model according to the failure criteria of the TR models, which shows that changing the failure criteria for the RB models gives a more accurate comparison of load capacity and strain to the reinforcing bar physical test results. Figure 5-36 gives the shear stress distribution of the adhesive

layer at the hole diameter, displaying an even distribution at 100% STL and a gradual decrease in stress at the deepest portion of the hole as the load is reduced.





(b)

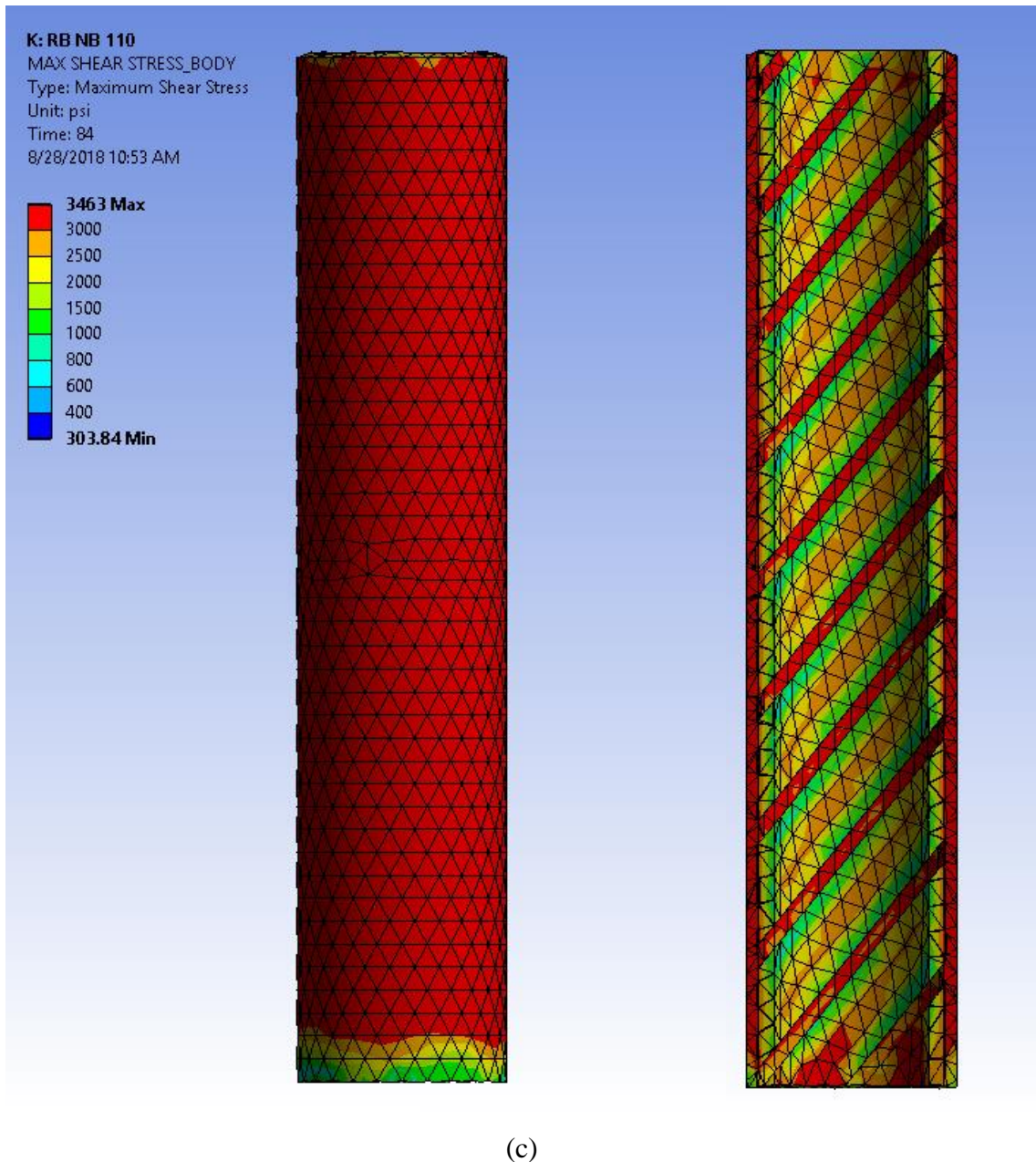


**Figure 5-34.** Shear stress contour plot of the adhesive layer of the RB-NB model at 104°F (40°C) before failure (a), at failure (b), and after failure (c) as load increases.

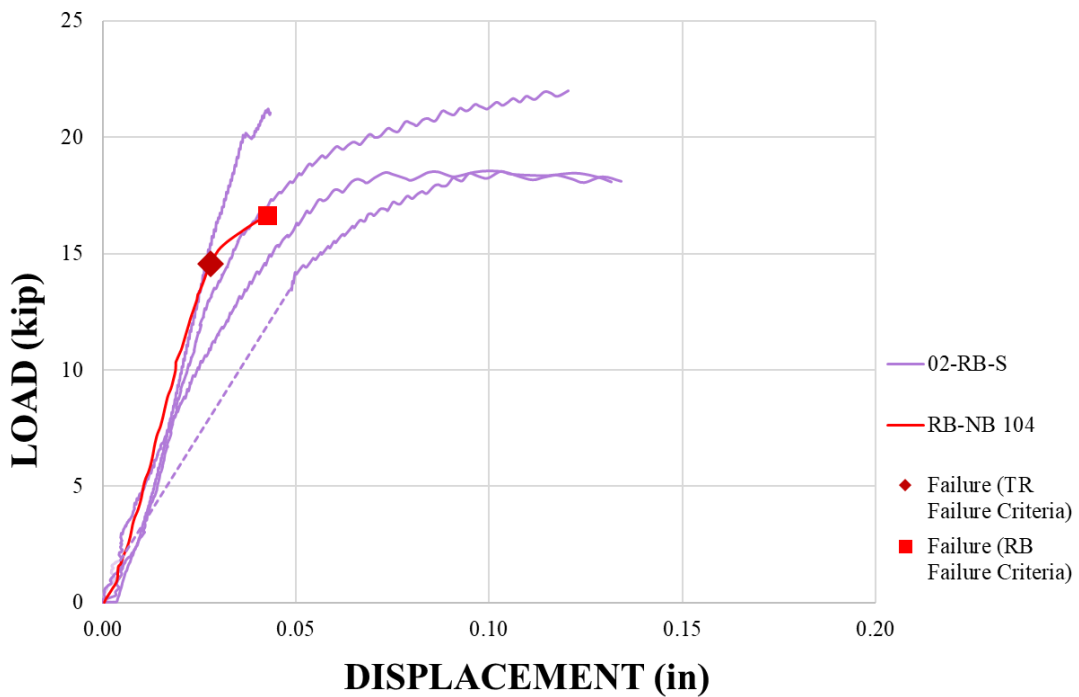


**Figure 5-35.** Material 2 Reinforcing Bar Test Results and RB-NB Model Results with assumed adhesive material properties at 104°F (40°C).

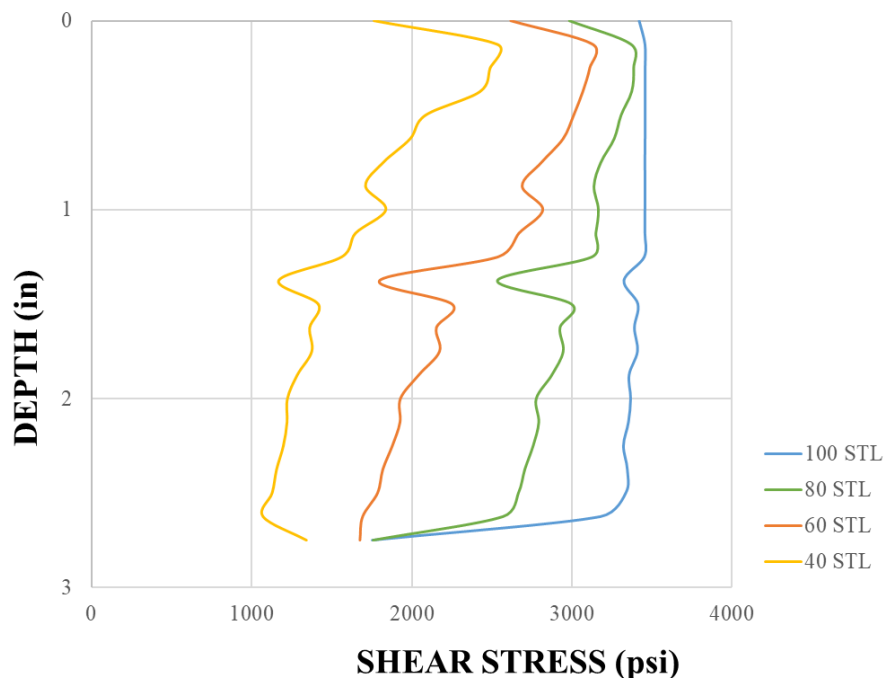


**Figure 5-36.** Shear Stress Distribution at the hole diameter for RB-NB at 104°F (40°C).

At assumed adhesive material properties at 77°F (25°C), the RB-NB model undergoes failure at 23.50 kips (104.53 kN) at a displacement of 0.03 in (1.02 mm), shown in Figure 5-37. The maximum shear stress observed at this point is 4934 psi (34 MPa) and the maximum equivalent stress observed is 8601 psi (59 MPa). A 30% increase in load capacity was determined from the RB-NB model run at 104°F (40°C), which follows the behavior of the material properties defined in Section 2.3 and Section 4.2.3.

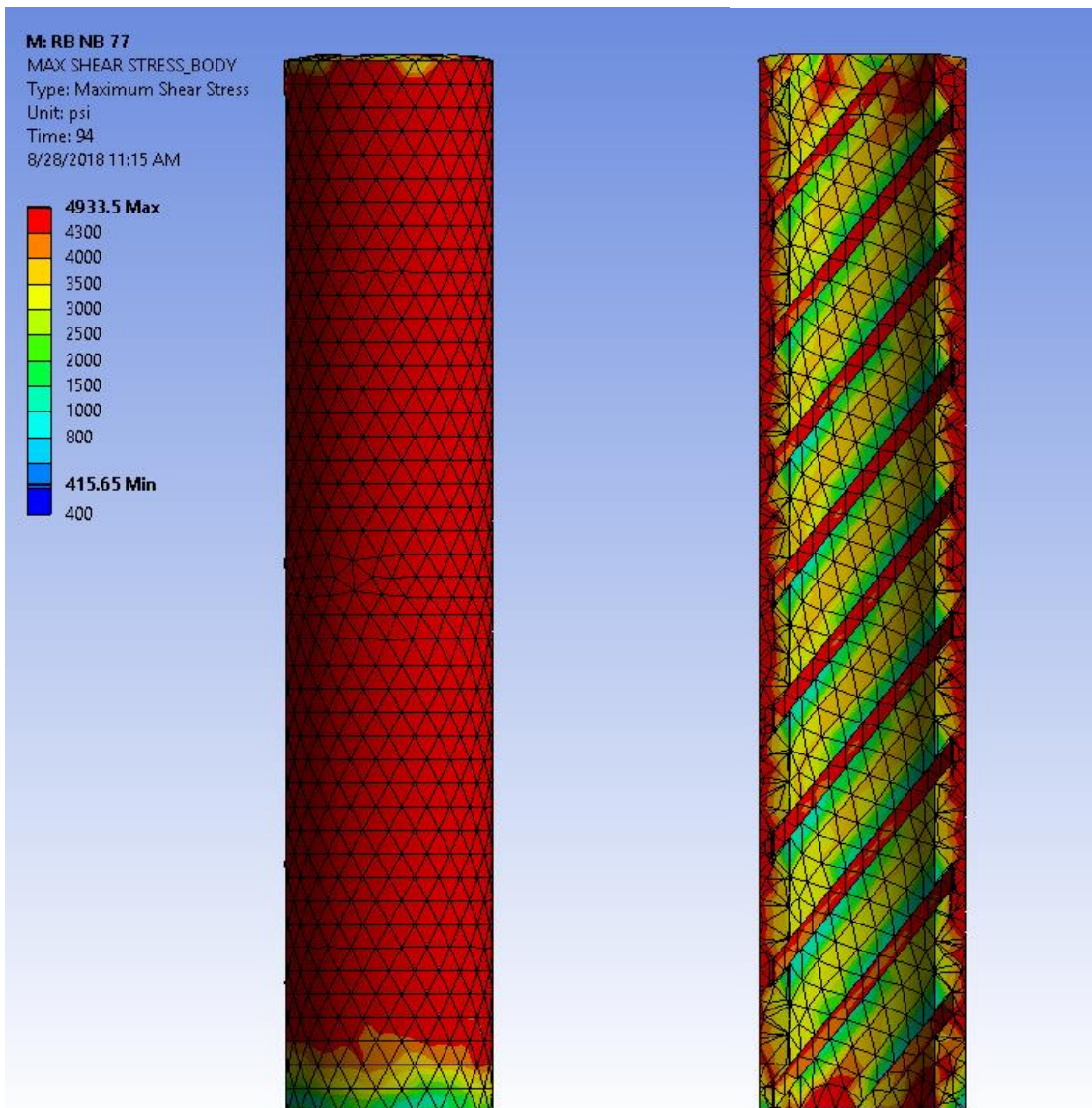


**Figure 5-37.** Shear stress contour plot of the outer face (left) and inner face (right) of the adhesive layer of the RB-NB model at 77°F (25°C) at failure.

At -40°F (-40°C), the RB-NB model reaches a maximum shear stress of 6308 psi (43 MPa) and a maximum equivalent stress of 11019 psi (76 MPa). As in previous models run at assumed adhesive material properties at -40°F (-40°C), failure could not be determined; the peak shear stress was unable to distribute evenly across the outer surface of the adhesive layer before the anchor exhibited failure and the model was unable to solve.

#### **5.3.4. RB-CB**

The RB-CB model simulated with assumed adhesive properties at 104°F (40°C) was observed to fail at 20.83 kips (92.66 kN) at a displacement of 0.03 inches (0.76 mm), reaching a maximum shear stress of 3573 psi (25 MPa) and a maximum equivalent stress of 6191 psi (43 MPa). This indicates that the additional adhesive layer at the bottom of the anchor increased the load capacity of the system by 20%, and that the force transferred from the anchor to the adhesive is also transferred to the bottom layer, further distributing the stress and enabling the adhesive to take more load. In the physical tests, the reinforcing bar exhibited 10% more capacity than the threaded rod specimens tested under the same parameters. The shear stress contour plot for the RB-CB model is shown in Figure 5-38 and the shear stress distribution at the hole diameter is shown in Figure 5-39. The RB-CB model at 104°F (40°C) best matched the load capacity of the physical reinforcing bar results, but did not match the stiffness, as seen in Figure 5-40.

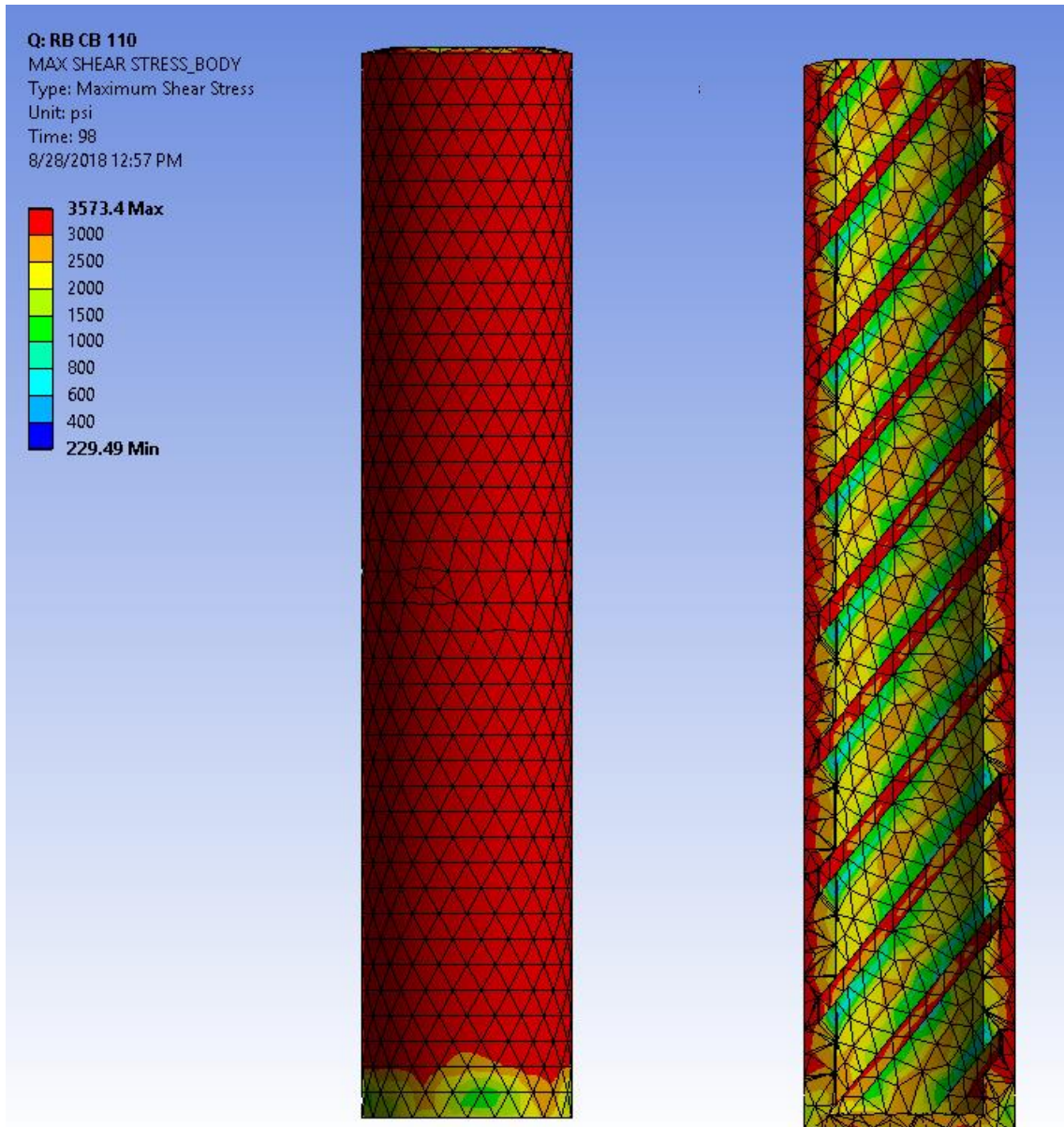


**Figure 5-38.** Shear stress contour plot of the outer face (left) and inner face (right) of the adhesive layer of the RB-CB model at 104°F (40°C) at failure.

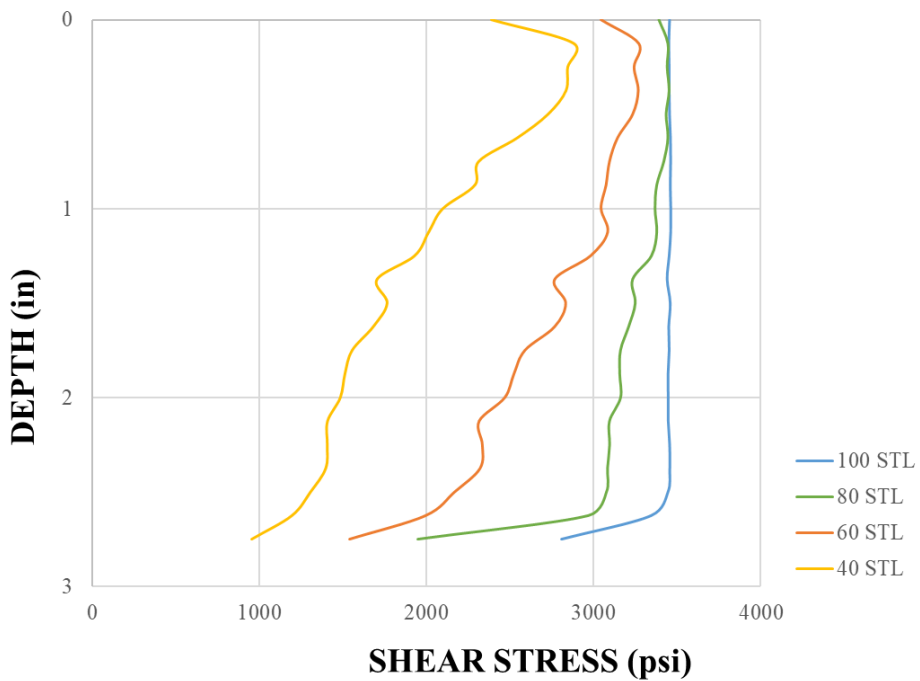


**Figure 5-39.** Shear Stress Distribution at the hole diameter for RB-CB at 104°F (40°C).

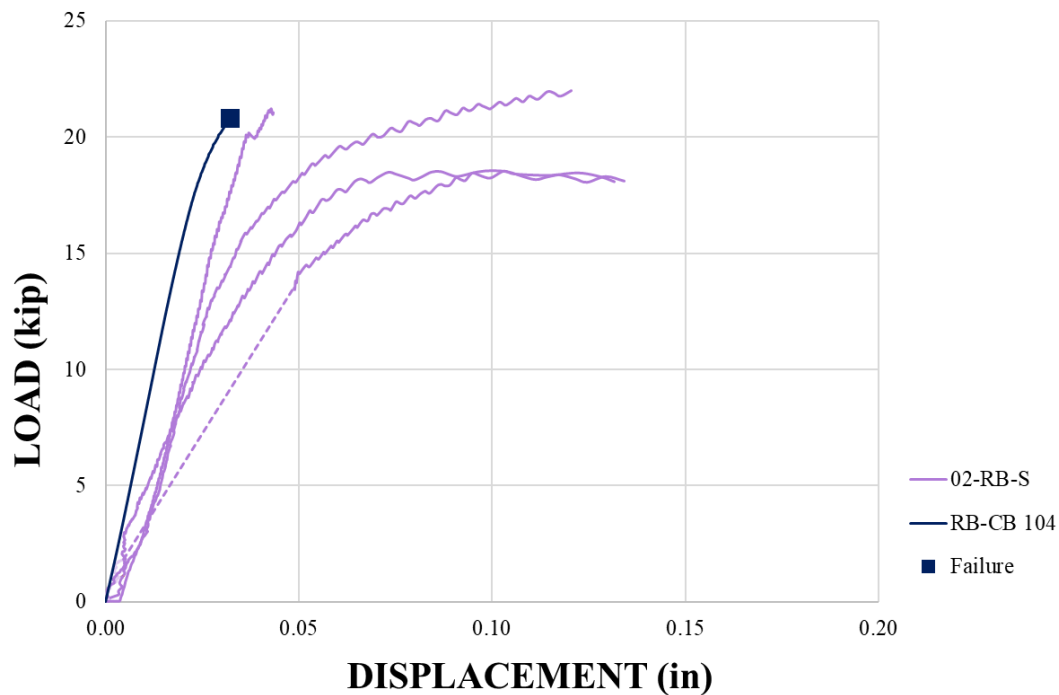


**Figure 5-40.** Material 2 Reinforcing Bar Test and FEM Results: Load vs. Displacement

At 77°F (25°C), the adhesive in the RB-CB model reaches a maximum shear stress of 4948 psi (34 MPa) and a maximum equivalent stress of 8600 psi (59 MPa). Failure of the adhesive could not be determined due to steel failure in the finite element model at increasing loads. Likewise, at -40°F (-40°C), failure could not be determined, but the RB-CB model reaches a maximum shear stress of 6084 psi (42 MPa) and a maximum equivalent stress of 10806 psi (75 MPa).

### **5.3.5. Comparison of the Physical Test and FEM Results**

Plotted in Figure 5-41 are the threaded rod physical test results tested at 110°F to 120°F (43°C to 49°C) compared with the TR-NB and TR-CB results simulated at 104°F (40°C). The TR-CB load vs. displacement curve is observed to be stiffer with failure occurring at a smaller displacement and higher load capacity, while the TR-NB load vs. displacement curve is observed to fit more accurately with the physical test results. Therefore, the TR-NB model with assumed adhesive properties at 104°F (40°C) will be used for further comparisons.

Figure 5-42 plots the reinforcing bar physical test results at 110°F to 120°F (43°C to 49°C) with the RB-NB and RB-CB results at 104°F (40°C). The reinforcing bar results show a greater coefficient of variation than the threaded rod results; the load vs. displacement of the RB-NB model is found to match closely with the lower bound of the physical test results, while the load vs. displacement of the RB-CB model approximately matches the test in the upper bound. As a result, the RB models appear more variable in whether the additional bottom adhesive layer contributes to the transfer of load; however, the RB-NB model follows the majority of the physical test results and therefore is considered the best fit.

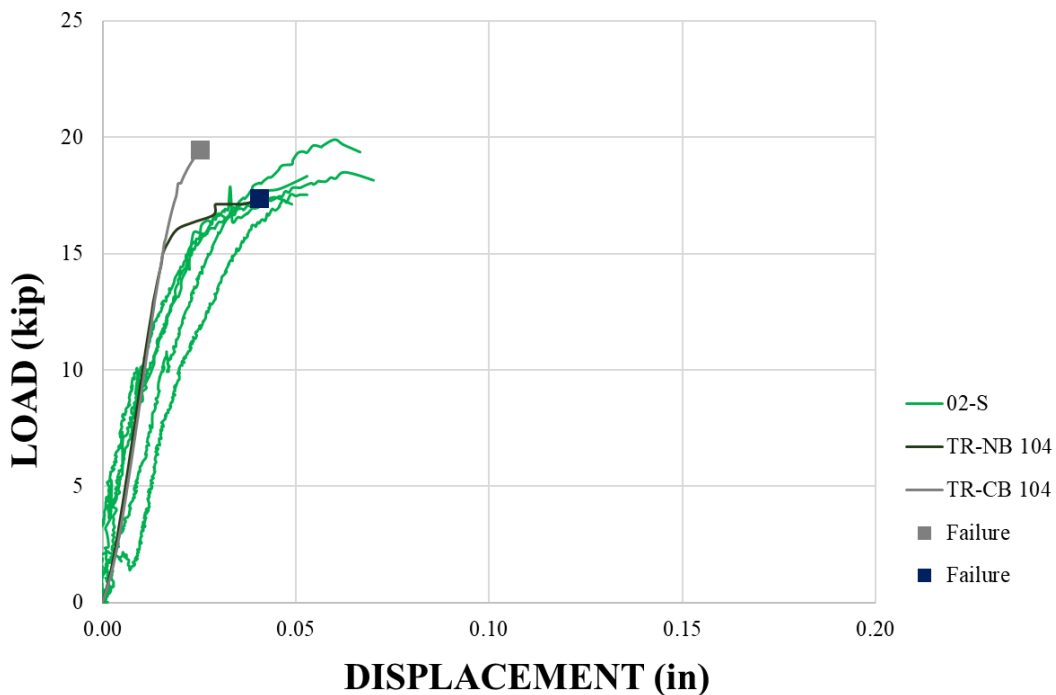


**Figure 5-41.** Material 2 Threaded Rod Results Compared With the TR-NB and TR-CB FEM Results: Load vs. Displacement.

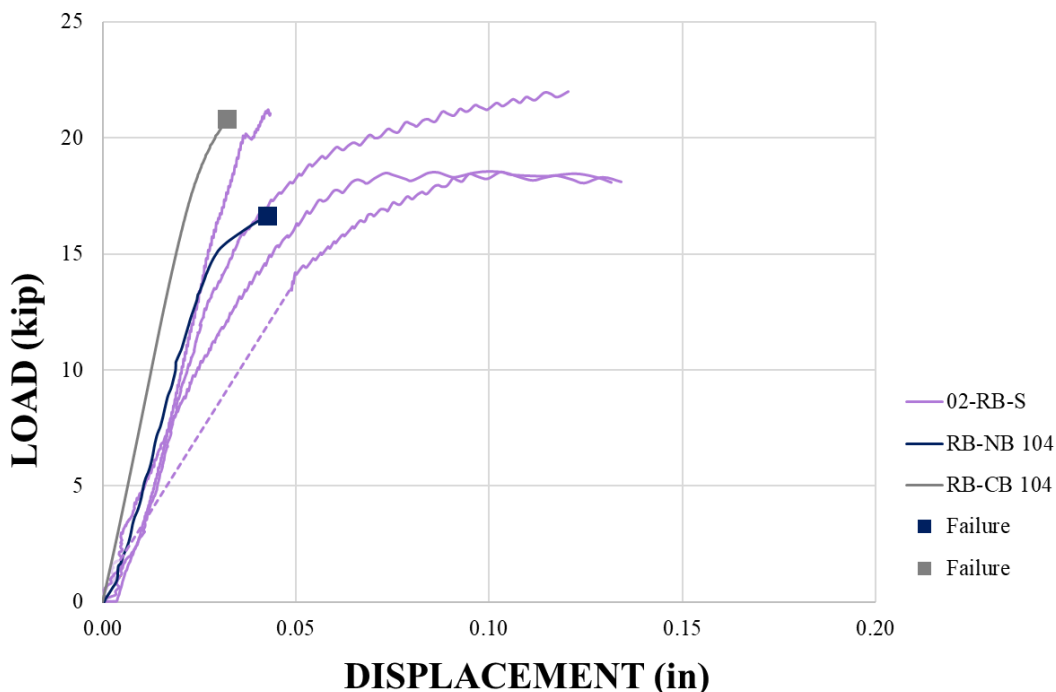


**Figure 5-42.** Material 2 Reinforcing Bar Results Compared With the RB-NB and RB-CB FEM Results: Load vs. Displacement.

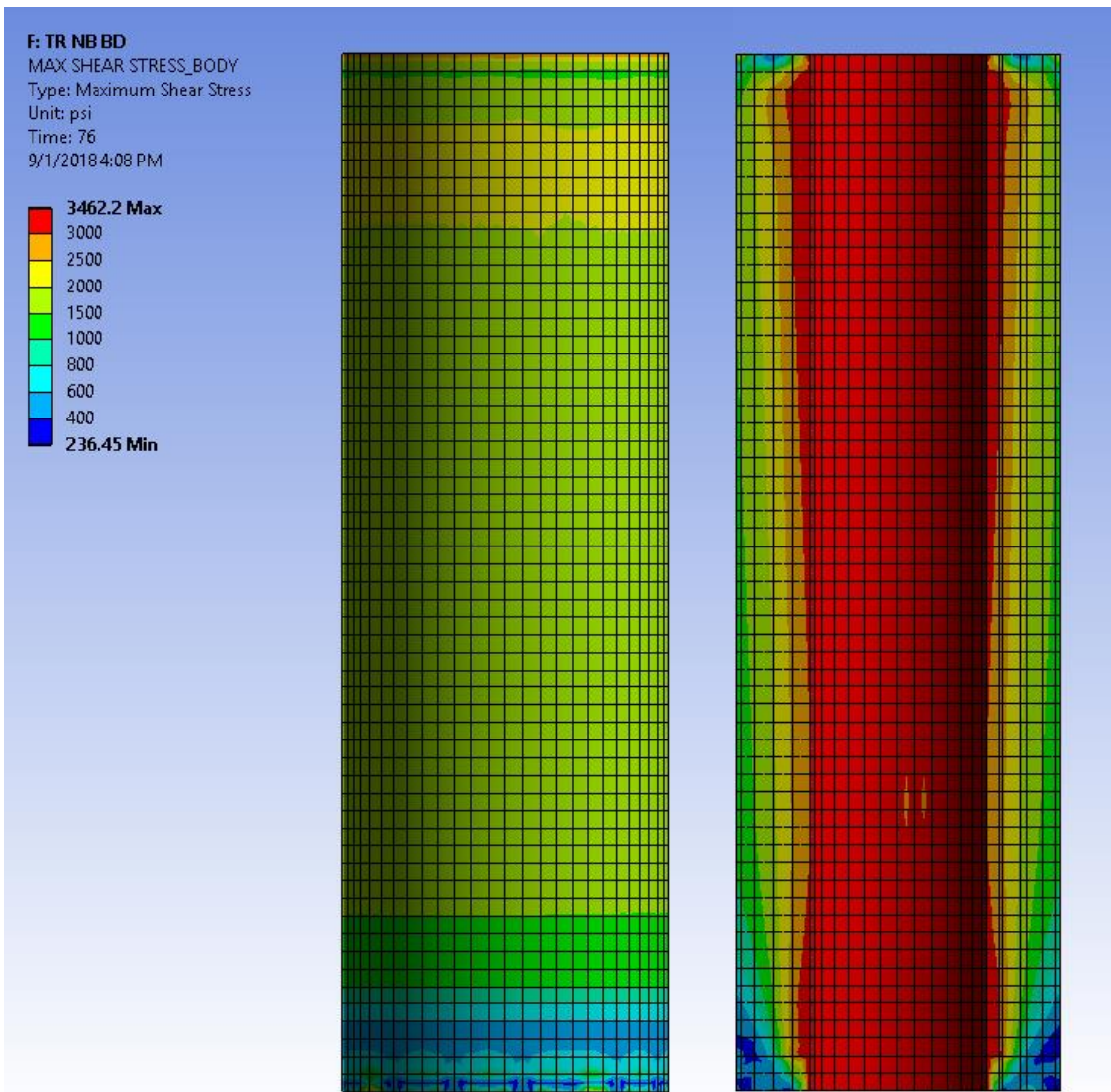
### 5.3.6. Larger Hole Diameter Results

Due to the better accuracy of the results of the TR-NB and RB-NB models at 104°F (40°C) to the physical testing results, the TR-NB and RB-NB models were used to investigate the behavior of a thicker adhesive layer. As such, the hole diameter for each model was increased to 0.875 in (22.23 mm) and both models were run at the assumed adhesive material properties at 104°F (40°C). Table 5-5 lists a summary of the larger hole diameter results.

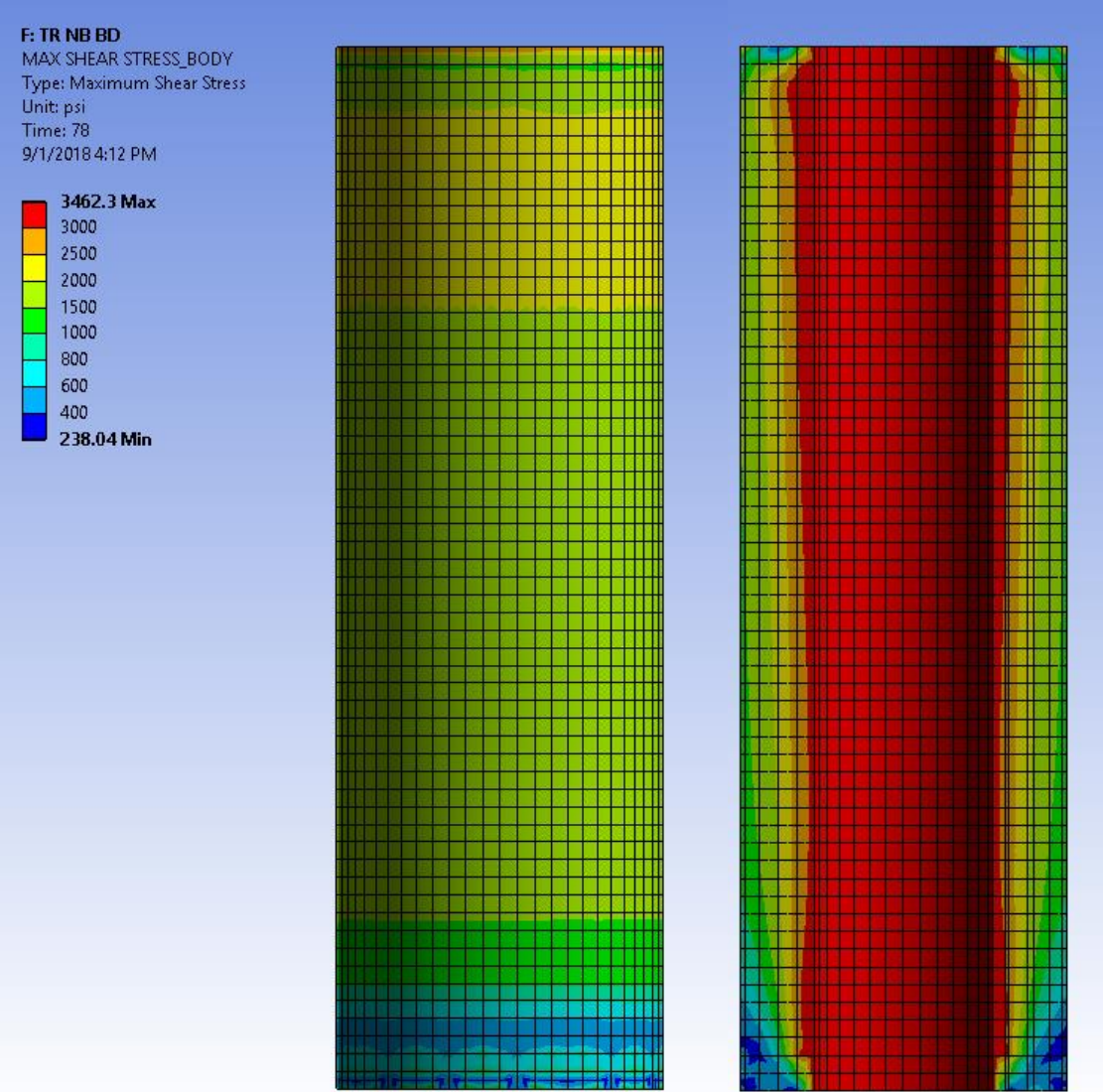
**Table 5-5. Summary of Finite Element (Larger Hole) Results**

MODEL	TEMPERATURE (°F)	LOAD (kip)	DISPLACEMENT (in)
TR-NB-BD	104	16.25	0.03
RB-NB-BD	104	19.17	0.04

In the TR-NB-BD model, the adhesive exhibits an even distribution of stress on the inner surface but does not penetrate to the outer surface before the anchor fails. If failure is assumed to be the point at which the adhesive shows an even distribution at the steel/adhesive interface without penetration to the outside face, then the TR-NB-BD model fails at 16.25 kips (72.28 kN) and reaches a maximum shear stress of 3462 psi (24 MPa) and a maximum equivalent stress of 5999 psi (41 MPa). A displacement of 0.03 inches (0.76 mm) is observed. This is shown in the progression of contour plots before failure, at failure, and after failure in Figure 5-43. In this case, the TR-NB-BD model displays lower performance than the TR-NB model.



(a)



(b)

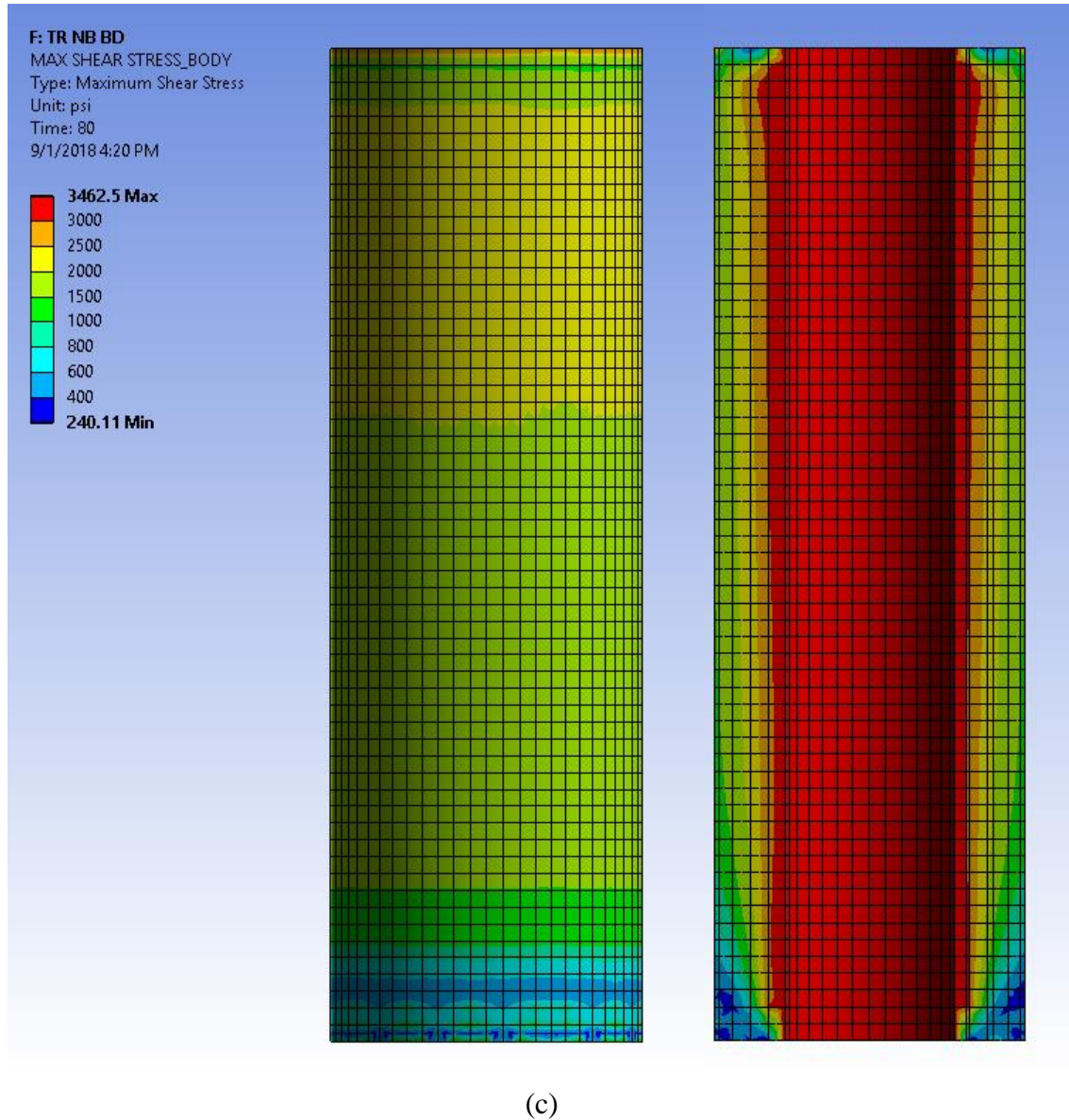


**Figure 5-43.** Shear stress contour plot of the adhesive layer of the TR-NB-BD model at 104°F (40°C) before failure (a), at failure (b), and after failure (c) as load increases.

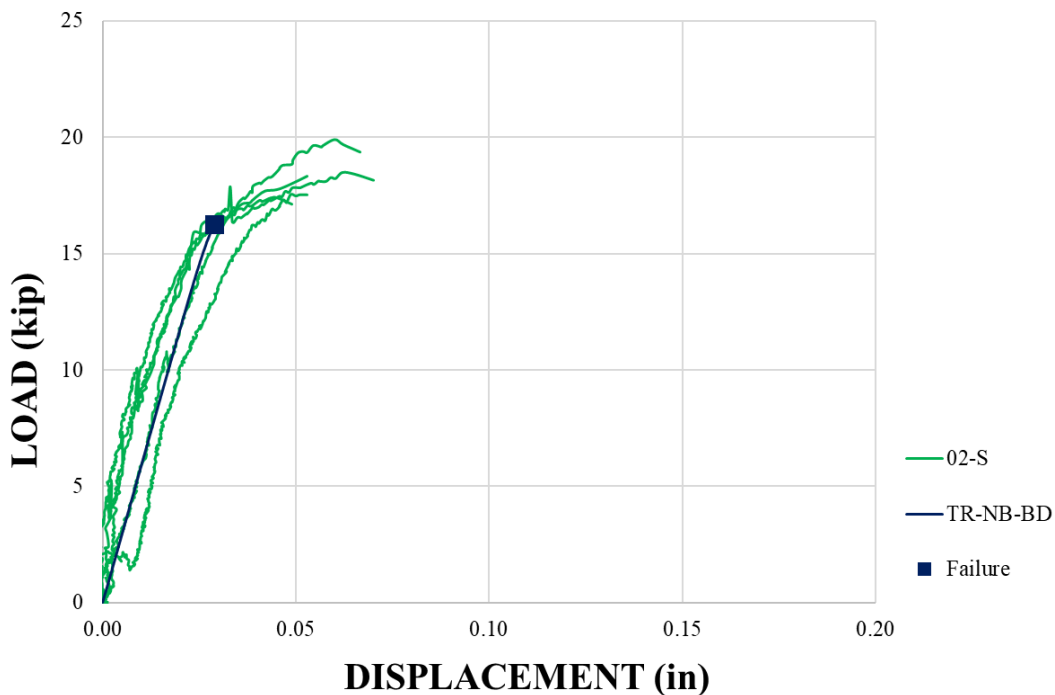
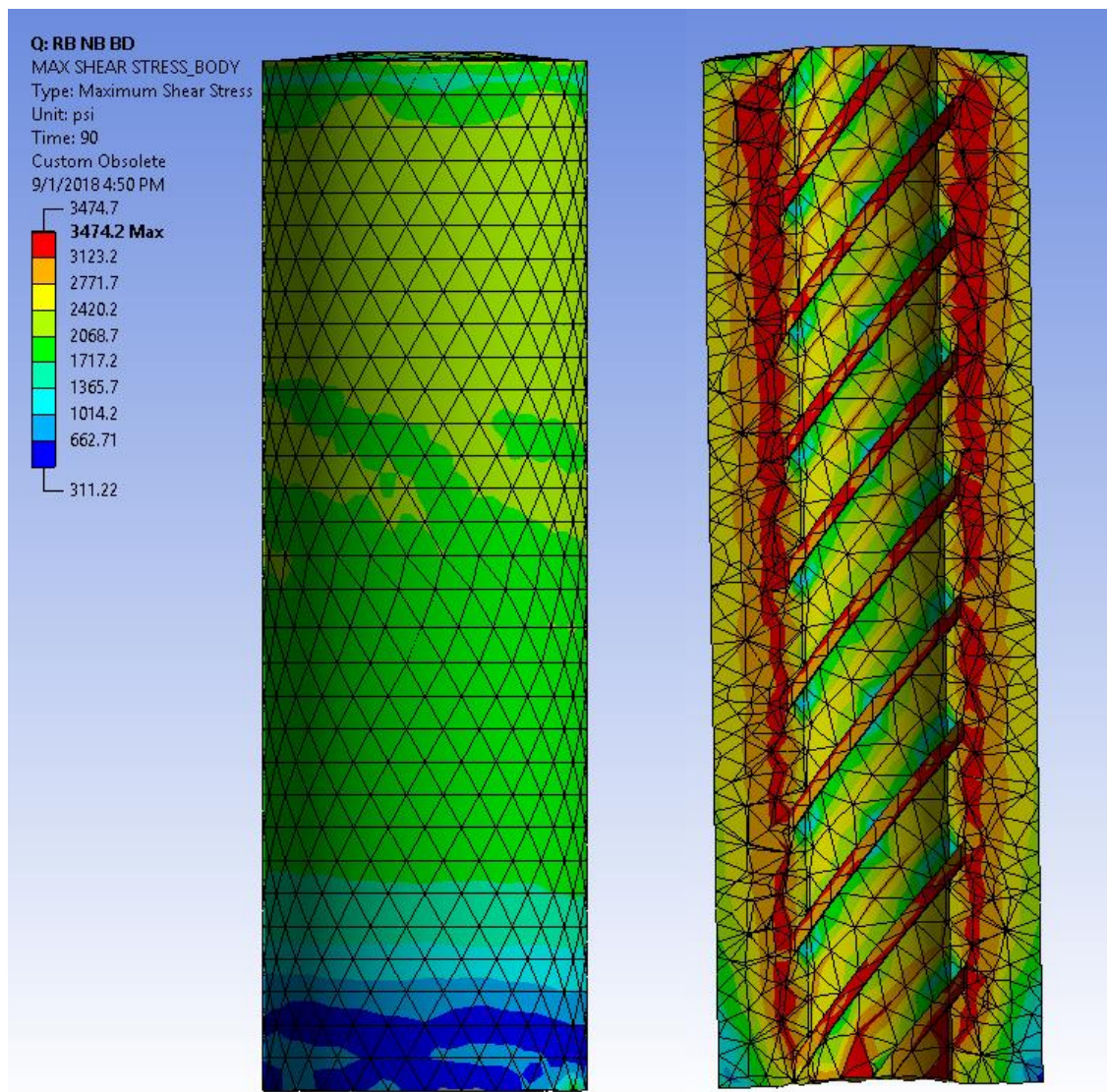
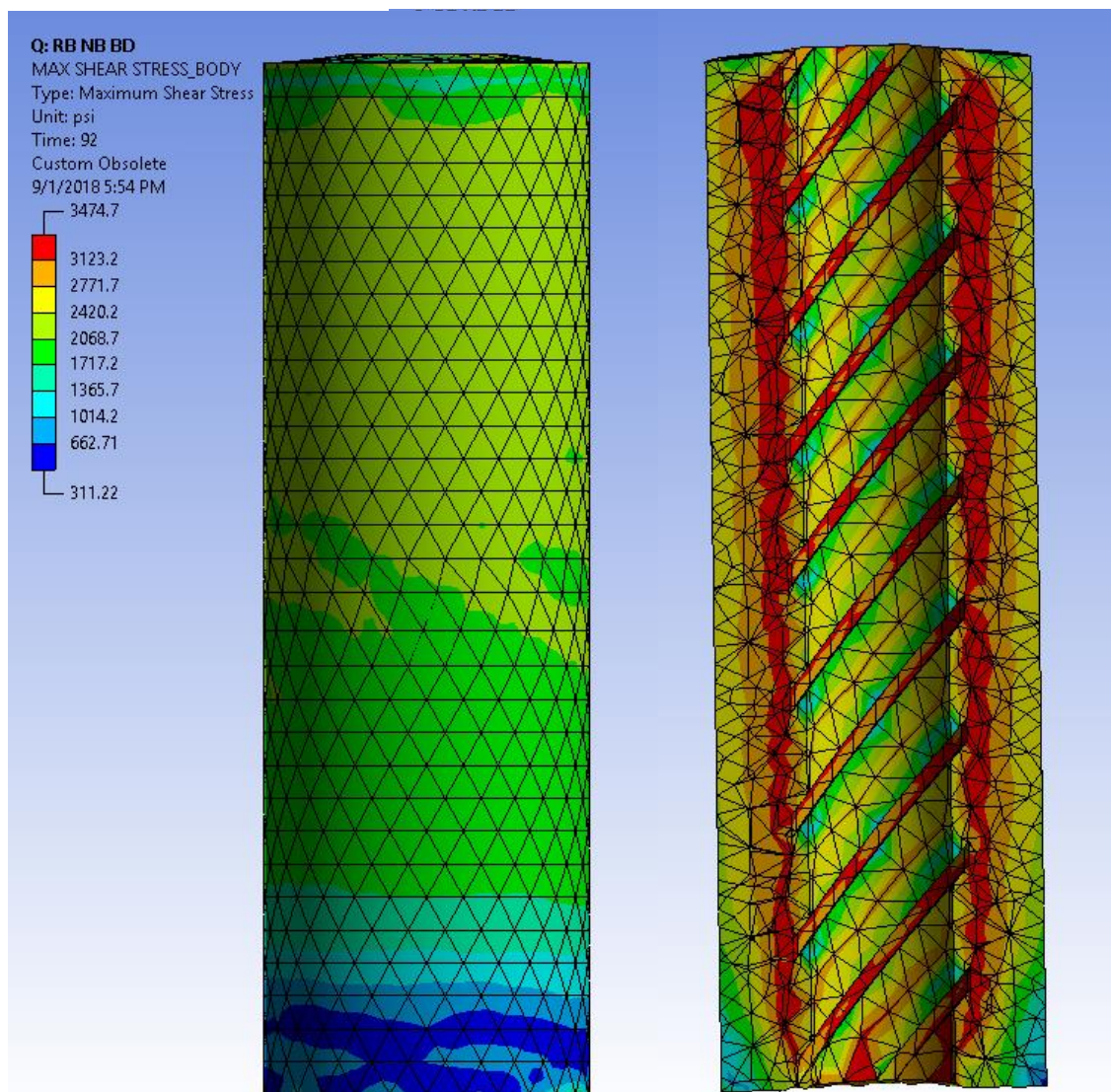


**Figure 5-44.** Material 2 Threaded Rod Test Results and TR-NB-BD Result: Load vs. Displacement.

In the RB-NB-BD model, the adhesive does not exhibit an even distribution of shear stress along the outer surface like in the RB-NB models. However, results show that as load increases, a concentration of peak stress occurs at the edge of the reinforcing bar lugs that eventually spreads and merges to form vertical bands from the top of the adhesive to the bottom, seen in Figure 5-45. If failure is assumed at this point, then the RB-NB-BD model fails at 19.17 kips (85.27 kN) at a 0.04 inch (1.02 mm) displacement, exhibiting higher performance than the RB-NB model. In addition, the adhesive reaches a maximum shear stress of 3469 psi (23.92 MPa) and a maximum equivalent stress of 6143 psi (42.35 MPa).



(a)



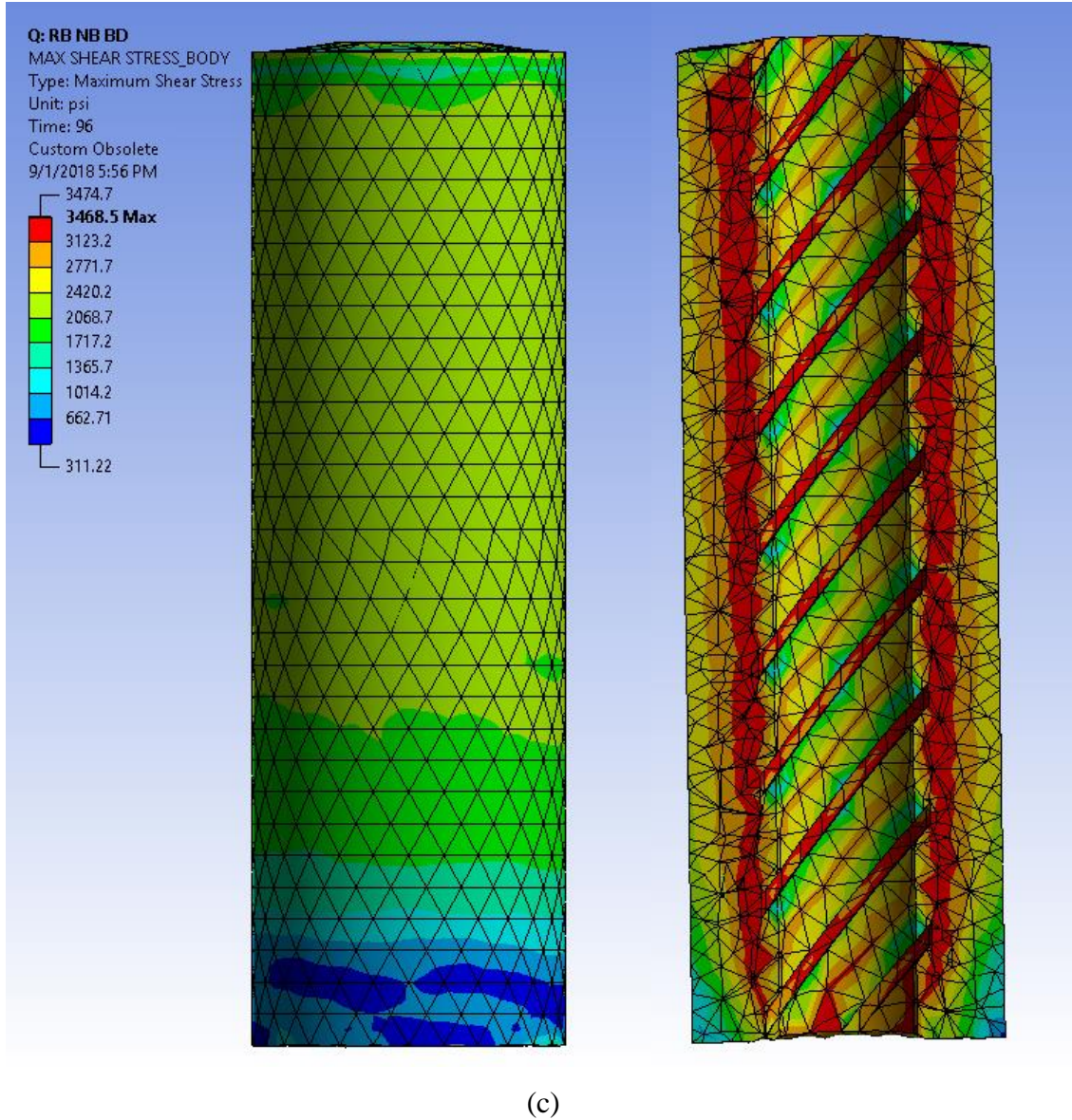


**Figure 5-45.** Shear stress contour plot of the adhesive layer of the RB-NB-BD model at 104°F (40°C) before failure (a), at failure (b), and after failure (c) as load increases.

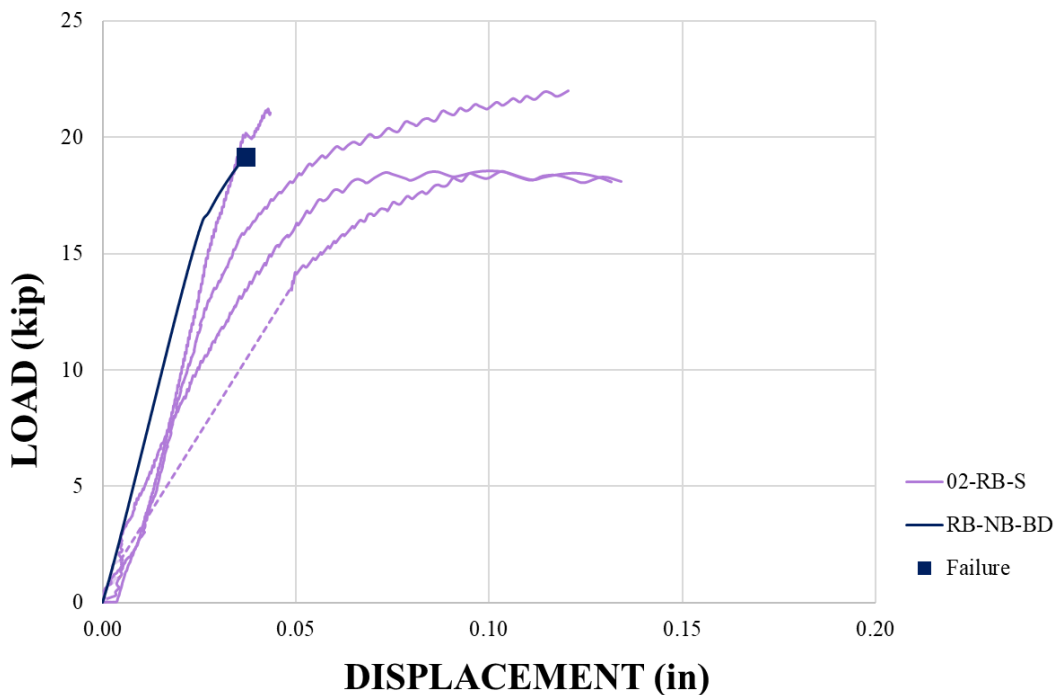


**Figure 5-46.** Material 2 Reinforcing Bar Test Results and RB-NB-BD Result: Load vs. Displacement.

#### 5.4. Summary

For the threaded rod finite element models, the failure criterion was defined as the point at which an even distribution of shear stress occurred at the inner surface of the adhesive layer and spread through to the outside surface of the layer. For the reinforcing bar finite element models, the failure criterion was observed to be the point at which an even distribution of shear stress occurred at the outer surface of the adhesive layer. Both threaded rod and reinforcing bar finite element models were run with and without an additional adhesive layer beneath the anchor to investigate changes in behavior and to determine which model fit more closely with the physical testing results; it was found

that the results of the NB models for both threaded rod and reinforcing bar with assumed adhesive properties at 104°F (40°C) exhibited the closest fit.

## **CHAPTER 6**

### **CONCLUSION**

The purpose of the study presented in this thesis was to investigate the effects of temperature on the load capacity and behavior of adhesive anchorage systems through the use of physical testing and finite element modeling. Physical tests were adopted from the procedure begun by Mendoza (2017) and Drolesch (2015) and temperature parameters were chosen based on in-service temperatures an anchorage system would most likely be exposed to during its service life.

Physical test results found that despite accommodating for the prevention of steel failure in the test design, in many cases for Material 1B the steel anchor would fail before the adhesive. Displacement readings were thus affected, measuring both adhesive displacement as well as steel yielding. Material 7, marketed for cold weather applications, experienced high performance in cold temperatures as expected, but as testing temperatures increased experienced reduced capacity. For Material 2, reinforcing bar anchors and threaded rod anchors were compared in static pullout tests. The reinforcing bar tests were found to have more capacity than the threaded rod tests but more variability. It is recommended that more testing be conducted with Material 2 before a conclusion can be reached about its behavior under changing temperatures.

Finite element models replicating both the threaded rod and reinforcing bar anchorage systems were simulated with assumed adhesive material properties at different temperatures. Failure was defined based on observations of the results; the adhesive exhibited more similar behavior than expected at all temperatures, showing little variation in strain. Load capacity predictions can be made based on the stress vs. strain curves for

adhesives under different temperatures given in Section 2.3. For the threaded rod models, failure was determined to be the point at which an even shear stress distribution occurred on the inner face of the adhesive and spread to the outer face. For the reinforcing bar model, failure was determined to be the point at which an even shear stress distribution occurred on the outer face of the adhesive. Overall, the finite element models showed lower capacity at elevated temperatures than ambient temperatures which did not match the experimental results. In addition, the models that lacked a layer of adhesive at the bottom of the hole exhibited the most load and strain similarities to the results of the physical tests of threaded rod models and a reasonable lower bound to reinforcing bar models.

When the hole diameter is expanded, failure of the threaded rod model was defined to be the point at which the anchor yielded, while failure of the reinforcing bar model was defined to be when a vertical band of peak stress occurred along the edge of the lugs along the length of the adhesive. From these criteria, it was found that the threaded rod model with a larger hole diameter displayed a lower load capacity than the same model with the manufacturer recommended hole diameter. On the other hand, the reinforcing bar model with a larger hole diameter exhibited more load capacity which matches manufacturer recommendations.

Limitations exist for this study. All tests were performed using a downward vertical installation direction, and as such, all results should only be attributed to downward vertical installation of anchorage systems. Overhead and horizontal installation tests were not conducted and may provide different results and conclusions.

## REFERENCES

- AASHTO TP-84. (2010). *Standard Method of Test for Evaluation of Adhesive Anchors in Concrete Under Sustained Loading Conditions*. Washington D.C.: American Association of State Highway and Transportation Officials.
- ACI 318. (2014). *Building Code Requirements for Structural Concrete (ACI 318-14) and Commentary (318R-14)*. Farmington Hills, MI: American Concrete Institute.
- ACI 355.4. (2011). *Qualifications of Post-Installed Adhesive Anchors in Concrete*. Farmington Hills, MI: American Concrete Institute.
- ASTM E488. (2010). *Standard Test Methods for Strength of Anchors in Concrete*. West Conshohocken, PA: ASTM International.
- Brockenbrough, R. (2006). *Structural Steel Designer's Handbook: AISC, AASHTO, AISI, ASTM, AREMA, and ASCE-07 Design Standards, Fourth Edition*. McGraw-Hill Professional.
- Chen, J., Young, B., & Uy, B. (2006). Behavior of High Strength Structural Steel at Elevated Temperatures. *Journal of Structural Engineering*, 132(12), 1948-1954.
- Cook, R., & Davis, T. (2009). *Adhesive Anchors in Concrete Under Sustained Loading Conditions*. Washington D.C.: National Cooperative Highway Research Program.
- Cook, R., Douglas, E., Davis, T., & Liu, C. (2013). *Long-Term Performance of Epoxy Adhesive Anchor Systems*. Washington D.C.: National Cooperative Highway Research Program.
- Cook, R., Kunz, J., Fuchs, W., & Konz, R. (1998). Behavior and Design of Single Adhesive Anchors Under Tensile Load in Uncracked Concrete. *ACI Structural Journal*, 9-26.
- Cook., R., & Burtz., J. (2003). *Design Guidelines and Specifications for Engineered Grouts*. University of Florida, Department of Civil & Coastal Engineering. Gainesville: Florida Department of Transportation.
- Davis, T. (2012). *Sustained Load Performance of Adhesive Anchor Systems in Concrete*. University of Florida.
- Droesch, D. (2015). *Bonded Anchors in Concrete Under Sustained Loading*. Amherst: University of Massachusetts Amherst.

- Dusel, J., & Mir, A. (1991). *Initial Evaluation of Epoxy Cartridges used for Anchoring Dowels into Hardened Concrete*. Sacramento, CA: California Department of Transportation.
- Ellis, B. (1993). *Chemistry and Technology of Epoxy Resins*. Springer, Netherlands: University of Sheffield.
- Fielder, B., Hobbiebrunken, T., Masaki, H., & Schulte, K. (2005). Influence of Stress State and Temperature on the Strength of Epoxy Resins. *11th International Conference on Fracture*, (pp. 32-43). Turin, Italy.
- Fuchs, W., Eligenhause, R., & Breen, J. (1995). Concrete Capacity Design (CCD) Approach for Fastening to Concrete. *ACI Structural Journal*, 92, 73-94.
- Gowariker, V., & Viswanathan, N. (1986). *Polymer Science*. New Delhi: New Age International (P) Ltd.
- ICC-ES AC308. (2013). *Acceptance Criteria for Post-Installed Adhesive Anchors in Concrete Elements*. Whittier, CA: ICC Evaluation Services Incorporated.
- Jordan, J., Foley, J., & Siviour, C. (2008). Mechanical properties of Epon 826/DEA epoxy. *Mech Time-Depend Mater*, 12, 249-272.
- Kim, M., Kim, S., Lee, S., Kim, J., Lee, K., & Yoo, D. (2017). Mechanical properties of ultra-high-performance fiber-reinforced concrete at cryogenic temperatures. *Construction and Building Materials*, 157, 498-508.
- Lange, J., Ekelof, R., St. John, N., & George, G. (1999). Transitions, Properties, and Molecular Mobility During Cure of Thermosetting Resins. *ACS Symposium Series*, 258-271.
- Ma, Q., Guo, R., Zhao, Z., Lin, Z., & He, K. (2015). Mechanical properties of concrete at high temperature--A review. *Construction and Building Materials*, 371-383.
- May, C. (1987). *Epoxy Resins: Chemistry and Technology, Second Edition*. CRC Press.
- McVay, M., Cook, R., & Krishnamurthy, K. (1996). Pullout Simulation of Postinstalled Chemically Bonded Anchors. *Journal of Structural Engineering*, 122(9), 1016-1024.
- Mendoza, M. (2016). *Performance of Adhesive and Cementitious Anchorage Systems*. Amherst: University of Massachusetts Amherst.
- Neuenschwander, M., Scandella, C., Knobloch, M., & Fontana, M. (2017). Modeling elevated-temperature mechanical behavior of high and ultra-high strength steels in structural fire design. *Materials and Design*, 81-102.

- NTSB. (2007). *Ceiling Collapse in the Interstate 90 Connector Tunnel, Boston, Massachusetts July 10, 2006*. Washington: National Transportation Safety Board.
- Ocel, J., & Provines, J. (2015). *Properties of Anchor Rods Removed from San Francisco-Oakland Bay Bridge*. McLean, VA: Federal Highway Administration.
- Okba, S., Nasr, E., Helmy, A., & Yousef, I. (2017). Effect of thermal exposure on the mechanical properties of polymer adhesives. *Construction and Building Materials*, 490-504.
- Rautenberg, J., Pujol, S., Tavallali, H., & Lepage, A. (2012). Reconsidering the use of high-strength reinforcement in concrete columns. *Engineering Structures*, 37, 135-142.
- Rawn, J., & Ouellette, R. (2018). *Organic Chemistry*. Academic Press.
- Shoukry, S., William, G., Downie, B., & Riad, M. (2011, June). Effect of Moisture and Temperature on the Mechanical Properties of Concrete. *Construction and Building Materials*, 25, 688-696.
- Yan, J., & Xie, J. (2017). Behaviours of reinforced concrete beams under low temperatures. *Construction and Building Materials*, 141, 410-425.